GAP JUNCTION FORMATION IN HEART VALVES IN RESPONSE TO MECHANICAL LOADING

by

Karen L. O'Malley

Submitted in partial fulfillment of the requirements
for the degree of Master of Applied Science

at

Dalhousie University
Halifax, Nova Scotia
June 2013

Dedication

To my parents, who instilled in me a love of learning.

Education is the kindling of a flame, not the filling of a vessel.

― Socrates

There is no end to education. It is not that you read a book,

pass an examination, and finish with education. The whole of life,

from the moment you are born to the moment you die, is a process of learning.

― Jiddu Krishnamurti

Table of Contents

List of Tables

List of Figures

Abstract

Valvular interstitial cells (VICs) are responsible for the maintenance of heart valve leaflet structure, however their responses to mechanical loading are not fully understood. Further characterization of VIC responses with regards to phenotype (quiescent or activated via α-smooth muscle actin [α-SMA]) and communication (through gap junction proteins connexins 43 and 26) were studied. Tissue strips from porcine aortic, pulmonary, and mitral valves were cyclically stretched in the circumferential direction at normal and above normal membrane tensions for 48 hours at 1 Hz, 37°C, and 5% CO_2. Unloaded tissues were statically incubated concurrently with loaded tissues, and fresh tissue controls were collected immediately. VIC phenotype was identified by α-SMA via immunohistochemical staining and cell enumeration, as well as by gene expression via RT-PCR. Gap junction protein Cx43 was also evaluated via immunohistochemical staining and cell enumeration and by gene expression via RT-PCR, whereas Cx26 was evaluated using immunohistochemical staining and cell enumeration only. Within the range tested, it was found that mechanical loading did not affect α-SMA or gap junction protein levels, nor were any differences in responses noted between valve types. However, the α-SMA gene expression level was significantly lower in the mitral valve compared to the aortic and pulmonary valves. This may indicate a difference in the genetic response pathways among the valves, but not in the functional outcomes. This difference may be explained by embryological origins, since the mitral valve, unlike the aortic and pulmonary valves, contains only VICs and no neural crest cells.

List of Abbreviations and Symbols Used

α-SMA	Alpha-smooth muscle actin
A_{260}	Absorbance reading at 260 nm
A_{280}	Absorbance reading at 280 nm
AR	Anitgen retrieval
AV	Aortic valve
aVIC	Activated valvular interstitial cell
C-terminus	Carboxy terminus
cDNA	Complimentary deoxyribonucleic acid
Cx##	Connexin ##
DMEM	Dulbecco's Modified Eagle's medium
DNA	Deoxyribonucleic acid
DNase	Deoxyribonuclease
ECM	Extracellular matrix
EDTA	Ethylenediaminetetraacetic acid
ELISA	Enzyme-linked immunosorbent assay
FA	Focal adhesion
FAK	Focal adhesion kinase
FBS	Fetal bovine serum
GJ	Gap junction
HIER	Heat-induced epitope retreival
HRP	Horseradish peroxidase
IHC	Immunohistochemistry
kDa	Kilodalton
MANOVA	Multivariate analysis of variance
MAPK	Mitogen-activated protein kinase
MMP	Matrix metalloproteinase
ms	Millisecond
MV	Mitral valve
N-terminus	Nitrogen terminus

obVIC	Osteoblastic valvular interstitial cell
P	Pressure
PBS	Phosphate buffered saline
PG	Proteoglycan
polyA	Polyadenylate
PV	Pulmonary valve
qVIC	Quiescent valvular interstitial cell
r	Radius
RNA	Ribonucleic acid
RNase	Ribonuclease
RT-PCR	Reverse transcription – polymerase chain reaction
SL	Semilunar valve
T	Tension
TBE	Tris/ borate/ ethylenediaminetetraacetic acid
TGF-β	Transforming growth factor-beta
TIMP	Tissue inhibitor of matrix metalloproteinase
TV	Tricuspid valve
TVP	Transvalvular pressure
UV	Ultraviolet
VEC	Valvular endothelial cell
VIC	Valvular interstitial cell

Acknowledgements

Chapter 1   Introduction

1.1   Heart Structure, Composition, and Function

The heart is a four-chambered pump that circulates blood through the lungs and body for nutrients and gas exchange. The valves ensure unidirectional blood flow, and open and close more than three billion times in a lifetime. The right side of the heart is responsible for pulmonary circulation, and the left side of the heart is for systemic circulation. Deoxygenated blood enters the right atrium from the vena cava where it is pumped through the right ventricle and pulmonary artery for gas transfer in the lungs. Oxygenated blood returns through the pulmonary vein to the left atrium and is pumped through the left ventricle and aorta for circulation through the body. (**Figure 1**)

The ventricles are separated from their arteries by the outflow or semilunar (SL) valves, so named because of their distinctive shape. They prevent retrograde flow from the arteries. The pulmonary valve (PV) is located between the right ventricle and the pulmonary artery. The aortic valve (AV) is located between the left ventricle and the aortic artery. The atria and ventricles are separated by the inflow or atrioventricular valves; the mitral (or bicuspid) valve (MV) in the left side of the heart, and the tricuspid valve (TV) in the right side of the heart. The atrioventricular valves also have chordae tendineae, tendonous fibrils that attach from the base of the leaflets to papillary muscles embedded in the ventricles. These prevent retrograde flow from the ventricles to the atria by preventing the valves from prolapsing into the atria when they close.

The heart has a specific and highly regulated pumping cycle with the average adult heart rate ranging between 60 and 70 beats per minute (1-1.167 Hz).[1] The opening and closing of the valves along with the contraction and relaxation of the atria and ventricles are coordinated for efficient blood flow. Systole makes up an approximate third of the cycle (~300 ms), and diastole the other two thirds (~600 ms).[2]
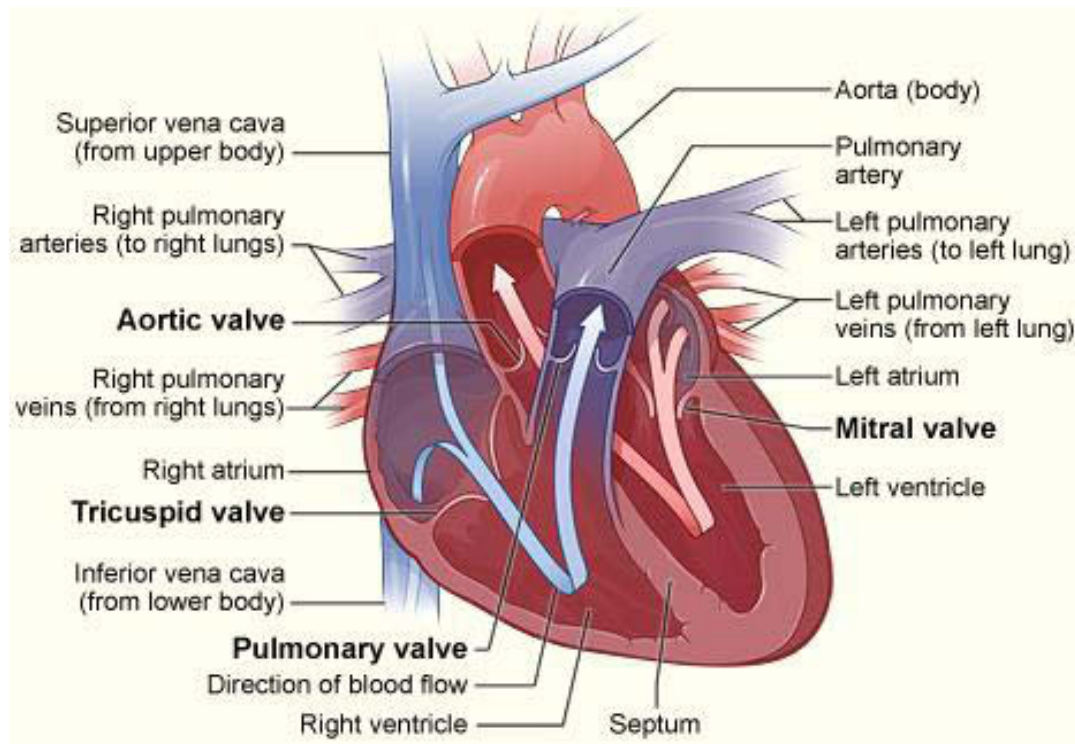
Figure 1 – Anatomy of the heart. (Figure from National Heart, Lung, and Blood Institute[3])

1.2 The Heart Valves

1.2.1 Valve and Leaflet Anatomy

Heart valves are an important part of an overall functional unit referred to as the valve root. The roots of the SL valves include the annulus, commissures, and leaflets. The atrioventricular valves have the same components, in addition to chordae tendineae and papillary muscles.[4] (**Figure 2**)
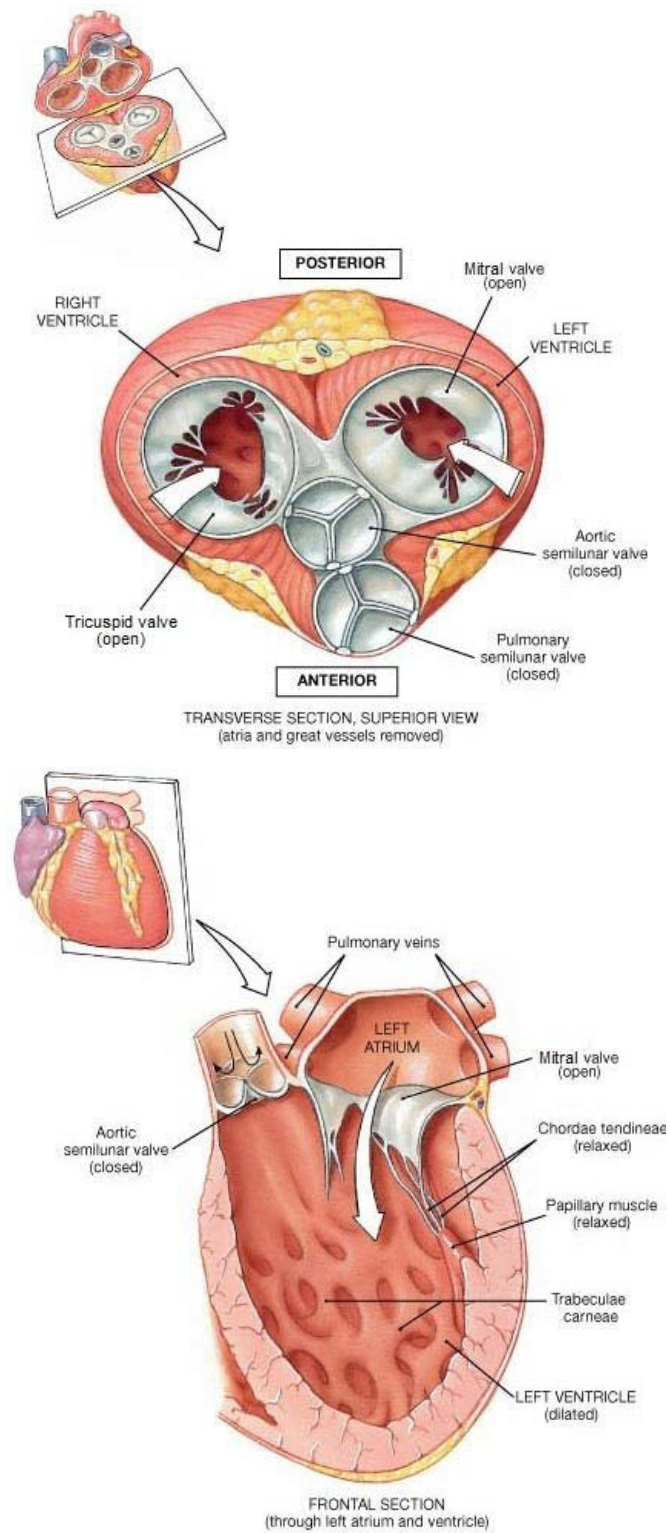
Figure 2 – Anatomy of the valves. They are shown during diastole. (Figure from Martini et al.[5])

The annulus is a fibrous structure composed mostly of collagen that surrounds and supports the valves.[4] The SL valves are similar in structure, though the PV leaflets are thinner than the AV leaflets, and the AV root also contains coronary ostia.[4] The ostia are the openings of the two coronary arteries, and they are located in the depressions behind the leaflets called the sinuses. The three leaflets are similar sizes and often referred to in the AV by their anatomical orientation to the coronary arteries as the left, right, and non-coronary (or posterior) cusps. For the PV, they are simply referred to as the left, right and anterior leaflets based on their anatomical orientation in the body. The valves attach in a crown-like fashion, with the curved base of the cusp attached at the annulus and the commissures (the point at which the leaflets meet) at the sinotubular junction. The free edge is the region that coapts with the neighbouring leaflets to provide a seal and prevent regurgitation. The center of the leaflet is referred to as the belly, and the region near the annulus as the base. (**Figure 3**)

The roots of the atrioventricular valves include the structures found in the SL roots in addition to the chordae tendineae and papillary muscles.[4] The MV is a two-leaflet valve and the leaflets are often referred to as anterior and posterior. The anterior leaflet is approximately two-thirds of the valve. As the name implies, the tricuspid valve (TV) has three leaflets, the anterior, posterior, and septal cusps. The chordae tendineae are located on the ventricular surfaces of the MV and TV. The papillary muscles are located in the walls of the ventricles, and they control the movement of the chordae.

1.2.2   Leaflet Structure and Components

The leaflet is a soft connective tissue that has a distinct trilaminar structure composed of the fibrosa, spongiosa, and ventricularis. It has valvular interstitial cells (VICs) dispersed throughout the interior, and is covered with a single-cell layer of valvular endothelial cells (VECs). The layers of the SL and atrioventricular valves are both highly organized, but their layers are not identical. (**Figure 4**)
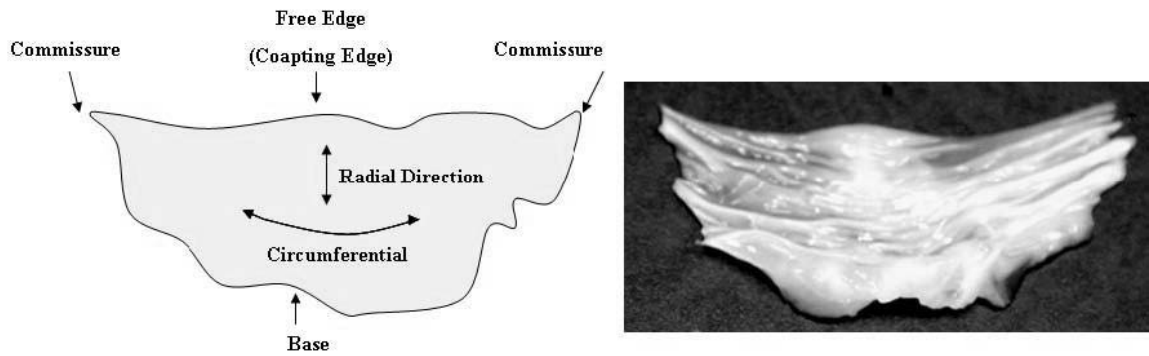
Figure 3 – An illustration (left) and an excised AV leaflet (right). The collagen bundles can easily be distinguished in the circumferential direction from the commissures. (Figure from Moeller[6])
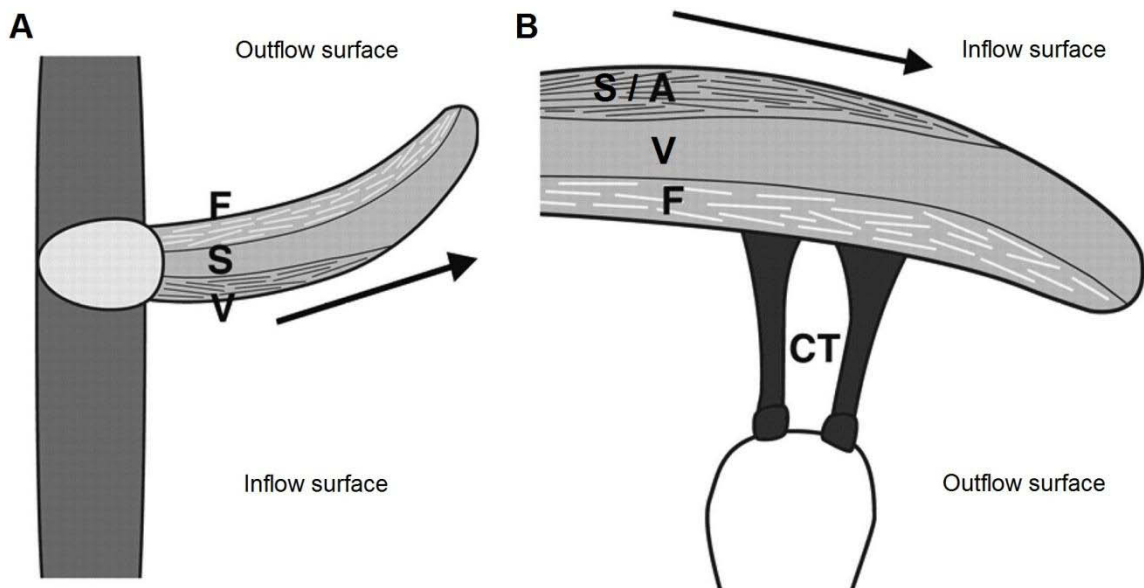
Figure 4 – Trilaminar structure of the valves. (**A**) The SL valves. (**B**) The atrioventricular valves. F – fibrosa; S – spongiosa; V – ventricularis; A – atrialis; CT – chordae tendineae. The arrows represent normal blood flow. (Figure adapted from Combs et al.[7])

The fibrosa is located on the outflow surface of the valve. It is the main load-bearing layer, and it dominates the valve's mechanical response.[2, 8] It is mainly composed of circumferentially arranged collagen fibres aligned relatively parallel to the free edge. The collagen fibre bundles attach to the heart wall near the commissures and blend with the annular collagen in order to assist in load transfer.[4] In healthy valves, the majority of the collagen is type I, which possesses high tensile strength.[2]

The spongiosa is located in the middle of the valve. It provides lubrication between the layers, flexibility, and dampens compressive forces during diastole.[9, 10] It is mainly filled with proteoglycans (PGs) that bind water, and a loosely arranged network of collagen and elastin fibres that mechanically link the inflow and outflow surfaces.[2, 4]

The ventricularis is located on the inflow side of SL valves and adjacent to the fibrosa in atrioventricular valves. It is composed mostly of elastin with some collagen fibres primarily oriented in the radial direction. The elastin dominates the mechanical response in the radial direction, maintains collagen fiber alignment, and allows collagen to quickly recoil.[11] The atrioventricular valves contain an additional layer called the atrialis, though it is often considered along with the spongiosa. It is has a similar composition and function to the ventricularis.[4, 12]

VECs are arranged in a single layer on the surface of the heart valves. VECs have been shown to be a distinct subtype of endothelial cell, in large part due to their different responses to shear.[13] Their main functions are to maintain non-thrombogenicity and are likely involved in signal transduction to VICs.[14]

VICs are interspersed throughout the leaflet structure. Their main function is to maintain and remodel the extracellular matrix (ECM). Further details can be found below (see Section 1.2.3).

1.2.3 VICs

There are multiple VIC phenotypes that have been proposed, three of which are commonly agreed upon – quiescent, activated, and osteoblastic VICs. Each phenotype has been shown to have different properties and functions. One of the most interesting aspects of VIC function is that their phenotype is plastic and reversible so as to change in order to meet changing physiological demands.[15]

Quiescent VICs (qVICs) are the normal VIC phenotype. They maintain the ECM and inhibit angiogenesis.[9] They make up the majority of VICs in healthy adult valves.

Activated VICs (aVICs) are associated with valve remodelling. They are connected with increased production of structural ECM proteins, such as collagen, remodelling enzymes, such as matrix metalloproteinases (MMPs) and tissue inhibitors of matrix metalloproteinases (TIMPs), and growth factors, such as transforming growth factor-beta (TGF-β).[9] They are commonly identified by the presence of alpha-smooth muscle actin (α-SMA), a contractile actin isoform that can be found in the cytoskeleton. Increased α-SMA expression levels have been shown in developing, diseased, and remodelling valve tissues.[15] aVICs are occasionally referred to as myofibroblasts because of their activated state (and qVICs as fibroblasts), however this is considered by many researchers to be an outdated term because the VIC population has distinct features, such as different proliferation and adhesion properties.[9]

Osteoblastic VICs (obVICs) are associated with calcification and hardening of leaflets. They are linked with increased chondrogenic and osteogenic proteins, such as osteopontin, osteocalcein, bone sialoproteins, and alkaline phosphatase.[9, 16] They are often identified by their expression of osteopontin.

One of the most interesting features of VICs is that their phenotype is plastic and reversible. Phenotypic expression profiles change during embryological development, postnatal development, and maturation, as well as in disease and injury response.[15, 17] VICs can become activated or revert to quiescence based on the needs of the valve, suggesting that they will respond and/ or normalize in order to restore a normal stress profile.[15] For example, aVIC expression is significantly higher during fetal development than during adulthood, and is higher in calcified adult valves compared to healthy adult

valves.[16, 17] Healthy adult valves contain mainly qVICs and some aVICs, but the specific proportions reported are variable and depend on the experimental model. The aVIC population has been reported to be less than 10% in normal human adult valves and ranging between 50-90% in isolated VIC culture conditions.[15] Further details of VIC mechanoresponsiveness can be found below (see Section 1.5.1).

1.2.4   Valve Origins and Development

Human heart development begins in the third week of pregnancy. At this point, the early heart is a tube filled with cardiac jelly, a gelatinous, non-cellular substance, that loops upon itself as it rapidly grows.[18, 19] There are several transition zones along the heart tube that further develop into additional cardiac structures, including the valves, and primitive chambers that mature into atria and ventricles.[19] Valve development begins in the fourth week of pregnancy when the cardiac cushions appear. Formation of the cardiac cushions is characterized by cellular migration and transformation. The overlying endothelial cells invade the cushions and begin to proliferate.[9] During this process, the cells undergo endothelial-to-mesenchymal transformation, becoming VICs.[9, 18] As the cushions grow, they begin to protrude into the heart tube and ECM deposition and remodelling begins.[7] From this point, they act to prevent blood backflow.[7] The details surrounding early valve development, however, remain poorly understood.

The first two valves to develop are the MV and TV (atrioventricular inflow valves) along with the ventricles. The AV and PV (SL valves) develop later with the outflow tract. In contrast to the atrioventricular valves, the SL valves also contain neural crest cells, in addition to local VICs. The neural crest cells immigrate to and become incorporated within the SL valves as well as the myocardium.[19] Their presence is required for normal valve development and aorticopulmonary septation, but their exact role in heart development remains disputed.

By the eighth week of pregnancy, the immature valves have formed, however they still do not have the distinct trilaminar structure that is a characteristic of adult valves. During protrusion, the valves are composed mostly of VICs with some PGs and collagen, and there is no stratification. By birth, the valves have gone from a bilaminar

structure containing the initial ECM to an incomplete trilaminar structure also containing elastin, although the ECM remains relatively unorganized.[17, 20] The trilaminar structure continues to develop after birth and is fully developed upon reaching adulthood.[17, 20]

1.3   Connexins

1.3.1   Adhesion Molecules, Connexin Structure and Function

VICs are connected to the ECM and one another via integrins, cadherins, and gap junctions (GJs). Integrins provide strong attachments between the cell and the ECM, whereas cadherins provide strong attachments between cells. Both of these attachment types, cell-ECM and cell-cell, link to the cell's cytoskeleton and have been implicated in signalling pathways.[21, 22] GJs are channels between joined cells that allow for the rapid and direct exchange of small molecules, such as inorganic ions (e.g. calcium, potassium, chloride), secondary messengers (e.g. cyclic adenosine monophosphate, inositol triphosphate), and other small molecules (e.g. amino acids).[23] These attachment components are often found in close proximity to each other in the cell membrane, and are thought to have reciprocal relationships and potentially integrated pathways.[24]

Gap junctions (GJs) are formed when two connexon hemi-channels from neighbouring cells combine. (**Figure 5**) Connexons are formed from six connexin proteins. Each connexin protein is composed of four transmembrane regions that are connected to each other by extracellular and cytoplasmic loops. Both the nitrogen and carboxy terminus (N- and C-terminus, respectively) are located in the cytoplasm. The majority of difference between connexin isoforms is due to variations in the C-terminus. Connexins are often identified by their weight, for example, connexin 43 (Cx43) has a molecular weight of 43 kDa. Whether GJs are open or closed is dependent upon and regulated by many factors, including transjunction potential, phosphorylation, and the presence of mechanical stimuli.[25]

Twenty-one types of connexins have been identified in humans. They are found throughout the human body, and Cx43 is the most ubiquitous.[24] They have a relatively

short half-life ranging between 1-5 hours.[26] They are found throughout the cell membrane, and are generally docked to connexins in neighbouring cells to form GJs. GJ clusters are often found at intercellular attachments sites, such as at the end of cellular projections (e.g. tendons) or at intercalated discs (i.e. heart). They may also be found independently, although they likely remain non-functional until multiple GJs cluster.[26] Connexin degradation may occur by annular junction formation, in which a portion of a cell membrane is phagocytised by the contacting cell, or by degradation within endosomes or lysosomes.[26]

Different yet often overlapping functions and properties of connexins are provided through two main means. Tissues often express multiple connexin isotypes in addition to variations in connexon components (i.e. homomeric or heteromeric) and channel formation (i.e. homotypic or heterotypic). This allows for a wider range of properties than homogenous formation would provide. These 'tunable' channels may have some functional overlap, and they largely work in concert with each other, but often cannot fully replace the function of an absent isoform.[24, 27] This explains why connexin knockouts and mutations frequently result in serious negative effects. For example, Cx43 knockout mice die at birth due to congenital cardiac abnormalities, and Cx43 mutation in humans is associated with oculodentodigital dysplasia, a genetic syndrome with ranging severity that primarily affects the eyes, teeth, and fingers.[24]
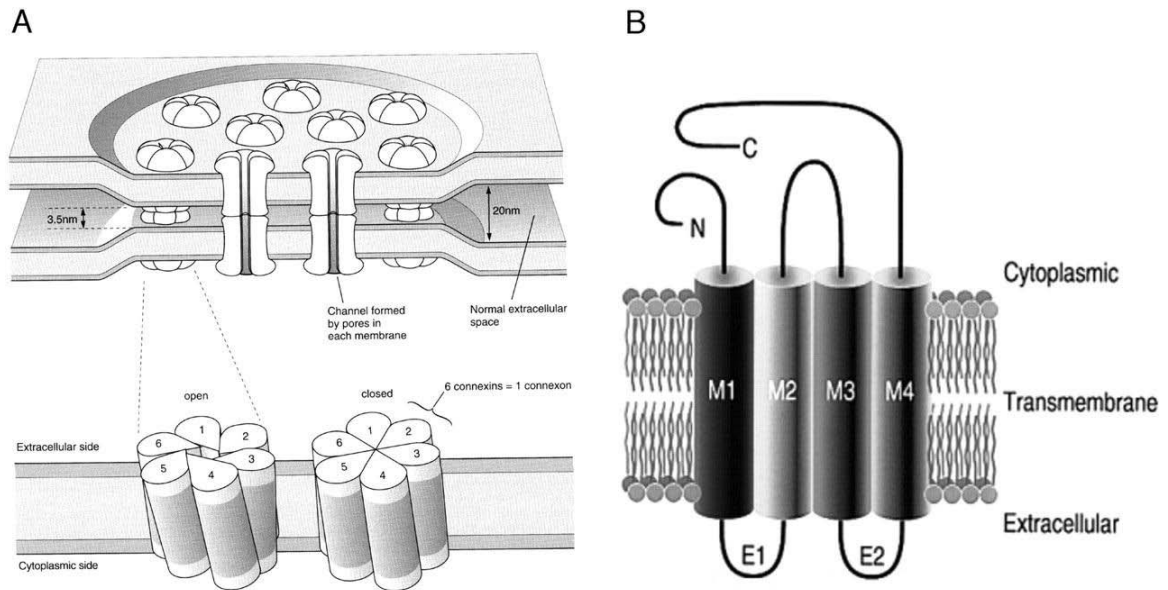
Figure 5 – GJ structures. (**A**) GJ channels are formed from two connexon hemichannels on closely apposed cells. Each connexon is formed from six connexins. (**B**) The connexin protein is composed of four transmembrane domains, two extracellular loops, and one cytoplasmic loop. The C-terminus is the most variable part of the structure among the different isotypes. (Figure adapted from Sohl et al.[28])

1.3.2   Connexins in Heart Valves

Two types of connexins have been identified in VICs, Cx43 and Cx26. Cx45 has also been identified, but in very low amounts.[21] Latif et al. found connexins dispersed throughout valve tissue and higher expression levels on the inflow side of the valves.[21] This suggests that VICs are connected through an intercellular network that may allow for communication and integrated responses to stimuli, such as mechanical stretch.

Cx43 is found in many tissues in the body and throughout the heart, including the valves.[21, 24] Its function is considered to be mainly regulated by phosphorylation, and there are 12 known sites for phosphorylation located on the C-terminus.[26] The initiation and downstream events of Cx43 phosphorylation remain poorly understood, and it is speculated that each connexin is regulated differently which complicates the elucidation of a mechanism.

Unlike Cx43, Cx26 is found in only a few tissues other than the heart valves, such as the skin, blood vessels, liver, and uterus.[23, 29-31] Cx26's regulation is not well understood, in large part because it is the only connexin that is not phosphorylated – likely due to its short C-terminus.

To date, Wang et al. have been the only group to study the link between connexin expression and mechanical conditions in VICs in heart valves.[32] In their study, hypercholesterolemic rabbits were shown to have increased Cx43 expression after three weeks compared to healthy rabbits, suggesting that intracellular communication was affected. Hypercholesterolemia induces leaflet thickening, inflammation, and calcification, which leads to alteration of the mechanical loading profile because of increased stiffness.[16, 32] Macrophages were also present, which have been associated with the inflammatory response and calcification.[16] It must be taken into consideration, however, that the observed effects on Cx43 may have been due to the presence of cholesterol or macrophages and not solely attributed to the altered mechanical conditions that arose from their presence. In fact, it may be a combination of these factors.

An increase in connexin expression in heart valves due to altered mechanical stretch may provide a protective remodelling response, based on their roles in other tissues (see Section 1.3.3). Increased connexin expression may more efficiently modulate the ECM structure to an appropriate stiffness in the various regions of the leaflets through coordination of VIC phenotype changes and biochemical signals. It may also offer a protective remodelling response to the VICs themselves by alteration of their cytoskeleton to be able to better withstand the 'new' mechanical environment.

1.3.3   Connexins in Other Soft Tissues

Connexins in other soft tissues were examined due to the limited data available for VICs in heart valves. Connexins in other soft tissues have been found to be required for proper tissue development, function, and remodelling. Their tunable channels allow for selectivity in the small signalling molecules they allow to rapidly exchange between cells. Importantly, this allows for specific and synchronous multicellular responses that can either be contained regionally or spread quickly throughout the tissue. Increases in

12

connexin expression have been associated with the onset and/ or rapid propagation of electrical impulses throughout tissues (i.e. heart, uterus), and quicker – although not necessarily better – remodelling or wound repair responses (i.e. blood vessels, tendons, skin), This suggests that connexins may have a role in VIC phenotype plasticity, which has been linked to the remodelling needs of the valve.[15] Connexin responses to mechanical stimulation in other soft tissues may offer insight into their responses in VICs, although connexin expression is regulated cell- and tissue-specifically.[29]

The focus in each of these sections is largely on Cx43 because of its ubiquity in the human body, however, Cx26 and other connexins are referred to when considered appropriate. In general, Cx43 expression is stretch sensitive and Cx26 expression is stretch insensitive, demonstrating that they are regulated differently.

1.3.3.1   *Heart*

The main connexin found in the myocardium of the heart is Cx43. Other connexins found in the heart include Cx40 and Cx45. Cx43 has been found to be required for proper impulse conduction and normal development and formation.[1] Experiments investigating acute responses have shown that increased Cx43 expression can be induced with mechanical stretch, which is thought to be associated with electrical and mechanical remodelling.[33, 34] Chronic pathological conditions generally show an overall decrease in Cx43 expression, with no discernible differences based on how the condition developed or its severity.[35, 36]

1.3.3.2   *Blood Vessels*

The main connexins found in smooth muscle cells in vascular walls are Cx43 and Cx26, and low levels of Cx37 and Cx40 are also present. Smooth muscle cells are mostly responsible for remodelling responses. Cowan et al. found that Cx26 was stretch insensitive, and that Cx43 was sensitive to static stretch.[30] Vascular Cx43 expression increases with increased forces due to changes in hemodynamic or mechanical

conditions, but the responses can be variable depending on the experimental model and vascular territory studied.[27, 37] For example, Cx43 expression increased in Cowan's model using cultured smooth muscle cells and static stretch, while both increased and decreased levels of Cx43 expression have been reported in hypertensive rats.[30, 37] In general, increased expression has been attributed to chronic remodelling due to prolonged increases of mechanical loads.

1.3.3.3   *Uterus*

The main connexins found in the myometrium of the uterus are Cx26, Cx32, and Cx43. Cx43 is thought to contribute to the electrical coupling between cells during labour. Its expression levels are normally low, and rise dramatically before the onset of labour.[38] The function of Cx26 is still currently unknown, but it is thought to be involved in maintaining the normal quiescent state. Its expression levels are highest during late pregnancy, and fall to low levels during labour.[38] The combination of stretch and progesterone were required for increased Cx43 expression. Cx26 was stretch insensitive, and required more complex conditions for elevation.[38]

1.3.3.4   *Tendons and Ligaments*

The main connexins found in tendons and ligaments are Cx32 and Cx43.[39, 40] These dense soft connective tissues are mainly composed of highly organized ECM, mostly collagen, and relatively few cells. The cells are usually spindle shaped (long and thin), with long projections in both the radial and longitudinal directions.[40] In tendons, Cx43 is found in both directions, and Cx32 is located only longitudinally.[39] Both connexins were found to be mechanically sensitive, and decreased GJs in these tissues have been implicated with decreased collagen production and decreased cell responses with the lack of integration of intercellular communication. [41-43]

1.3.3.5   *Skin*

The main connexins found in the dermis and epidermis of the skin are Cx26, Cx30, and Cx43.[31] Connexin expression is typically low immediately after a skin wound. This is thought to help facilitate cellular migration.[44] In contrast, the early healing response of Cx26 and Cx30 shows increased expression. Their functions are unknown, but they are thought to be involved in the regulation of cell proliferation, differentiation, and migration.[31] Cx43 appears to have a more complex role in the healing response. Initially, it is usually low, and transient inhibition has been shown to promote a positive healing response. This includes increased cell proliferation and migration, reduced inflammation and scarring, and more rapid wound closure. In contrast, chronic inhibition (greater than 7 days) has been shown to interfere with healing and normal homeostasis.[31]

1.4   Biomechanics of the Heart Valves

1.4.1   Mechanical Environment

Heart valves experience a number of forces over their cardiac cycle. Valves in this complex mechanical environment experience shear, bending, pressure, and stretch, and opposite sides of the valves experience very different environments. An overview of these forces can be found in **Figure 6**.

Shear is experienced while the valves are open. The ventricular and atrial inflow surfaces of the leaflets experience laminar shear as blood flows past them. The fibrotic outflow surfaces experience oscillatory shear from the pooling of blood. When the valve is closed, it also experiences shear as the blood pools in the sinuses. Shear mostly affects VECs as they are at the surface, but they have been shown to modulate VIC responses within the interior of the valve tissue.[45]

Bending stresses occur as the valves move between their open and closed positions. The curvature of the leaflets, especially in the belly, change during these movements. This bending stress induces tension on the ventricular and atrial inflow

15

surfaces and compression on the fibrotic outflow side with the base of the leaflets acting as a hinge. Elastin in the ventricularis and atrialis allows for further extension and flex of the inflow surface compared to the fibrotic outflow layer where high tensile strength collagen predominates.
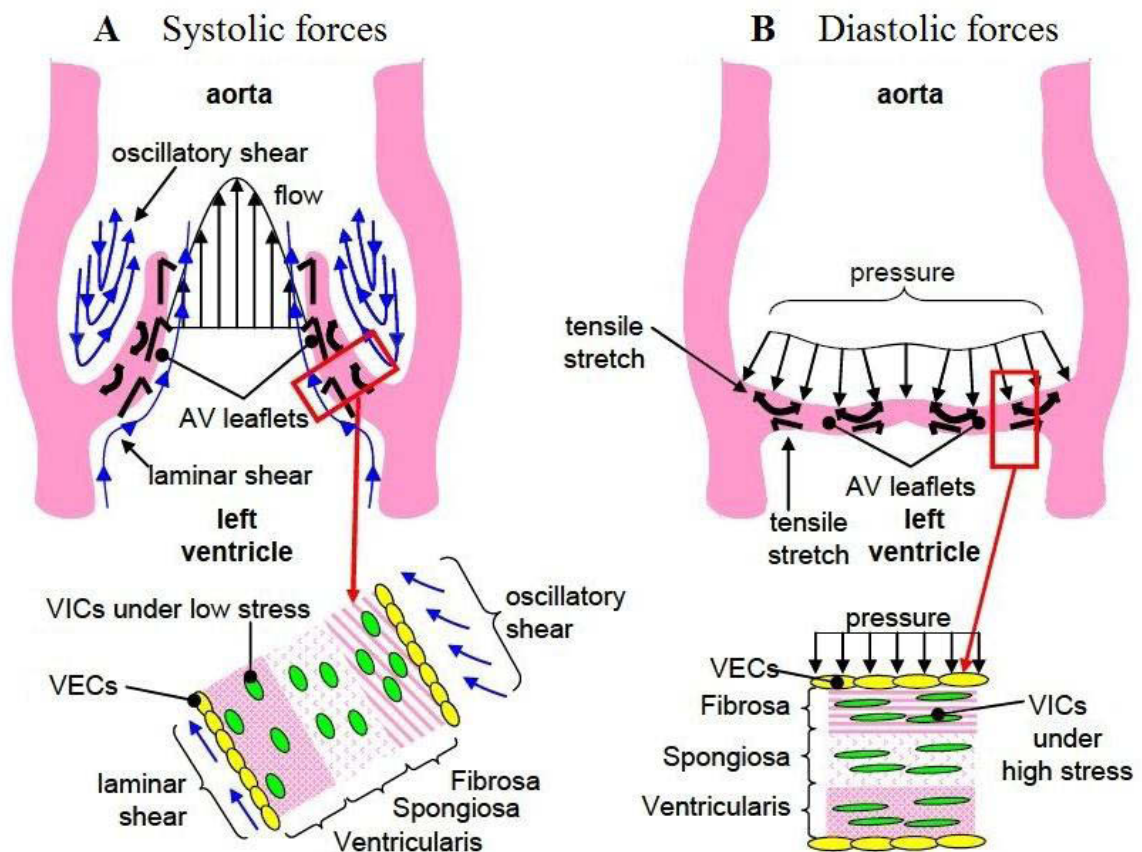
Figure 6 – An overview of mechanical forces along and within the leaflets, as demonstrated on the AV. The orientation of ECM and VICs change in response to these forces. (**A**) The AV is open during systole. Open valves experience shear. Valves undergo bending stress as they move between the open and closed positions. (**B**) The AV is closed during diastole. Closed valves experience tension as they stretch to coapt and pressure is exerted by the blood. (Figure adapted from Balachandran[46])

The transvalvular pressure (TVP) gradient the leaflets experience varies over the course of the cardiac cycle, and the maximum is reached when the valves are closed. In a healthy human adult, the maximum TVP in the PV is 10 mmHg, 25 mmHg for the TV, 80 mmHg for the AV, and 120 mmHg for the MV.[47] This force is mainly supported by collagen in the fibrosa.

The TVP across the valve induces stress within the leaflets. Stress is generally not used in normalizing the forces applied to heart valves due to the leaflet thickness being non-uniform and difficult to measure. However, membrane tension can be calculated via the Law of Laplace:

$$T = \frac{\Delta P \cdot r}{2}$$

Where T is tension, P is the TVP, and r is the radius of curvature, assuming the valve is closed and spherical. r is assumed to be 10 mm for the AV and PV, and 13.4 mm for the MV.[48, 49] This yields units of force per unit length (N/m), with calculated values close to literature values. The maximum tension values found in the literature for each of the valves are 8 N/m for the PV, 18 N/m for the TV, 60 N/m for the AV, and 90 N/m for the MV.[50, 51]

Tensile stretch of the leaflets is greatest during valve closure. The valves extend in both the radial and circumferential directions so that the free edges can coapt and form a tight seal through which blood cannot regurgitate. Valve leaflets experience approximately 30% stretch in the radial direction and 10% stretch in the circumferential direction.[2] There is less stretch in the circumferential direction due to the orientation of the strong collagen fibres, and greater stretch in the radial direction due to the orientation of the extensible elastin fibres and the splay between collagen fibres.[2, 11]

Valve leaflets display anisotropic, non-linear, and viscoelastic biomechanical properties. Anisotropy refers to material properties of the leaflets being directionally dependent with different mechanical responses observed in the circumferential and radial directions. These responses are non-linear because the slope of the stress-strain curve increases with increasing strain.[11] (**Figure 7**)

Soft tissues, including heart valves, are viscoelastic.[52] A viscous material will flow with the application of force, but does not return to its original state upon force

removal. An elastic material deforms proportionally with the application of force, and returns instantly to its original state upon force removal. This linear relationship specifies that stress is directly proportional to strain. Heart valves are considered viscoelastic because they exhibit properties of both viscous and elastic materials, and their stress-strain behaviour is time dependent. As such, viscoelastic responses can include creep, stress relaxation, or hysteresis. Hysteresis is the dissipation of energy between loading and unloading.[52] Creep is the gradual increase in strain under sustained stress. Stress relaxation is the gradual decrease in stress under sustained strain. (**Figure 7**) Grashow et al. suggests that valves are quasi-elastic, not viscoelastic, because they display stress relaxation but not creep.[50] This seems unlikely because the two concepts have been shown for other soft tissues, and early data from Pierlot et al. shows that valve material does indeed display creep.[52, 53]
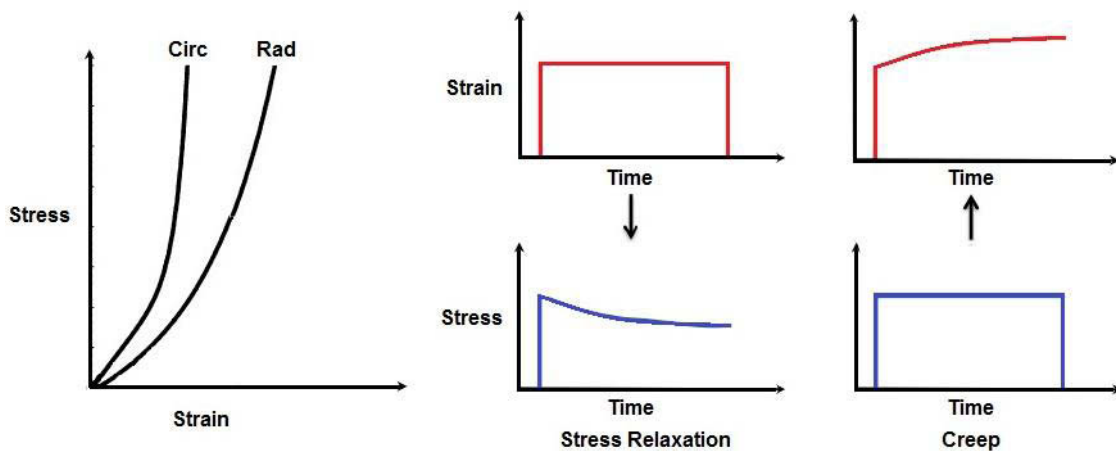
Figure 7 – Graphical representations of anisotropy and non-linearity, stress relaxation, and creep.

1.4.2   Mechanotransduction

The process by which mechanical forces are detected by cells and in turn transformed into biochemical signals is referred to as mechanotransduction. Tensegrity, a concept proposed by Ingber,[54] is a popular and well-supported theory proposed to unify many small pieces of data into an integrated and complex model for mechanotransduction. He suggests that the process occurs based on complex bidirectional pathways that are used to produce a concerted response through pre-stressed hierarchical networks in order to transfer and specifically focus stresses.[54] The tensegrity model is based on interactions between the architecture of the organ, the cell structure, and mechanosensitive molecules.[54] Many different components have been implicated in this response, including cell-cell adhesions, cell-ECM adhesions, the ECM, and the cellular cytoskeleton, membrane, and nucleus.[54] The absence of slack and pre-stress in the system allows for an immediate response to change to be transmitted throughout the hierarchical components. The interconnected networks balance forces among one another, so changes occur at multiple scales simultaneously in order to restore order after mechanical perturbations.

VIC nuclei in the heart valve leaflet have been shown to deform under loading.[55] Deformation of the nuclei occurs concurrently with collagen straightening and compaction which strongly indicates that there is a tight and direct connection between the cell and the ECM. (**Figure 8**) TEM images showing close association between VICs and collagen, the ability of VICs to produce force, and the elucidation of the specific VIC integrins which are known to bind to collagen all support this concept of integration.[22, 55, 56] Together, these points suggest that the tensegrity model of mechanotransduction can be applied to VICs within heart valve leaflet tissue.
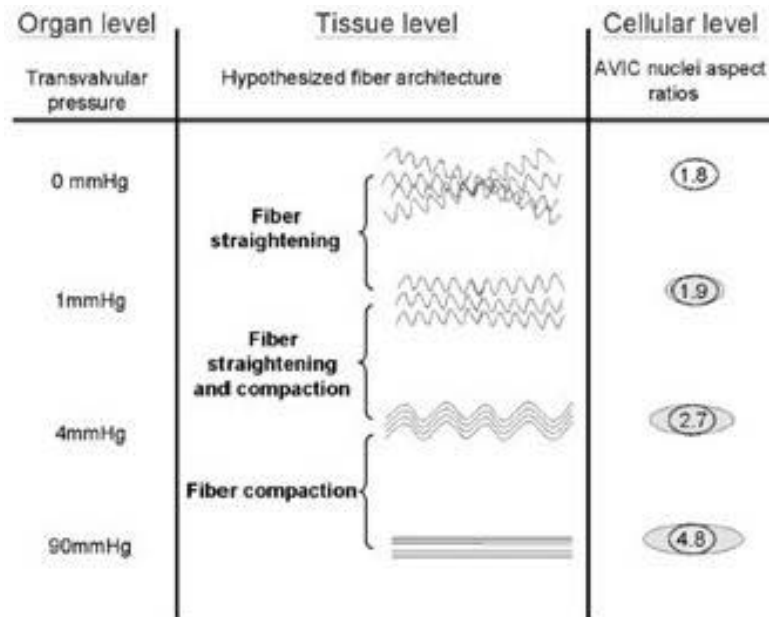
Figure 8 – The effects of TVP on aortic VIC nuclear aspect ratios and the concurrent effects on valvular collagen. (Figure adapted from Huang et al.[55])
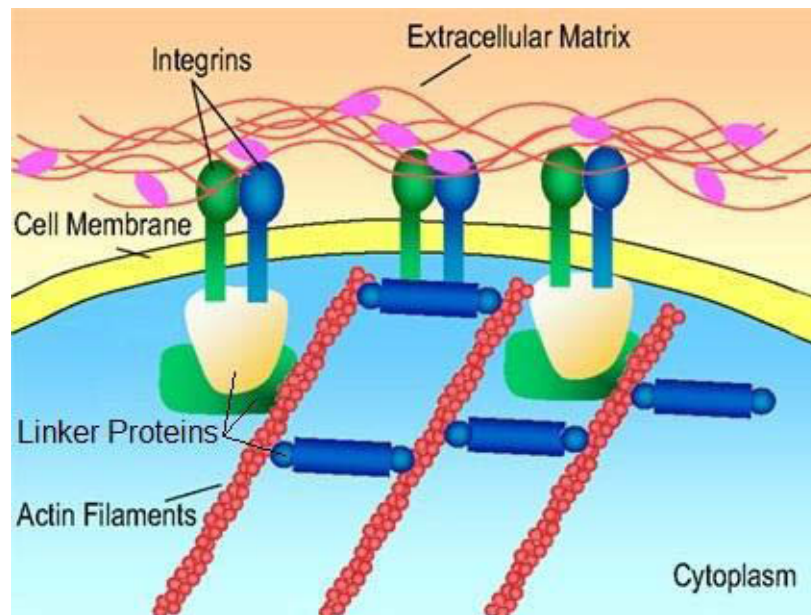
Figure 9 – Components connecting the cell and ECM. (Figure adapted from Rao et al.[58])

VICs are strongly bound to collagen in the ECM via membrane-bound integrins. The most common integrins found in VICs are α2β1 and α3β1.[22] The strength of the association is based on the formation of focal adhesions (FAs). FAs are formed from a cluster of integrins, and in general, their size increases with force.[57] Integrins also provide intracellular connections. In the cytosol, integrins are associated with actin microfilaments through linking proteins (e.g. talin, vinculin, and α-actinin), and by extension with the cytoskeleton and the nucleus.[22] (**Figure 9**) Actin is one of the main cytoskeletal proteins that form an interconnected scaffold within the cell in order to provide structure and shape, and the cytoskeleton is further integrated with the cell membrane and nucleus. Due to this integration, mechanical stimuli may be sent throughout the cell and stimulate many potentially mechanosensitive pathways.

VICs are tightly bound to each other through two types of adhesive junctions, the adherens junction N-cadherin and the desmosomal junction desmoglein.[21] These membrane-bound junctions provide strong cell-cell attachments, and also closely link their cytoskeletons. Linker molecules on their cytosolic membrane bind to actin microfilaments (adherens) and intermediate filaments (desmosomes), and have been implicated in transcription modulation.[21] Close association of adhesive junctions and GJs have been shown to occur both morphologically and temporally suggesting that they influence one another.[21, 59]

There are a number of response pathways proposed for connexins that form the GJs in VICs. Integrins are potential mechanotransducers of force to connexins. Integrins have been shown cause downstream modulation of connexins in response to stretch in myocytes, and the responses differed based on the matrix proteins upon which they were cultured.[33, 60] This suggests that changes in the ECM can affect changes in GJs via integrins. Connexins themselves may also be mechanosensitive. There are many proteins that become activated with changes in mechanical loading of the cell due to conformational changes that expose activation sites or open a channel for the passage of molecules because of movement of the membrane or the cytoskeleton.[54] This is a possibility because connexins are tightly integrated into the cell membrane, and it has been suggested that connexins in general, and Cx43 specifically, are attached to cytoskeletal microtubules and possibly actin.[41, 61] Banes et al. suggested that Cx43 in

tendon fibroblasts is associated with the actin cytoskeleton independently of integrins.[41] Another opinion is that connexins are modulated by mechanosensitive transcription factors present in the cell. Both of the previously listed mechanisms were shown to be possible based on work from Cowan et al.[30] They showed that Cx43 in blood vessels from rats increased with stretch independent of translation of other proteins, although their results could also be due to a mechanosensitive signalling cascade or transcription factor already present in the cell.

Currently, the exact signalling pathways for GJs are poorly understood. The simple linear pathways most often studied are confounded by bi-directional cross-talk, complex and integrated signalling cascades, and feedback loops. Some likely molecules that have been implicated in a number of studies include focal adhesion kinase (FAK), which is involved in integrin signalling, mitogen-activated protein kinase (MAPK), which has been implicated in both integrin and connexin signalling, and c-Fos, which is involved in transcription regulation.[59, 61, 62]

1.5 Evidence of Valvular Remodelling

1.5.1 Induction of Changes

Current research has shown that valves will remodel based on changes in their mechanical environment, no matter how the change occurred. Interestingly, the mechanism that has been suggested for remodelling in valves is similar to the developmental changes that occur during valve formation and maturation.[17, 20] This remodelling process provides a positive and functional change in normal hearts. In diseased and injured valves, this response leads to changes that are compensatory but overall dysfunctional and detrimental. This may occur as a result of the constant cyclic loading of the valve. Any damage, whether congenital, acquired, or due to regular maintenance, may cause a long-lasting response as the tissue constantly adapts to its new structure or hemodynamics.[10]

1.5.1.1   *Mechanical Conditions*

Physiological changes may be induced by alterations in the biomechanical or hemodynamic environment. This can be observed during perinatal development, pregnancy, and the Ross procedure. During the fetal-to-neonatal transition, there is a relatively rapid change in blood pressure due to closure of the shunts that had served to bypass pulmonary circulation during fetal development.[63] Before birth, SL heart valves experience the same maximum TVP, 50 mmHg. After birth, the AV on the left side is under increased pressure, 70-80 mmHg, and the PV on the right side is under decreased pressure, 30 mmHg. Total collagen content remains the same in both valves, but the AV experiences increased remodelling compared to the PV. This is based on reduced collagen cross-linking stability in the AV as determined by the immature-to-mature collagen cross-link ratio and higher aVIC expression.[17, 63] Collagen content increases during fetal development with the gradual increase in systemic blood pressure, and then the collagen levels remain stable during postnatal maturation, although the fibres thicken and become more organized.[17, 64]

During pregnancy, blood volume and cardiac output increase.[65] Collagen becomes more stable in all of the valves, and valve thickness and collagen content increase in both SL valves.[65]

In the Ross procedure, a healthy low pressure PV replaces a damaged high pressure AV, and a prosthetic valve replaces the PV. This is an acute increase in load on the PV, from 10 N/m to 60 N/m. This 6-times increase is much higher than an increase due to hypertension (1.5-2 times higher), but AV and PV failure occur at nearly the same strain (1500 N/m for the AV) which is about a 25-times safety factor.[66-68] After placement, the PV autograft leaflets thicken due to increased collagen and cellularity, and VICs become activated.[15, 69, 70]

Investigations of VICs have also included their responses to different types of isolated mechanical stimuli, including shear, pressure, and stretch. These studies have shown that shear and pressure can maintain leaflet collagen, but not VIC phenotype.[71-73] Cyclic stretch has been shown to increase both leaflet collagen and aVIC expression levels in a load-dependent manner.[74-76] Compared to fresh tissues, unloaded tissues had

reduced aVIC expression, tissues that had been stretched at near-physiological levels had similar aVIC expression, and tissues that had been stretched at above-physiological levels had increased aVIC expression.[75-78] Two of these studies had similar methodologies and found an interesting difference in aVIC responses. Balachandran et al.[75] found increased aVIC content after 48 hours of isolated cyclic stretch, while Merryman et al.[77] found significant increases in aVICs after 2 weeks of isolated cyclic stretch or earlier if the tissue was in the presence of TGF-β. This suggests that cyclic stretch does affect VIC phenotype, but the extent to which it does remains inconclusive, and that phenotype regulation may be more complex.

1.5.1.2   *Pathological Conditions*

Pathological conditions are also known to induce change. They are most often observed with age, disease, or drugs.[10] Aging is often associated with stenosis (orifice narrowing), fibrosis (leaflet thickening), and myxomatous degeneration ('floppy' leaflets). Stenosis is often associated with calcification, and it is one of the most common causes for valve replacement.[16] The ongoing hardening of the leaflets eventually reduces leaflet motion and causes obstructed blood flow. Progression is often associated with inflammatory processes, including fibrosis and angiogenesis, and this state has been associated with many of the same risk factors as atherosclerosis.[10, 16] Investigation into the calcification process has shown the presence of aVICs, obVICs, ECM remodelling proteins, and osteogenic growth factors and cytokines, including TGF-β.[9, 10, 16, 79] Myxomatous degeneration is due to the inappropriate accumulation of PGs, and affected leaflets have increased extensibility, decreased stiffness, and disrupted collagen, which usually causes regurgitation.[80] The decreased leaflet stiffness causes the valves to improperly coapt and may also result in prolapse. This is most commonly observed in the MV.[10] Increased levels of aVICs and remodelling proteins, such as MMPs, have been shown.[10, 81, 82]

Diseases, such as rheumatic fever and endocarditis, can also cause valve inflammation leading to dysfunctional remodelling. Fibrosis is the most common alteration, and depending on the nature of the remodelling, the outcome may either be

stenosis or regurgitation.[10] Many of the known drug-induced valvulopathies are associated with serotonin receptors, and cause a plaque to form that leads to stenosis and/or regurgitation.[10]

These pathologies may not have initiated because of mechanical conditions, but remodelling still occurs, and the mechanical loading of the leaflets changes because the ECM structure and composition has been altered. The remodelling processes that change the stiffness of the ECM structure induce changes in VICs because they have shifted from their normal stretch set point. Increased ECM stiffness causes decreased stretch, and therefore the effective load that the cell senses is decreased because there is less deformation.

1.5.2 Valve Treatment Options

Currently, the only way to treat dysfunctional or diseased valves is through valve replacement.[16, 83] Three of the most common valve replacement types are mechanical, bioprosthetic, and homograft valves. They all provide treatment, however their lifetimes are limited, and they each have a specific set of drawbacks.[83] Mechanical valves require concurrent administration of anticoagulation drugs due to their thrombogenicity, and are more prone to infections than other alternatives. Bioprosthetic valves are treated porcine or bovine tissue. They degrade or fail quicker than mechanical valves and are prone to calcification, especially in children. Homograft valves are cryo-preserved human tissue and have similar characteristics as bioprosthetic valves, but their supply is very limited. Another surgical replacement option is the Ross procedure. This is a technically demanding surgery in which a healthy PV replaces a damaged AV, and a prosthetic valve replaces the PV. It is considered the procedure of choice for children and young adults, but its availability is limited due to the complexity of the surgical procedure.[84]

Tissue engineered heart valves (TEHVs) are considered a viable alternative for the future as they are expected to be able to grow, repair, and remodel for the lifetime of the patient without adverse effects.[83] Research has greatly advanced, but this remains an unrealized clinical concept.

1.5.3 Evidence for Differences in Remodelling: Environmental Conditioning or Embryological Origins?

Research on heart valves increasingly shows that they can be classified based on the environmental conditions they experience in vivo. The larger stresses experienced by the valves in the left side of the heart are associated with increased remodelling. For example, the changes in TVP during the fetal-to-neonatal transition for the AV and PV show differences in cell phenotype and ECM structure. aVIC content in neonates, which was similar during gestation, is higher in the AV and lower in the PV, before decreasing overall by childhood.[17] AV leaflets become thicker and contain more elastin.[17, 85] This adaptive response suggests that changes in mechanical conditions initiate the remodelling response, and once these changes have created a stable mechanical loading profile, there is a return of the VICs to quiescence and normal maintenance.[15]

This can also be seen in pulmonary autografts used in the Ross procedure. PV leaflets become thicker within a few months of the Ross procedure, due to increased collagen and cellularity.[69, 70, 86] aVIC expression is increased following implantation, and decreases with time to nearly baseline levels.[15, 70]

This load-modulated behaviour is further supported by collagen stability research. Collagen stability is lower in the AV compared to the PV as demonstrated by more immature cross-links.[63] Stability has also been shown to be inversely proportional to TVP based on decreasing denaturation temperatures and fewer mature cross-links (stability: $MV < AV < TV < PV$).[87] These studies suggest that valves in higher stress environments could be primed for increased remodelling or may accrue more damage. It may also indicate that their more open structure makes it easier to assemble new components during the repair and remodelling response.

Work on isolated and cultured VICs has also shown interesting left-right relationships. Aortic and pulmonary VICs have similar contractile behaviour, although aortic VICs are able to generate force significantly faster than pulmonary VICs.[88] VIC stiffness, aVIC expression, and collagen synthesis markers are higher in the AV and MV compared to the PV and TV.[88, 89] The differences in stiffness and contractility displayed by cells suggest that VICs are adapted to their imposed environmental stresses.

Interestingly, phenotype and cell structural proteins also show evidence for the effect of embryological origins. aVIC expression and collagen synthesis markers are higher in the valves on the left side of the heart in comparison to those on the right, but the levels were also higher in the SL valves (AV and PV) compared to their atrioventricular counterparts (MV and TV, respectively).[89] These differences were insignificant in both cells and tissues between the AV and MV, but were significant for the PV and TV. The results require additional study for confirmation, however they show that embryological origins may modulate the magnitude of VIC responses.

Additional evidence for the influence of origins comes from calcification potentials. VIC calcification potentials at basal levels and when supplemented with osteogenic media show that the high-pressure left side leaflet cells have greater activity than the right side, but also that the SL valves (AV and PV) have greater activity than their atrioventricular counterparts (MV and TV, respectively).[90]

This is further supported clinically. The AV and MV have higher failure rates than the PV and TV, and replacement due to failure occurs more often for the AV than the MV.[91, 92] Overall, these results strongly suggest that origins do influence VIC function, although it seems to be secondary to their environmental conditioning.

Chapter 2   Rationale

VICs maintain the ECM and have a variable phenotype. qVICs are responsible for normal maintenance, and aVICs are considered the remodelling phenotype because of their increased ECM turnover and enzyme production.[9] VIC responses have been investigated in vivo for normal growth and degenerative conditions[15] and through ex vivo isolated mechanical stimuli of shear,[71] pressure, [72, 73] and stretch.[75, 77] Some evidence seems to point to cyclic stretch as the primary VIC phenotype regulator because of relatively acute responses (48 hours) that have been observed,[75, 93] however contradictory evidence suggests that VIC phenotype changes do not become significant until after an extended period (2 weeks).[77]

GJ-mediated communication is required for appropriate and efficient remodelling responses in a number of different tissues. Very little research has been done on communication between VICs through studies of gap junctions and their components Cx43 and Cx26. A study by Wang et al. showed that induced sclerosis in a rabbit model increased Cx43 expression, and was associated with both VIC activation and macrophage infiltration.[32] There have been no studies to determine the effect of isolated cyclic stretch on VIC communication.

This study is focussed on testing heart valves with isolated cyclic stretch to try to provide additional understanding of VIC phenotype responses and provide new information on communication responses. The use of multiple valve types (AV, PV, and MV) also allows for comparisons between environmental conditions (low and high TVP) and embryological origins (with and without neural crest cells).

The ex vivo model is appropriate because it provides a reasonable representation of the physiological environment because the cells and ECM are maintained in their native configurations and attachments. It also allows for comparisons to studies with similar methodologies.

This study will provide a better understanding of remodelling pathways in order to better understand common degenerative processes and will have applications to TEHV fabrication.

Chapter 3 Hypotheses

Overall hypothesis: Tissue stresses affect VIC responses by altering phenotype and communication, and cell origins have a negligible impact on VIC responses. Specifically, increasing mechanical loads will change the VIC phenotype from quiescent to activated, and the number of gap junctions will increase. These responses will be greater in tissues from native high tension conditions.

Supporting hypotheses:

Phenotype and communication

1. Increased mechanical loading of heart valve tissues will result in increased production of gap junction protein Cx43 in VICs. Increased mechanical loading of heart valve tissues will not affect production of Cx26 in VICs.
2. Increased mechanical loading of heart valve tissues will result in VIC phenotype changes from qVICs to aVICs.
3. Increased mechanical loading of heart valve tissues will result in increased production of Cx43 in the aVIC phenotype compared to the qVIC phenotype.

Classification: embryological origins vs. environmental conditioning

4. Mechanical loading of heart valve tissues from native high tension (AV) conditions will result in higher levels of gap junction protein production and VIC phenotype changes compared to low tension (PV) conditions.
5. Mechanical loading of heart valve tissues which have cells originating from different embryological cushions [i.e. in outflow (AV, PV) versus inflow (MV)] will result in similar changes in the levels of gap junction protein production and VIC phenotype changes.

Chapter 4   Methods

The following sections detail the general experimental methods used for this study. Material, chemical, and instrument details can be found in Appendix A – Supply List. Solution details can be found in Appendix B – Solutions.

4.1   Mechanical Stimulation

Six fresh pig hearts (5-6 months) used for this study were collected from Oulton's Meats (Windsor, NS). One heart at a time was collected immediately after butchering, and gross excision of the valves (AV, MV, and PV) was performed on site. Upon removal, the valves were vigorously agitated and rinsed thrice with ice-cold, sterile PBS in individual sterilized jars. They were then transported in new sterilized jars containing ice-cold, sterile PBS with 1.5% ampicillin-streptomycin. Upon return to the laboratory, the valves were rinsed twice in PBS, once in DMEM containing 10% FBS and 1% ampicillin-streptomycin, and then the leaflets were excised using sterile technique.

Strips 5 mm wide were taken from the body of each of the leaflets (AV, MV, and PV) in the circumferential direction. (**Figure 10A**) The circumferential loading direction was chosen based on the architecture of the leaflets. Collagen fibre alignment is largely circumferentially oriented and is correlated with VIC deformation, therefore loads applied in this direction to the tissue should transfer to the ECM and VICs.[55] The AV and PV had one strip taken from each of the three leaflets whereas three strips were taken from the larger anterior leaflet of the MV. (**Figure 10B**) The designations of each leaflet strip undergoing different loading conditions were randomized for all valves. Circumferentially oriented samples of fresh tissue were also collected from the remaining leaflet for each valve after obtaining excised leaflet tissue strips for mechanical loading experiments. The leaflets were kept moist with DMEM containing 10% FBS and 1% ampicillin-streptomycin until tested.

A   **B**
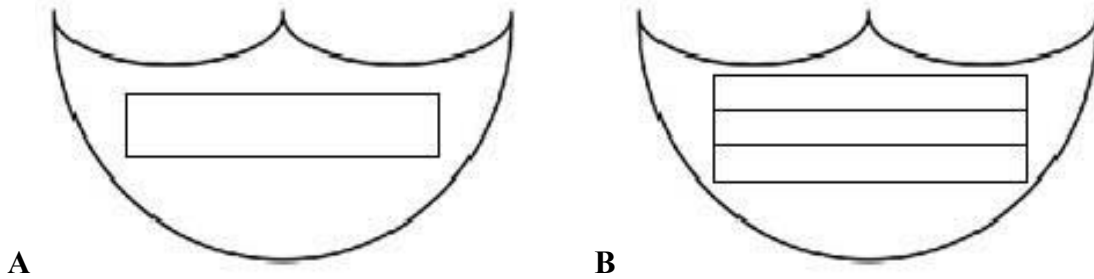
Figure 10 – Preparation of tissue strips from the valve leaflets. Samples were taken from the belly of the leaflet in the circumferential direction. **(A)** One strip was taken from each of the three AV and PV leaflets. **(B)** Three strips were taken from the larger anterior leaflet of the MV.

Valve leaflet strips in preparation for mechanical loading experiments were secured into the custom-made grips using a custom-designed gauge block to ensure a constant gauge length of 7 mm. (**Figure 11E-F**) After being secured into the grips, the lower and upper grips were placed with an alignment slide guide used to prevent tissue rotation during loading in order to avoid off-axis confounds. (**Figure 11G**) Finally, appropriate weights were added to the bottom grip corresponding to the desired membrane tension values at near-physiological levels (low load) and at 1.5-times higher levels (high load), as shown in **Table 1**. The high-load levels are representative of moderate in vivo hypertensive conditions.[66] In vivo tensions in the valves are due to pressures perpendicular to the leaflet surfaces. They can be calculated using the Law of Laplace, and have been confirmed experimentally for the AV and MV.[50, 51] The weights required for the desired experimental membrane tension values were calculated using the in vivo tensions and the width of the tissues, to take into account the 'perpendicular' force required to induce the appropriate membrane tension. The weights were so low for the near-physiological PV values that a larger difference of two times near-physiological tension between the 'low' and 'high' loads was thought to be required in order to potentially detect any differences. The applied weights used to achieve each desired tension also accounted for the opposing buoyant force of the media on the lower grip and weights when submerged. All of the loading apparatus components were made either of

31

stainless steel or polyethylene terephthalate (Dacron; lower grip for the PV) to allow for sterilization before use. (**Figure 11A-D**)

The grips and leaflet strips were then placed into one-use sterilized high-density polypropylene containers, and DMEM containing 10% FBS, 1% ampicillin-streptomycin, and 1% fungizone was added to a level that ensured the tissues would remain immersed. The tops of the polypropylene containers were then securely wrapped with sterile surgical cloth to prevent contamination after removal from the laminar flow hood and subsequent placement into the loading apparatus within a cell culture incubator. For unloaded controls, fresh tissue from each valve was placed in individual wells in a 6-well tissue culture plate. All tissues were placed in a cell culture incubator maintained at 37°C and 5% CO_2 for 48 hours with the mechanically stimulated samples attached to a custom-made apparatus designed to cyclically load the leaflet tissue at 1Hz. (**Figure 12**) The upper grip holding the samples was attached to a moving arm that cyclically raised and lowered the bottom grip and weight assembly, loading and unloading the samples.

After 48 hours, the incubated samples (unloaded and mechanically stimulated) were removed from the incubator and then cut into thirds. The middle sections of the tissue strips were prepared for immunohistochemical analysis, and the remaining two thirds of the tissues were utilized for reverse transcription and polymerase chain reaction (RT-PCR) analysis.
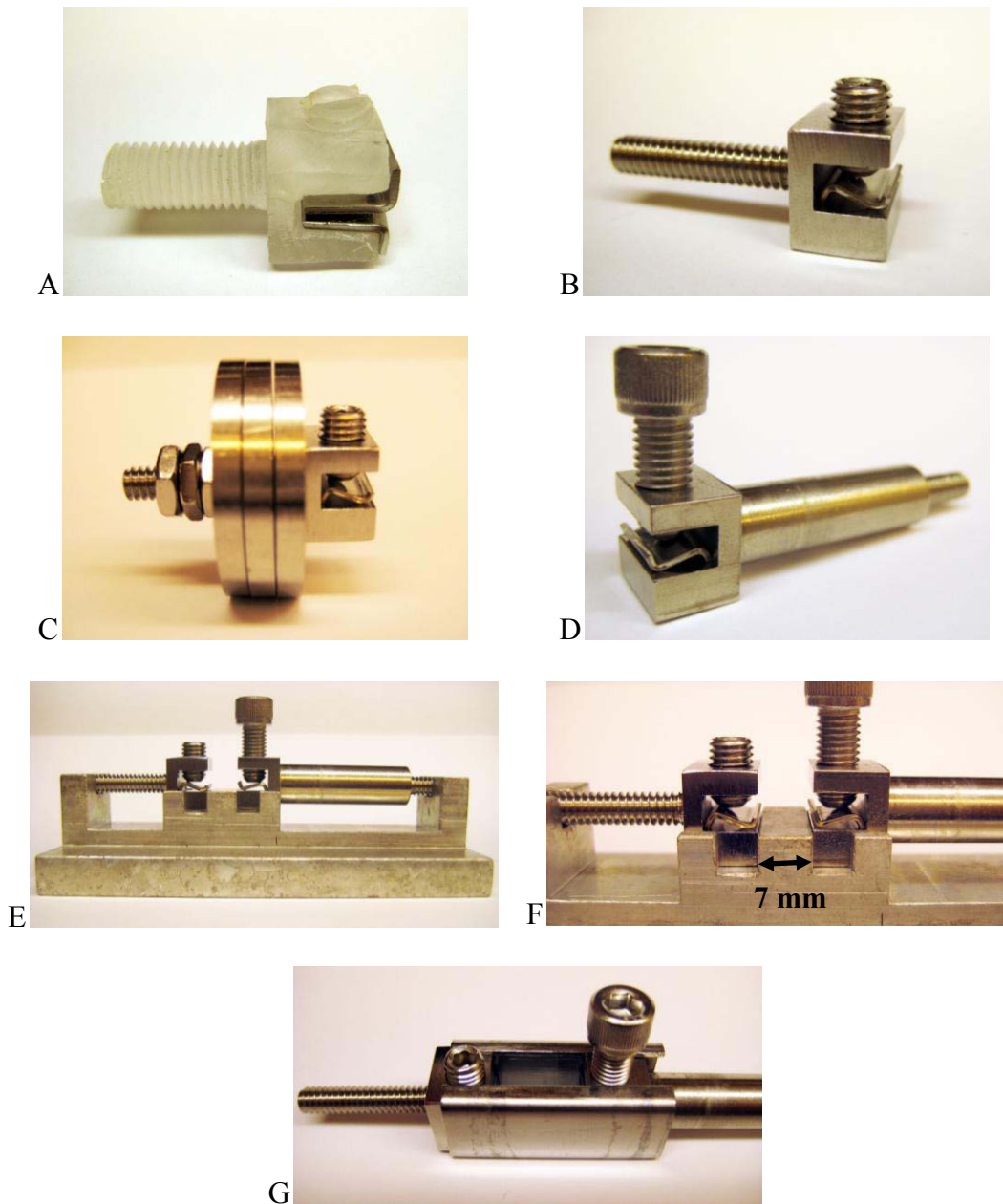
Figure 11 – Custom components designed for the mechanical stimulator. **(A)** The lower grip for the PVs made from Dacron. Tissue strips were held between the two textured, stainless steel flat plates. **(B)** The lower grip for the AV and MV. Tissue strips were clamped using an S-shaped stainless steel plate. **(C)** The lower grip showing the attachment of stainless steel weights and nuts. Various combinations were used to provide the required force for each leaflet. **(D)** The stationary upper grip. **(E)** An overview of grip components and attachments, and the gauge block used for ensuring consistent gauge length. **(F)** A close-up of the direct gripping region showing the 7 mm gauge length. **(G)** The upper and lower grip in the slide guide that was used to prevent tissue rotation.

Figure 12 – Inside view of the incubator showing the mechanical stimulation apparatus with samples in place. The upper grip holding the samples was attached to a moving arm that cyclically raised and lowered the bottom grip and weight assembly, loading and unloading the samples. Unloaded samples were maintained in separate wells in a culture plate shown on the bottom shelf.

Table 1 – Experimental tension values.

Valve	Low-Load (Near Physiological)		High-Load (1.5 x Physiological)	
	Membrane Tension (N/m)	Weight Required (g)	Membrane Tension (N/m)	Weight Required (g)
Aortic	60	30	90	45
Mitral	90	45	135	68
Pulmonary	8	4	16†	8

† For the high-load condition, the PV was subject to tensions corresponding to two times the physiological load.

4.2   Immunohistochemical Procedures

Samples for immunohistochemistry (IHC) were fixed in 10% neutral buffered formalin for three days, and then transferred to 70% ethanol before processing and paraffin embedding. Embedding was carried out by the Histology Research Services Laboratory at Dalhousie University. After embedding, the tissues were sectioned at 5 μm thickness, mounted on silinated slides, and dried at 57°C for a minimum of 12 hours.

Tissues were stained for various markers following the steps outlined in **Table 2**. Briefly, slides were deparaffinised and subjected to antigen retrieval using a pressure cooker. Endogenous peroxidases were blocked with hydrogen peroxide and protein block. The primary antibody was applied overnight, and the signal was amplified with the application of a biotin link, followed by streptavidin-horseradish peroxidase (HRP). Diaminobenzidine-HRP was applied for visualization, and then the slides were counterstained with Mayer's hematoxylin. They were dipped in Scott's water, dehydrated, and sealed with glass cover slips.

Optimal antibody concentrations were determined by applying graduated concentrations to continuous sections from the same tissue, and evaluated based on amount and intensity of staining. The Cx43antibody stained the protein in the cell membrane, and the α-SMA antibody stained the protein in the cytoskeleton. Since VIC phenotypes are on a spectrum because of their plasticity and reversibility, and qVICs do not present α-SMA, its presence was considered a marker for the activated phenotype.[15] Further details of the primary antibodies and their respective heat-induced epitope retrieval (HIER) buffers can be found in **Table 3**. All samples from one heart were stained simultaneously for each antibody, plus three additional slides for a negative control (no antibody), an isotype control, and a positive control (tissue was antibody-specific). Upon staining completion, randomly selected sections were digitally photographed at 400x magnification, and analyzed using a semi-quantitative method. Details of the semi-quantification methods can be found below (see Section 4.4.1).

Table 2 – Procedure for IHC staining. All solutions, except for HIER buffers, phosphate-buffered saline (PBS), and antibodies, were provided by the Histology Research Services Laboratory.

Solution	Time
Xylenes	5 minutes
Xylenes	5 minutes
Xylenes	5 minutes
100% Ethanol	2 minutes
100% Ethanol	2 minutes
100% Ethanol	2 minutes
95% Ethanol	2 minutes
95% Ethanol	2 minutes
70% Ethanol	2 minutes
70% Ethanol	2 minutes
Tap water	Brief rinse
Distilled water	3-5 minutes
PBS x 3	Brief rinses
HIER in antibody-dependant buffer	127°C peak temperature
2% hydrogen peroxide in PBS	10 minutes
PBS x 3	Brief rinses
Protein block	10 minutes
Primary antibodies	Overnight (~22 hours)
PBS x 3	Brief rinses + 5 minute soak
Biotinylated universal link	30 minutes
PBS x 3	Brief rinses + 5 minute soak
Streptavidin-HRP	30 minutes
PBS x 3	Brief rinses + 5 minute soak
Tap water	Brief rinse
Diaminobenzidine-HRP	7 minutes
Tap water	Brief rinse
Mayer's hematoxylin solution	2 minutes
Tap water	Brief rinse
Scott's water	Brief rinse (until samples turned blue)
Tap water	Brief rinse
70% Ethanol	20 dips
70% Ethanol	20 dips
95% Ethanol	20 dips
95% Ethanol	20 dips
100% Ethanol	20 dips
100% Ethanol	20 dips
100% Ethanol	20 dips
Xylenes	2 minutes
Xylenes	20 dips
Xylenes	20 dips

4.3   Reverse Transcription and Polymerase Chain Reactions

Samples for RT-PCR were maintained in RNAlater® at 4°C for three to seven days, and frozen at -80°C within seven days. RNA was extracted from heart valve tissues with RNeasy® Mini Kits. Directions of the manufacturer were followed. Each sample was first disrupted in cryogenic vials with a combination of 3 mm and 1 mm glass beads in 600 µL Buffer RLT® and 6 µL β-mercaptoethanol using a micro dismembrator. The lysate was separated by centrifugation, and an equal proportion of 70% ethanol was added to the supernatant to provide ideal binding conditions. The supernatant solution was then loaded onto the RNeasy® silica membrane. RNA bound to the membrane prior to being eluted and was washed three times to eliminate contaminants. Concentrated total RNA was then eluted into ribonuclease- (RNase) and deoxyribonuclease-free (DNase) water. The RNA samples were then frozen at -80°C, concentrated using a lyophilizing freeze dryer (-50°C), and stored at -80°C until analyzed using RT-PCR.

The concentration and quality of the RNA samples were measured using a spectrophotometer. Concentration was determined by measuring the absorbance at 260 nm (A_{260}). Quality was determined by the A_{260}/ A_{280} ratio, where 1.7-2.1 was considered acceptable.[94] The quality of the extracted RNA was also initially examined by looking for sharp bands on a 1% agarose gel during electrophoresis.

An appropriate amount of each RNA sample solution was taken such that 2 µg of total RNA was used for RT. The methodology and chemical components were from the SuperScript® III First-Strand Synthesis System. Each sample was denatured, annealed, and then incubated for complimentary DNA (cDNA) synthesis. The reaction was terminated, and any remaining RNA template was removed by digestion with RNase H. cDNA synthesis reaction products were stored at -80°C until PCR was performed. All samples from one heart were completed at the same.

After determining appropriate annealing temperatures and extension times for the primers, PCR optimization was completed by ensuring the process was continuing to amplify and had not reached a plateau. This was done by using the same starting cDNA material, annealing and extension parameters, and varying the numbers of cycles (18, 25, 30, and 35). The general PCR thermal cycling program can be found in **Table 4**, and

primer-specific details can be found in **Table 5**. The primers for Cx26 did not work, which was determined by testing a range of annealing temperatures.

PCR was done following the FastStart PCR MasterMix manufacturer's protocol. 2 μL of the cDNA solution, 2 μL each of the forward and reverse primers (12.5 μM), 25 μL MasterMix, 0.5 μL Taq DNA polymerase, and DNase- and RNase-free water were mixed for a total reaction volume of 50 μL. The primers were custom designed by Dr. Yong Wu against human DNA using BLAST® (GenBank®, National Center for Biotechnology Information). All samples from one heart were run at the same time for each primer. A negative control (no cDNA) was run concurrently to ensure there was no RNA or DNA contamination. Electrophoresis using agarose gels (1.5%) were then run to visualize expression levels. One valve per primer was run (e.g. Cx43: AV – Fresh, No, Low, High) with β-actin (i.e. β-actin: AV – Fresh, No, Low, High), in addition to a 100 bp ladder. The gel was then developed in TBE (Tris/ borate/ ethylenediaminetetraacetic acid) solution with ethidium bromide for 20 minutes to visualize the DNA, and then the gel was imaged under ultraviolet (UV) light. Band sizes were measured using densitometry as outline below (see Section 4.4.2).

Table 3 – IHC antibody details

Antibody	Dilution	Isotype Control	HIER Buffer
Cx43	1:200	IgG	Citrate buffer, pH 6
Cx26	1:50	IgG	Citrate buffer, pH 6
α-SMA	1:100	IgG2a	Tris-ethylenediaminetetraacetic acid (EDTA) buffer, pH 9

Table 4 – General PCR program. The lid temperature was 105°C to prevent evaporation.

Step	Temperature (°C)	Time (min:sec)
Activate	94	3:00
Denature*	94	00:15
Anneal*	Primer-specific	00:20
Extend*	72	Primer-specific
Final extension	72	10:00
Safety step	4	60:00

* Repeated 30 times.

Table 5 – Primer sequences and experimental parameters.

Primer	Sequence	Annealing Temp (°C)	Extension Time (s)
Cx43	F: 5'-TAG ACA GGT CTG AGT GCC TGA AC-3' R: 5'-AAG CGT ATT TTG GAG ATC CAC AGT C-3'	64	60
α-SMA	F: 5'-GTG GCT ATT CAG GCG GTG CTG-3' R: 5'-CTT CGT CGT ACT CCT GTT TGC TG-3'	62	40
β-Actin	F: 5'-GAC AAT GGC TCC GGC ATG TGC-3' R: 5'-CAT GAG GTA GTC GGT CAG GTC-3'	56	30

4.4   Image Analysis

4.4.1   Semi-quantification of Immunohistochemistry Images

Three to nine images of each stained leaflet tissue section prepared by IHC staining were taken at 400x magnification to enable, at minimum, at least 100 cell nuclei to be manually counted. The images were imported to Photoshop® and a colour correction process was conducted on the images to more easily differentiate between the blue nuclei and the brown positive antibody stain. The levels were balanced so that the 0-255 histogram covered the full spectrum range. Contrast and intensity were increased to the same level for all images. These processing steps maintained the image information, and were identical in order to allow for comparisons across multiple images.[95] These images were then opened in ImageJ© (National Institutes of Health, Maryland) and overlaid with a 100 μm^2 randomly-oriented point grid. (**Figure 13**) Nuclei were counted if they were under a cross point, and excluded if they contacted the edge of the image, irrespective of whether they were under a point. The total number of cell nuclei and the nuclei in positively stained cells were counted in order to give the percent positive expression. All observations were made blinded to tissue type and loading condition. The results for each leaflet tissue and mechanical loading condition were statistically analyzed as outlined below (see Section 4.5).

4.4.2   Densitometry of RT-PCR Gels

ImageJ© provides a dedicated macro to compute and plot a densitometric histogram of individual lanes on gels. Briefly, the images were contrast inverted, the lanes selected, and the peaks corresponding to the intensities of the bands of interest in the histogram were determined. The intensities of the bands of interest were normalized to the values of β-actin, which was used as a reference, or housekeeping, gene. The results for each leaflet tissue and mechanical loading condition were then analyzed using the statistical analyses outlined below (see Section 4.5).
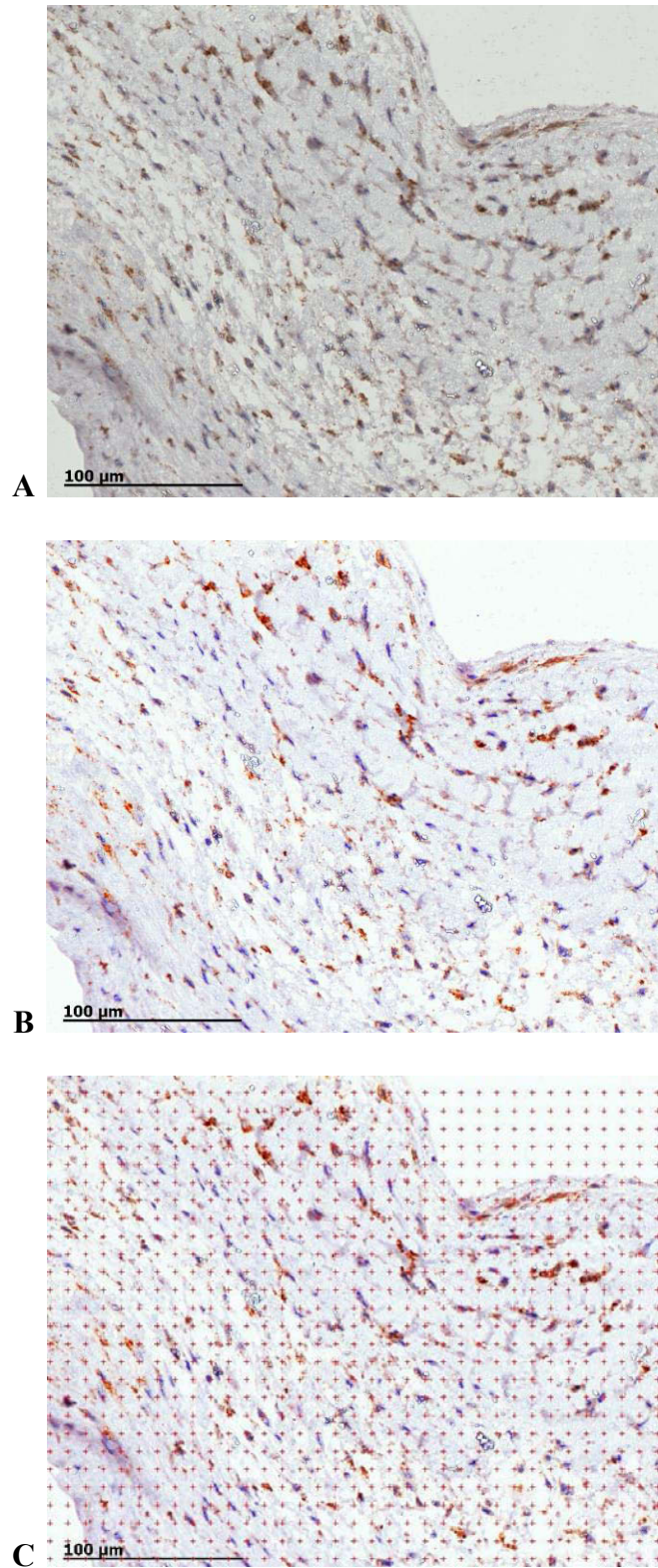
Figure 13 – Visualization of image processing steps on a 400x photo. **(A)** Original image. **(B)** Image after editing in Photoshop®. **(C)** Image with overlay of offset grid.

4.5   Statistical Methods

The experimental design of the study included the pairing of all valve types within each heart (AV, MV, PV), and tissue samples from each valve were exposed to each loading regime (fresh, no load, low load, and high load). This enabled data from all hearts to be pooled to look at inter-heart valve comparisons or separated to look at intra-heart valve comparisons, thereby reducing heart-to-heart variability and increasing statistical power. Initial comparisons were made using a two-way multivariate analysis of variance (MANOVA) with repeated measures to determine the significance of valve type and loading condition. Relationships were further investigated with a one-way MANOVA with repeated measures if the two-way MANOVA was significant and there were no interactions. Post-hoc comparisons for determining where significant differences lie were made using the Dunnett test for parametrically distributed data or the Dunn test for non-parametrically distributed data. Data distributions were determined using the Shapiro-Wilk test for normality. Differences were considered significant if the p-value ≤ 0.05. All tests were performed using JMP® version 9 (SAS Institute Inc., North Carolina). Data was expressed as mean $\pm$ standard error of the mean (SE).

Chapter 5   Results

The raw data for each component of the study can be found in Appendix C – Raw data.

5.1   α-SMA

5.1.1   RT-PCR

A two-way repeated-measure MANOVA on α-SMA expression was used to compare loading condition and valve type for the AV and PV. The effects of both valve type ($p = 0.22$) and loading condition ($p = 0.10$) were found to be not significant, and there was no interaction between valve type and loading condition ($p = 0.53$). A statistical analysis incorporating the MV data was not possible as expression levels were very low and required the use of different RT-PCR run conditions for detection. RT-PCR data can only be compared between samples that have been run under the same reaction conditions.[96] Based on this result, the MV was considered significantly different from both the AV and PV without statistical analysis because of the lack of detectable expression at a specified level that indicated expression in the PV and AV. There were measurable levels in the MV from two hearts, and one of the hearts had measureable levels for only two conditions. Each step of the RT-PCR process was performed simultaneously for the three valves of each heart, so it was concluded that this difference between hearts for the MV values of α-SMA was unlikely to be experimental variation. Large differences in gene expression levels were investigated by testing samples at increasing cycle numbers: 30 (comparison to other samples), 33, 36, and 39 cycles. These tests showed that MV tissues from the four remaining hearts had visible expression only at higher cycles, either 36 or 39 cycles (**Figure 14**), which corresponds to approximately 50-500 times lower expression compared to the AV and PV.

Gene expression levels for the AV are shown in **Figure 15**. When expressed relative to fresh tissue, unloaded tissues had 0.61 ± 0.16-fold expression, low-load tissues

had 0.24 ± 0.14-fold expression, and high-load tissues had 1.41 ± 0.78-fold expression (**Table 6**).

Gene expression levels for the PV are shown in **Figure 16**. Relative to fresh tissue, unloaded tissues had 0.97 ± 0.56-fold expression, low-load tissues had 0.99 ± 0.44-fold expression, and high-load tissues had 2.48 ± 0.91-fold expression (**Table 6**).

Gene expression levels of the valves for the unloaded, low load, and high load conditions expressed relative to their fresh tissues are shown in **Figure 17-Figure** 19. The MV was considered different from both the AV and PV because it had no expression at the level of detection of the other valve tissues.
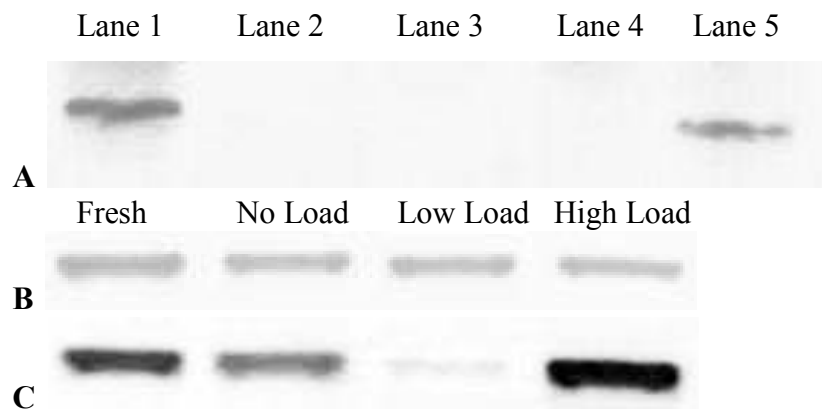
Figure 14 – Representative images of α-SMA RT-PCR gels. The contrast has been increased in these images for clarity between the bands and the background. **(A)** Image of a gel showing the results of cycle tests for α-SMA in the MV. Lane 1 shows a band for AV-Fresh at 30 cycles for comparison. No bands are visible for MV-Low in lanes 2-4 corresponding to 30, 33, and 36 cycles, respectively. An α-SMA band is visible only at 39 cycles in lane 5. **(B)** The housekeeping gene, β-actin, remained unchanged across all loading conditions. **(C)** α-SMA bands at 30 cycles for each loading condition for an AV sample are shown for comparison.
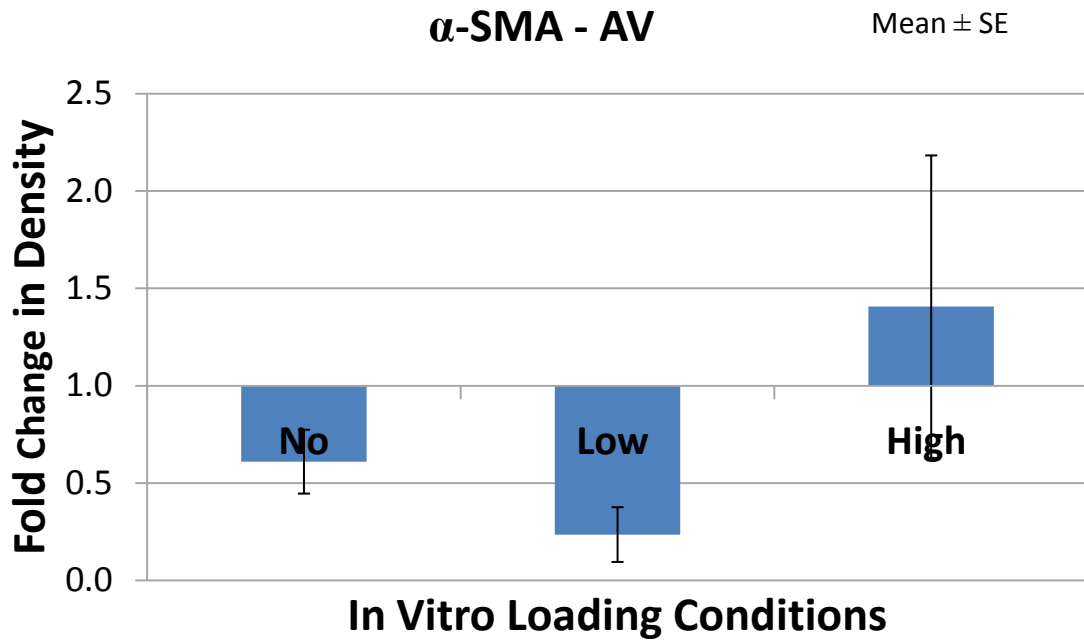
Figure 15 – Average α-SMA expression of the AV for each loading condition expressed relative to the fresh condition. (n = 6)
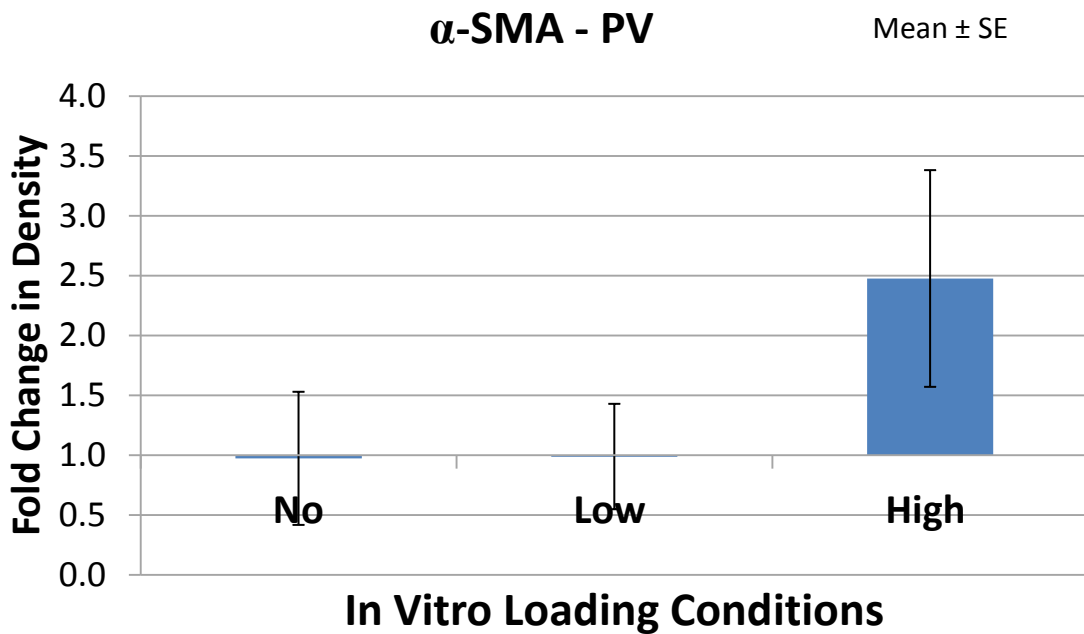
Figure 16 – Average α-SMA expression of the PV for each loading condition expressed relative to the fresh condition. (n = 5)
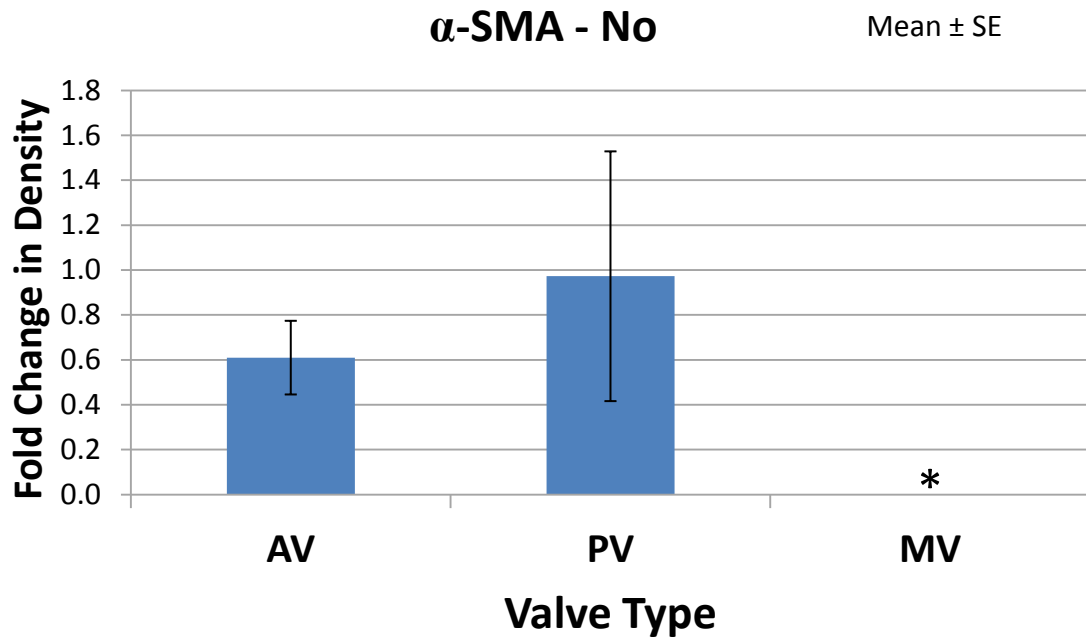
Figure 17 – Average α-SMA expression in unloaded tissue for each valve expressed relative to their respective fresh tissues. The asterisk (*) marks the MV as different because its RNA levels were not detectable under the same conditions as the AV and PV. (AV: n = 6; PV: n = 5; MV: n = 6)
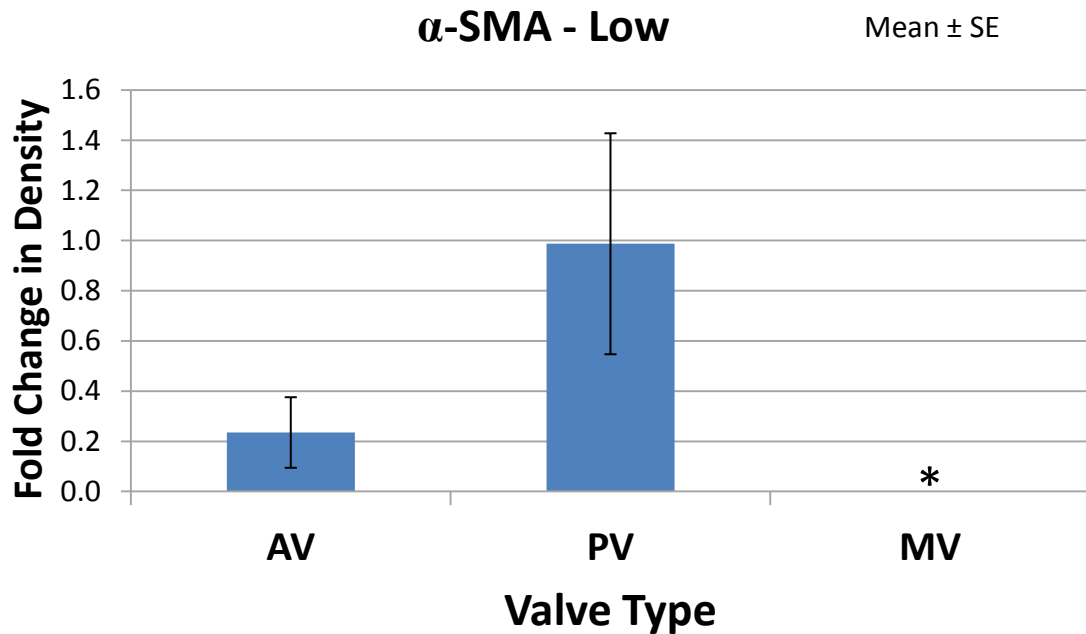
Figure 18 – Average α-SMA expression in low-load tissue for each valve expressed relative to their respective fresh tissues. The asterisk (*) marks the MV as different because its RNA levels were not detectable under the same conditions as the AV and PV. (AV: n = 6; PV: n = 5; MV: n = 6)
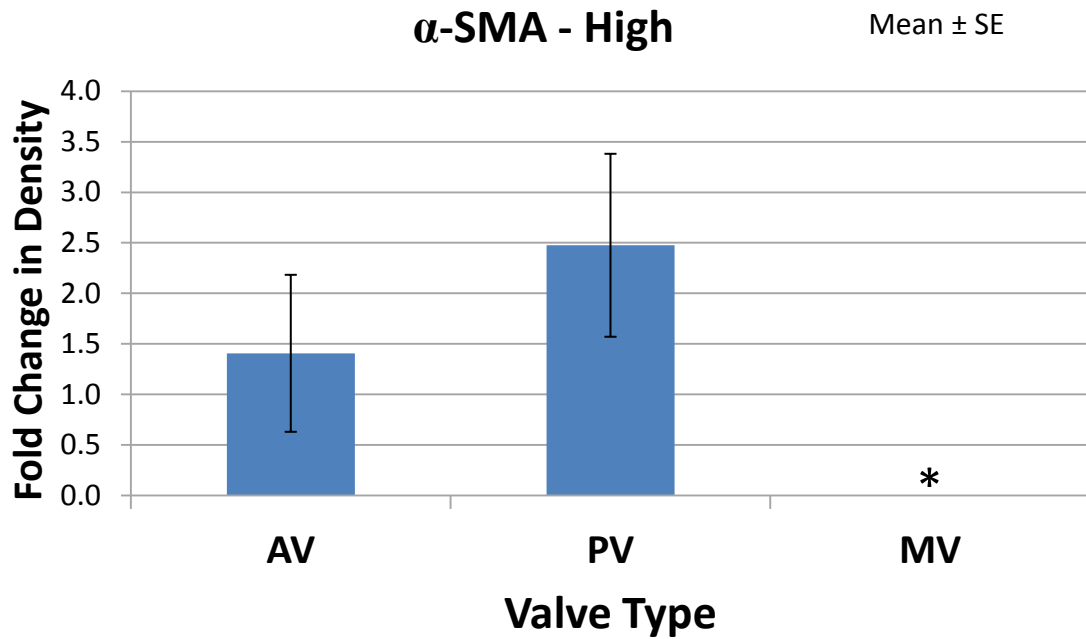
Figure 19 – Average α-SMA expression in high-load tissue for each valve expressed relative to their respective fresh tissues. The asterisk (*) marks the MV as different because its RNA levels were not detectable under the same conditions as the AV and PV. (AV: n = 6; PV: n = 5; MV: n = 6)

Table 6 – Average α-SMA expression levels relative to fresh tissue for individual valves for each loading condition with associated SEs. BD – below detection conditions (AV: n = 6; PV: n = 5; MV: n = 6)

Valve	Loading Condition							
	Fresh		No		Low		High	
	Fold Units	SE	Fold Units	SE	Fold Units	SE	Fold Units	SE
AV	1.0	0.0	0.6	0.2	0.2	0.1	1.4	0.8
MV	BD	-	BD	-	BD	-	BD	-
PV	1.0	0.0	1.0	0.6	1.0	0.4	2.5	0.9

5.1.2 Immunohistochemistry

A two-way repeated-measure MANOVA on α-SMA percent positively stained cells was used to compare loading condition and valve type. Results showed no significant interaction ($p = 0.47$) and that there were no significant differences between valve types ($p = 0.90$). No significant difference was observed within loading condition, although the p-value was just above significance ($p = 0.058$) (**Figure 20**). α-SMA positively stained cells were $53 \pm 3\%$ in fresh tissues, $38 \pm 5\%$ in unloaded tissues, $46 \pm 5\%$ in low-load tissues, and $44 \pm 5\%$ in high-load tissues (**Table 7**).
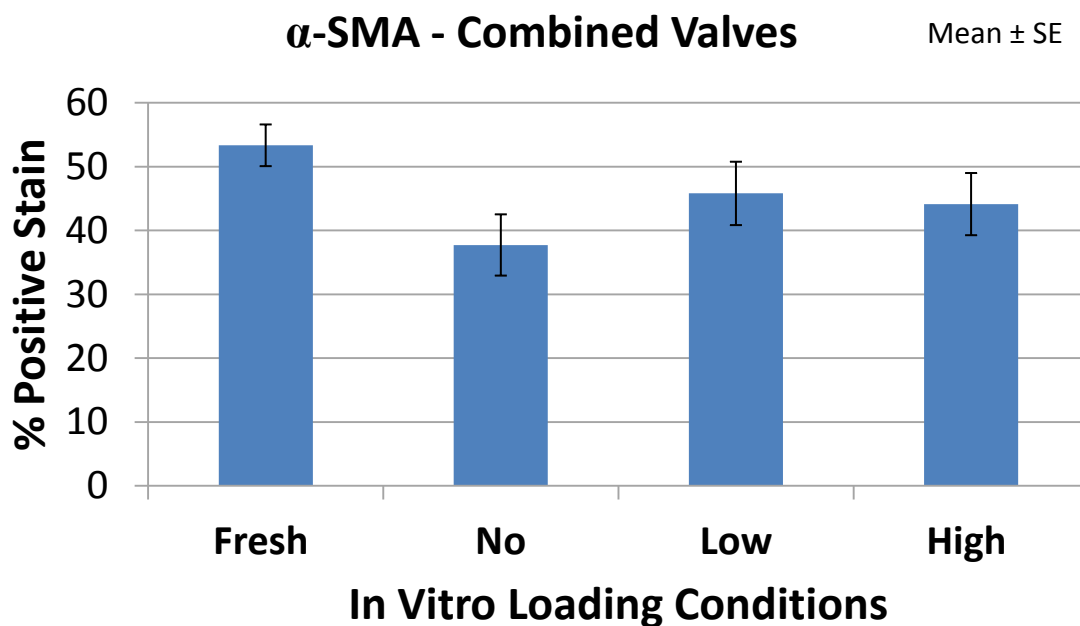
Figure 20 – Average percentage of α-SMA IHC positively stained cells for pooled valve types for each loading condition. (AV: n = 6; PV: n = 6; MV: n = 6)

Table 7 – Average percentage of α-SMA IHC positively stained cells of individual valves and pooled valve types with associated SEs. (AV: n = 6; PV: n = 6; MV: n = 6)

Valve	Loading Condition							
	Fresh		No		Low		High	
	% Positive	SE	% Positive	SE	% Positive	SE	% Positive	SE
AV	54	7	43	10	45	8	39	9
MV	55	5	33	10	45	7	37	9
PV	51	6	37	6	44	12	56	7
Pooled	53	3	38	5	46	5	44	5
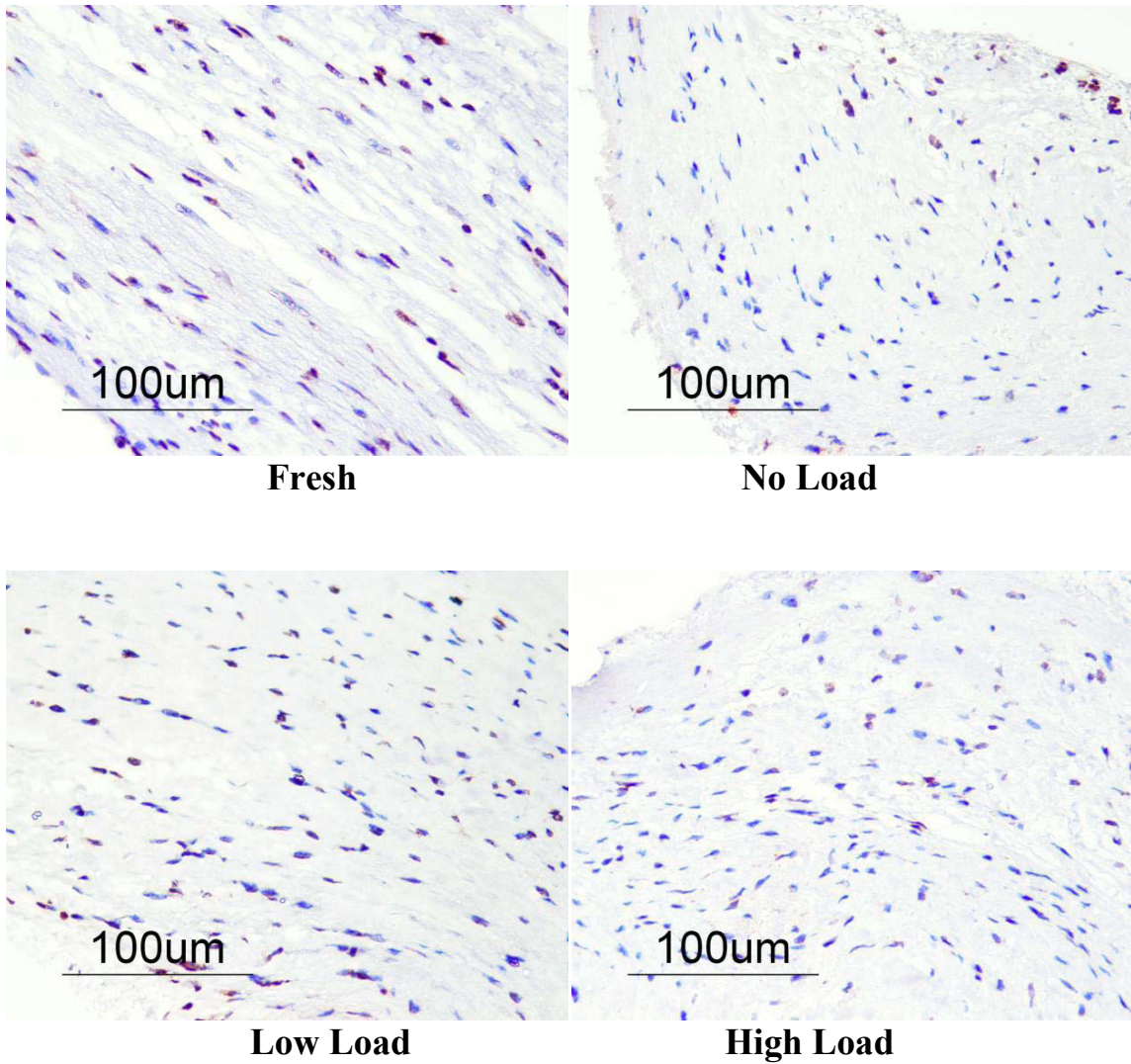
Figure 21 – Representative IHC images at 400x magnification of α-SMA for each loading condition. All images are from the PV.

5.2   Cx43

5.2.1   RT-PCR

A two-way repeated-measure MANOVA on Cx43 expression was used to compare loading condition and valve type. Results showed no significant interaction ($p = 0.47$), no significant differences between valve types ($p = 0.82$), and no effect due to loading condition ($p = 0.078$) (**Figure 22**). Cx43 expression relative to fresh tissue was 1.63 ± 0.26-fold in unloaded tissues, 2.41 ± 0.44-fold in low-load tissues, and 1.90 ± 0.44-fold in high-load tissues (Table **8**).
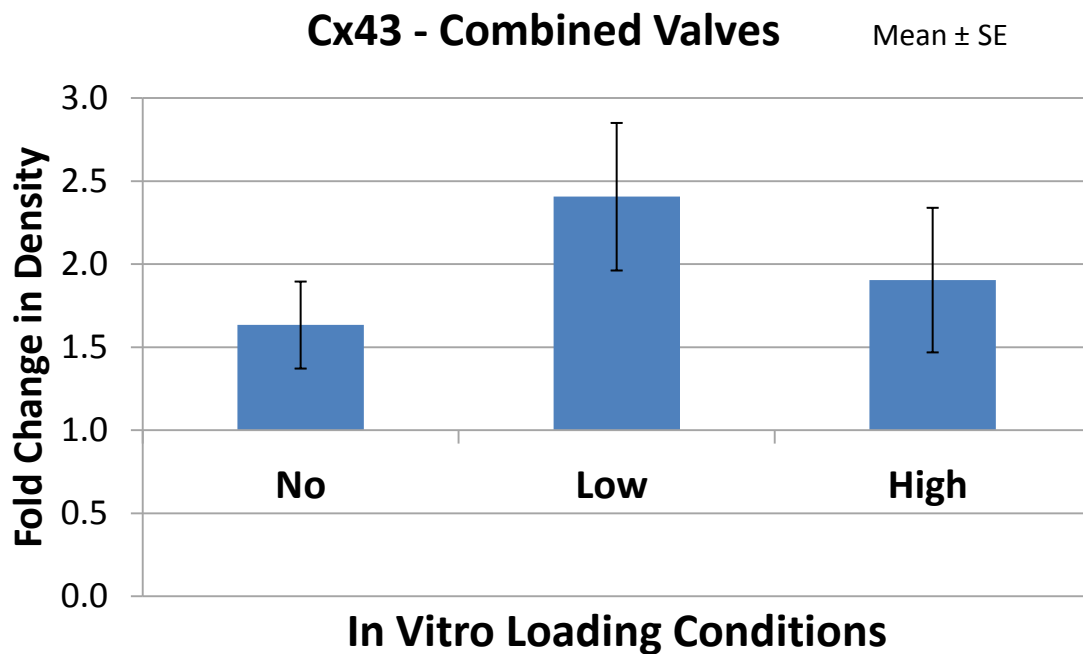
Figure 22 – Cx43 expression for pooled valve types for each loading condition expressed relative to the fresh condition. (AV: n = 5; PV: n = 6; MV: n = 6)

Table 8 - Average Cx43 expression levels relative to fresh tissue of individual valves and pooled valve types with associated SEs. (AV: n = 5; PV: n = 6; MV: n = 6)

Valve	Loading Condition							
	Fresh		No		Low		High	
	Fold Units	SE	Fold Units	SE	Fold Units	SE	Fold Units	SE
AV	1.0	0.0	1.5	0.3	2.9	0.6	2.7	0.8
MV	1.0	0.0	1.5	0.5	2.4	0.7	1.5	0.7
PV	1.0	0.0	1.9	0.6	2.0	1.0	1.7	0.9
Pooled	1.0	0.0	1.6	0.3	2.4	0.4	1.9	0.4

5.2.2   Immunohistochemistry

A two-way repeated-measure MANOVA on Cx43 percent positively stained cells was used to compare loading condition and valve type. Results showed no significant interaction ($p = 0.44$), and that there were no significant differences between valve types ($p = 0.73$) or due to differences in loading condition ($p = 0.13$) (**Figure 23**). Fresh tissue had $45 \pm 5\%$, unloaded tissues had $42 \pm 4\%$, low-load tissues had $53 \pm 4\%$, and high-load tissues had $54 \pm 5\%$ of positively stained cells (**Table 9**).

Cx43 - Combined Valves

Mean ± SE
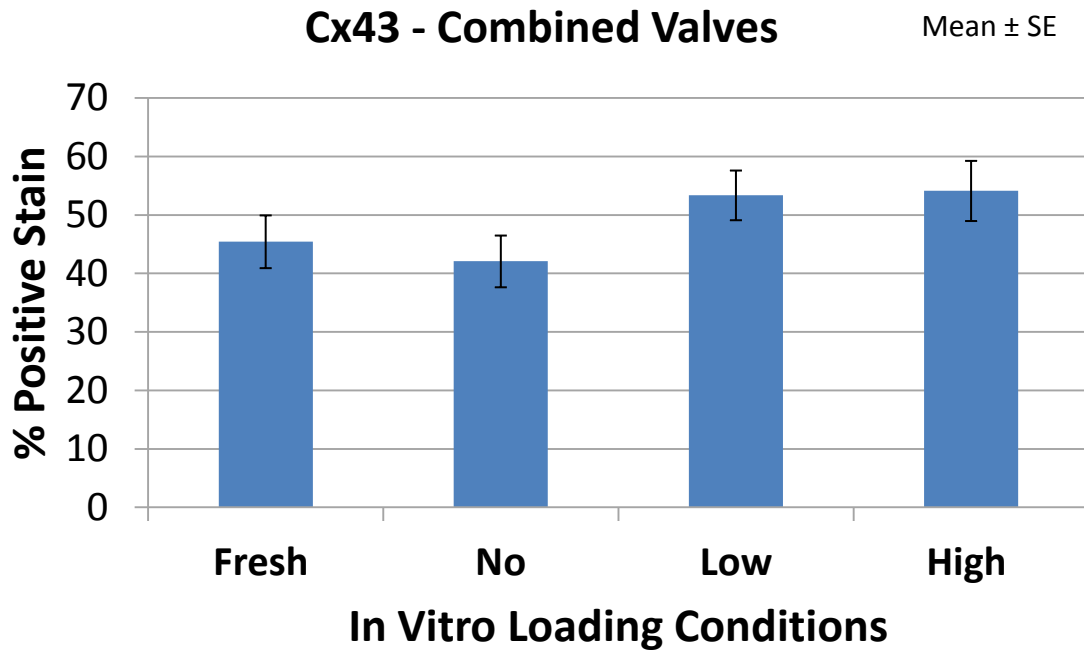
Figure 23 – Average Cx43 IHC positively stained cells for pooled valve types for each loading condition. (AV: n = 5; PV: n = 3; MV: n = 5)

Table 9 - Average Cx43 IHC positively stained cells for individual valves and pooled valve types with associated SEs. (AV: n = 5; PV: n = 3; MV: n = 5)

Valve	Loading Condition							
	Fresh		No		Low		High	
	% Positive	SE	% Positive	SE	% Positive	SE	% Positive	SE
AV	47	9	42	5	48	3	49	9
MV	48	8	49	10	61	10	55	10
PV	42	8	35	7	53	9	60	9
Pooled	45	5	42	4	53	4	54	5

Fresh **No Load**

Low Load **High Load**
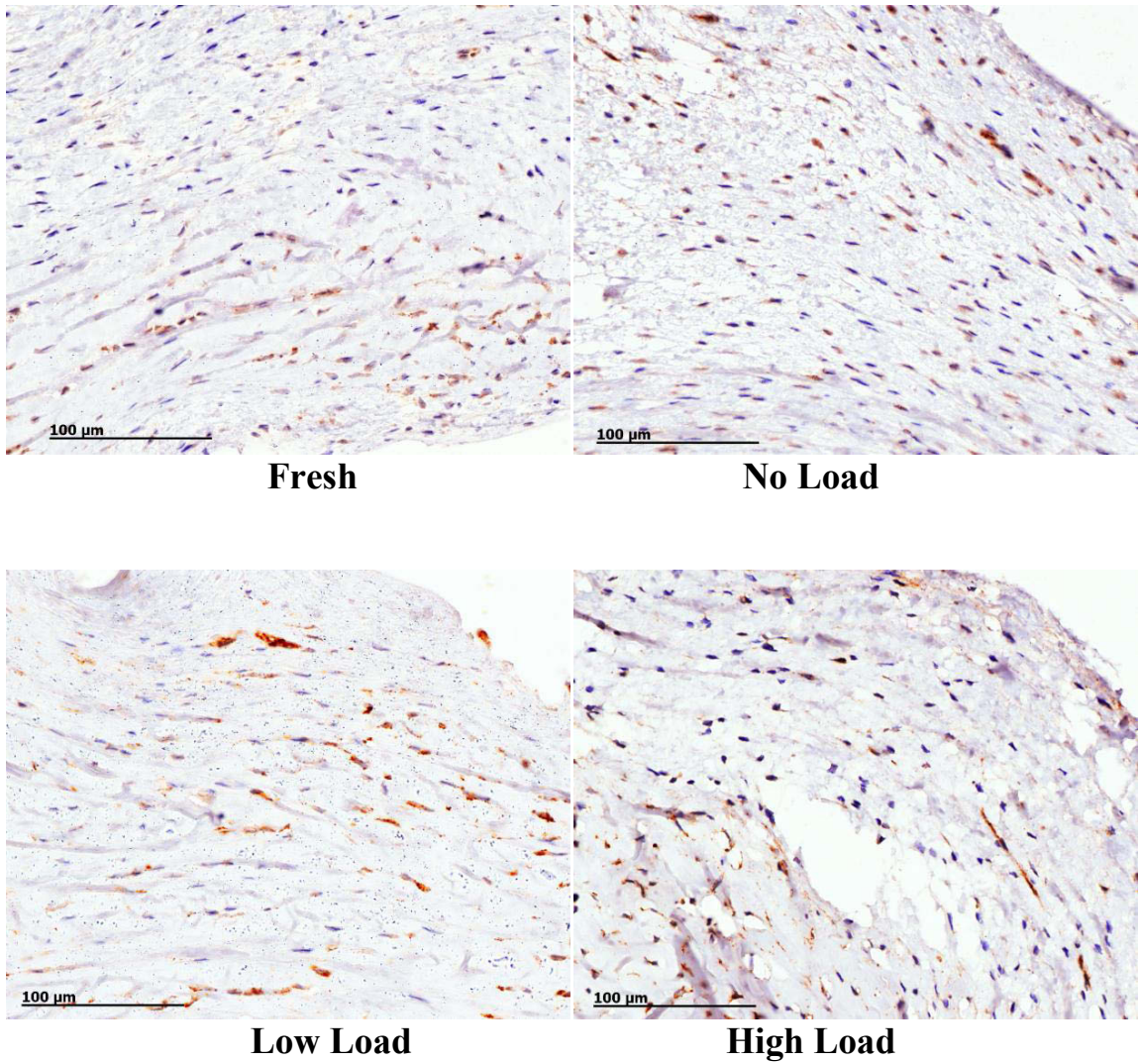
Figure 24 – Representative IHC images at 400x magnification of Cx43 for each loading condition. All images are from the MV.

5.3   Cx26

A two-way repeated-measure MANOVA on Cx26 percent positively stained cells was used to compare loading condition and valve type. Results showed no significant interaction ($p = 0.58$), and that there were no significant differences between valve types ($p = 0.97$) or loading condition ($p = 0.80$) (**Figure 25**). Fresh tissue had $56 \pm 3\%$, unloaded tissue had $57 \pm 4\%$, low-load tissues had $60 \pm 6\%$, and high-load tissues had $54 \pm 4\%$ positively stained cells (**Table 10**).
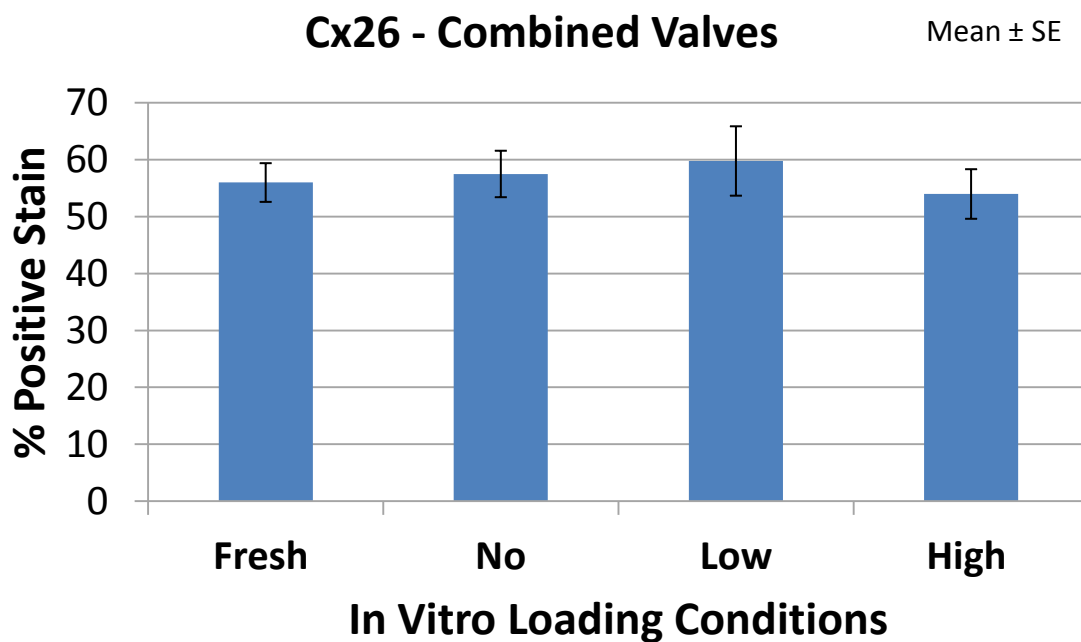
Figure 25 – Average Cx26 IHC positively stained cells for pooled valve types for each loading condition. (AV: n = 6; PV: n = 6; MV: n = 6)

Table 10 - Average Cx26 IHC percentage of positively stained cells for individual valve types and pooled valve types with associated SEs. (AV: n = 6; PV: n = 6; MV: n = 6)

Valve	Loading Condition							
	Fresh		No		Low		High	
	% Positive	SE	% Positive	SE	% Positive	SE	% Positive	SE
AV	57	6	68	4	54	7	52	6
MV	54	8	53	9	65	12	51	7
PV	57	4	51	7	60	13	59	10
Pooled	56	3	57	4	60	6	54	4
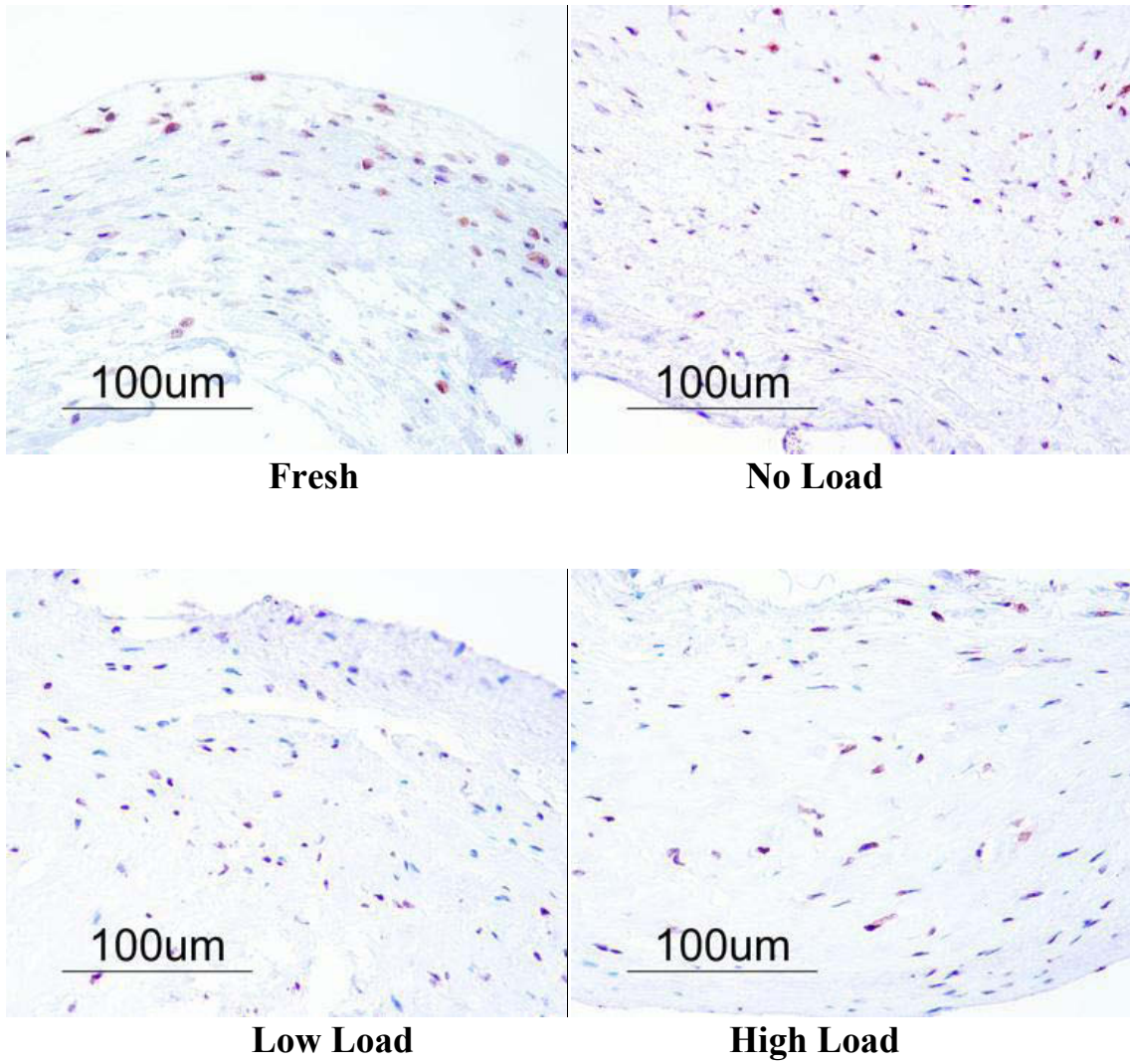
Figure 26 – Representative IHC images at 400x magnification of Cx26 for each loading condition. All images are from the AV.

Chapter 6   Discussion

6.1   General Discussion

6.1.1   Connexins

VIC communication as determined by connexin expression was not significantly affected by either loading condition or valve type. Baseline proportions of Cx43 and Cx26 were similar across valve types,[21] and did not change under different mechanical conditions. Further, based upon these results, it was found that under the loading conditions explored presently, connexins are likely unable to be used to classify valve responses based on either cell origins or native tissue stresses.

It may be possible that while the tissues were stretched, the VICs did not experience deformation because of lack of adhesion to the ECM, however, it is known that VICs are closely attached to collagen.[55] Collagen is aligned primarily in the circumferential direction, the same direction as the tissues were stretched, therefore the lack of response was unlikely to be due to a lack of force transmission to the VICs. Nuclear deformation, considered a reasonable approximation for cellular deformation, has been shown to occur with increasing tissue stress.[55] GJs are also present throughout the cellular membrane without polarity.[21] The imposed uniaxial circumferential stretch that was applied to the tissues can be assumed to have been transmitted to the VICs and their GJs.

Based on the results from this study, however, Cx43 expression was unaffected by loading condition. In contrast to these observations, based upon evidence in the literature, the mechanical environment has been shown to affect Cx43 expression. Cx43 has been shown to be mechanosensitive in many different soft tissues, including blood vessels, heart, uterus, and tendons. [30, 34, 38, 43]

One possibility to explain the mechanical unresponsiveness of Cx43 in this experimental model is that it may be sensitive to a different type of mechanical stimulus than stretch. Heart valve tissues have been shown to respond differently dependent upon

the type of mechanical stimulation. For example, in cultured AV tissues, α-SMA increased with cyclic stretch applied circumferentially, decreased with cyclic pressure applied using a sealed pressure chamber, and did not change when both circumferential cyclic stretch and cyclic pressure were applied in combination in a stretch-pressure chamber.[72, 75, 93]

Another possible explanation may be that Cx43 requires additional chemical factors for the response to mechanical stretch to be potentiated. Merryman et al. showed that VIC activation was substantially increased in the presence of TGF-β and cyclic stretch compared to either stimulant individually.[77] The sensitivity of VICs to biochemical mediators may include their GJs as well. In the uterus, increased Cx43 expression was achieved through the combination of both stretch and the hormone progesterone.[38] This biochemical component may also explain the increased Cx43 expression in heart valves of hypercholesterolemic rabbits.[32] Hypercholesterolemia led to sclerotic-like conditions, including leaflet thickening, VIC activation and proliferation, and the presence of macrophages. Macrophages are associated with the inflammatory response, and release cytokines, chemokines, and growth factors, including TGF-β, which may have influenced GJ expression.[97] The mechanical functionality of leaflets changes with ECM remodelling, and Cx43 may require the presence of the additional biochemical signals for increased expression, or they may exaggerate smaller changes that were otherwise undetectable in the model used in the present study.

A further explanation for the observed results in this study is that Cx43 expression remained the same, but the functionality of the GJ channels changed. Cx43 can be present in both a phosphorylated or unphosphorylated form.[98] Both forms have been found in VICs, however the proportions of each have not yet been determined.[21] The role of GJ phosphorylation remains unclear, but it is likely regulatory and has been linked to changes in permeability (gating open or closed, and electrical and molecular conductivity), assembly, and degradation.[99] The majority of Cx43 is phosphorylated in heart tissue, however there are proportional differences even within the same organ (e.g. myometria and atria of the heart).[98, 100] In the current study, no distinctions were made for phosphorylated forms, and GJ functionality tests were not performed. Based on the short-half life of GJs (1-5 hours) and the experimental duration (48 hours), the phosphorylated

proportion may have changed, but the overall expression levels had time to be altered by the imposed mechanical conditions, similar to the responses seen in other soft tissues.

Finally, another possible explanation for the lack of Cx43 responsiveness in the current study is the range of loading conditions used. The choice of loading conditions used in the present study corresponded to physiological and 1.5-times physiological loads. It is possible that the above-physiological loads were not large enough to elicit measurable responses within the experimental timeframe. Severe hypertension is considered closer to two times higher the normal physiological tensions, and may have been able to elicit a significant response in this model. However, this should be validated using a model that can induce established changes (i.e. collagen or another valvular protein) to confirm the current result.

Cx26 is likely not mechanosensitive, which is in agreement with its response in other soft tissues. This may be due to the range of stretch examined, as outlined above, however a similar lack of response to stretch for Cx26 has been noted in blood vessels and the uterus.[30, 38]

Another possible explanation for why Cx26 was mechanically unresponsive is that it may be mechanosensitive, but not in the circumferential direction used to impose loads on the leaflets in this study. Potentially, Cx26 may be oriented in primarily one direction, that is radially as opposed to circumferentially, similar to the uniaxially-oriented Cx32 of fibroblasts within tendons.[39] If this were true, a radial loading component may be required to stimulate Cx26. However, this is unlikely because Cx32 in tendon fibroblasts is longitudinally oriented, which is the primary loading direction of tendons, and heart valve leaflets primarily support loading in the circumferential direction. Additionally, images from Latif et al. showed no cellular polarity in GJ distribution in VICs that has been noted in tendon fibroblasts.[21]

Alternatively, Cx26 may be biochemically sensitive to hormones, such as seen with progesterone in the uterus, or cytokines, as identified in the wound response of the skin.[31, 38] Cx26 was also found to have different temporal expression compared to Cx43 in the uterus and the skin,[29, 31, 101] so the time scale of this study (i.e. 48 hours) may not have been appropriate. Different regulation of connexin isoforms in the same tissue is a reasonable assumption since they have different functions.[26] Even if there is some

functional overlap, one isoform of a GJ cannot completely compensate for the loss of another isoform. For example, in contrast to Cx43, Cx26 is not phosphorylated.[99] It would be reasonable to conclude that they are also differentially regulated in heart valves.

6.1.2   α-SMA

α-SMA protein expression was not significantly affected by loading condition, although the *p*-value was just above significance ($p = 0.058$). This was an unexpected result because of results from previous work on the AV using similar experimental models. From previous studies, when compared to fresh tissue, it was expected that α-SMA content in AV leaflets would have decreased in unloaded tissues, had similar levels with cyclic loading at near-normal tension, and higher levels at increased tension.[75, 93] An analysis of the current study design in contrast to those in the literature was conducted to determine what components may have contributed to differences in results.

There have been a number of studies looking at the isolated effects of the different hemodynamic components, including shear, pressure, and stretch. Most of these studies have been investigations into collagen, PGs, and VIC phenotypes as marked by α-SMA. Most valve research has been on the AV and some work has been done on the MV, largely because degeneration and/ or failure are much more common for these valves than the PV or TV.[91]

Shear is more important for VECs than VICs because VECs are at the leaflet surface and experience it directly. However, VICs can be affected by shear and their response is modulated by VECs.[45] VICs are activated under shear stress in the absence of VECs, and are mostly quiescent in the presence of VECs. Another study found that shear maintains leaflet collagen, but not aVIC levels.[71] This same effect has been shown for pressure changes, where collagen synthesis but not VIC phenotype is maintained.[72, 73]

Cyclic stretch has been shown to increase collagen content and activate VICs in a load-dependent manner.[74, 75] Interestingly, a study investigating the combination of pressure and cyclic stretch in AV tissues showed that they had opposing effects on VIC activation.[93] Pressure alone decreased aVIC content, stretch alone increased aVIC content, and the combination maintained aVIC content. This suggests the individual

components of valvular hemodynamics each have a role in tissue homeostasis and that they maintain normal basal levels when combined. It also demonstrates that cyclic stretch impacts VIC phenotype.

Experiments that directly compared aVIC content in fresh tissues to tissues that had been mechanically stimulated with isolated cyclic stretch at near-physiological levels have not been conducted. A study that compared fresh AV tissues and those under near- and above-normal stretch looked at cell proliferation, apoptosis, collagen content, and remodelling enzymes such as MMPs and TIMPs, but not aVIC content.[74] Other AV tissue studies investigating changes in VIC phenotype with isolated cyclic stretch at above-normal levels resulted in increased aVIC expression compared to near-normal levels[93] (absent comparisons to fresh and unloaded tissues) and unloaded tissues[75] (absent comparison to near-normally stretched tissues). An intact AV organ culture system showed that combined mechanical hemodynamics (pressure, shear, bending, and stretching) and regulated oxygen content in a near-normal environment maintained native valve ECM and phenotype.[78] This study found that aVIC content decreased in unloaded tissues compared to fresh and mechanically stimulated tissues. They attributed this to the stretch component from flexing (open/ close) and tensile stretch (coaptation and sealing) because previous studies showed that isolated pressure and shear were unable to maintain the VIC phenotype.[71-73]

Remodelling responses to changes in loading conditions in the MV are similar to the AV. When remodelling was studied by induced mechanical means (tethering of chordae),[102] or by looking at degenerative pathways (myxomatous),[15, 82] the chronic response included VIC activation, similar to SL valve responses.[17] Lacerda et al. have shown that cyclic stretch causes VIC activation in a load-dependent manner by examining different levels of stretch from unstrained to pathological amounts.[76] α-SMA content increased with increasing amounts of stretch.

The load-dependent relationship for α-SMA may also explain its lack of responsiveness in the present study. As mentioned for the connexins, the range of loading conditions, especially the above-physiological load, may not have been sufficient to elicit a significant increase in this model.

α-SMA content was expected to change in a predictable manner to mechanical stretch based on the research mentioned above and on the similarities in the stimulation component of the study by Balachandran et al.[75] Some of these differences are discussed.

One difference between studies was the manner of inducing tension in the tissues. For the current study, load-control was used. Weights were applied to give the desired membrane tension, which would have remained constant throughout the experiment, and the loading protocol would allow creep to occur. In the study by Balachandran et al.,[75] strain-control was used. The load, and therefore the membrane tension, was not monitored. Strain was determined based on deformation, and remained constant throughout the experiment. This would mean the tissue would stress relax because the stretch is to the same extent at every cycle – the mean strain was unchanged. The membrane tension experienced by the tissue would have decayed to an asymptote in the study by Balachandran et al., and in the present experiment the stress remained constant. The viscoelastic responses cannot be ignored, however if the membrane tension was significantly reduced due to stress relaxation, it would be expected that the current study would have demonstrated a larger increase in α-SMA than that by Balachandran et al., but this was not the case. Therefore, although the membrane tension profiles would be different, this was not necessarily the main determinant in the differences in α-SMA expression between the two studies.

Comparison between studies by Merryman et al.[77] and Balachandran et al.[75] offers an interesting difference, considering that both used a strain-controlled methodology on circumferentially oriented AV tissues. Merryman et al.[77] found no difference in α-SMA expression between fresh, unloaded, and 15% cyclically strained tissues after 7 days. Compared to fresh tissues, α-SMA expression only became significantly increased for strained tissues after 14 days or in the presence of TGF-β (n = 4). Determination of α-SMA levels was done using a quantitative ELISA (enzyme-linked immunosorbent assay) method to provide protein concentrations of the tissue samples. Balachandran et al.[75] found that compared to fresh tissues, α-SMA expression increased with 15% cyclic strain after 48 hours (n = 8). Determination of α-SMA levels was done using semi-quantitative IHC and immunoblot methods. The sample sizes and α-SMA quantification methods were different, but both studies found α-SMA increased with 15% cyclic stretch,

although, interestingly, it took much longer in the Merryman et al. study for the increase to become significant. This raises the possibility that the reported significant differences in α-SMA expression due to cyclic stretch may be somewhat small and that the presence of hormones or other signalling chemicals may be required for biologically significant results.

Cell enumeration methodology was another difference between the present study and that by Balachandran et al.[75] There is no universal scoring system, but stereology is one of the most widely accepted practices and was used for this study.[103-105] The accuracy of this technique is based on statistics and sampling, and the main determinant of precision is inherent biological variability.[103, 105] This was confirmed experimentally as the pooled SEs were ≤ 5%, and are similar to other studies that had significant IHC components.[15, 17] Balachandran et al. used a method based on cell area.[75] The percent positive stain was determined based on the area coverage of the positive stain compared to the area of the leaflet. Variability in cell sizes would likely affect these ratios. Preliminary IHC evaluation for this study used the area method (data not shown), but was changed to stereology because of its well-documented and evaluated procedures. In many papers from the Balachandran et al. research group, α-SMA IHC results and SEs are only provided as ratios in figures,[75, 93] and some papers do not provide direct values, even within a figure (either percentages or ratios).[71-73, 78] The differences between conditions are illustrated only with ratios and comparison between studies is challenging. Additionally, although IHC evaluation is semi-quantitative by nature, effect sizes cannot be determined in the absences of these numbers.

The lack of confirmation of results between these studies, especially for the fresh to unloaded tissue relationship, likely indicates a lack of statistical power in this study. The *p*-value was just above significance for loading condition ($p = 0.058$). There may be no effect at all or there may be an effect, but it was small because it was not detectable with the current statistical power. For the present IHC data, with n = 6 for each treatment group and 20% standard deviation, the largest difference of 15% (between fresh and unloaded tissues) could not be identified. A sample size of n ≥ 8 would have been required for this difference to achieve significance. Other studies with significant IHC components have generally had n = 8-12.[15, 17, 74, 75] Aikawa et al. have been able to detect

20% differences.[15, 17] Based on the overall body of work, it had been expected that there would be significant differences in α-SMA expression due to the imposed mechanical conditions.

In the current study, there were no differences in α-SMA protein expression across valve types. Similarly, Aikawa et al. found no differences in α-SMA expression between the AV and PV,[17] although Merryman et al. found that the AV and MV had higher α-SMA protein levels than the PV and TV.[89] The different results in these studies may be due to the quantification methods used. Aikawa et al. determined α-SMA levels using histological cell enumeration, and was based on the presence or absence of α-SMA for each cell. Merryman et al. determined α-SMA levels using a quantitative ELISA method. The choice of quantification method may also explain why no differences were found between valves in the present study, which was based on the presence or absence of α-SMA in cells, similar to the study by Aikawa et al.

The lack of difference in protein levels between valve types from different native loading conditions, specifically the AV and PV, was unexpected because of the previously mentioned work by Merryman et al., and also because of research that had shown load-modulated relationships between the valves for collagen and VIC behaviour.[87, 89] The lack of difference between valve types from different embryological cushions, specifically the AV and MV, was expected as origins were proposed to have a lesser influence on remodelling responses than native loading conditions. Together, these suggest that VIC remodelling responses cannot be classified by either their native loading environment or their embryological origins, and that their responses may require more complex factors than the present experimental model included.

In the current study, there was a significant difference in α-SMA gene expression levels. The MV had transcription levels approximately 50-500 times lower compared to the AV and PV. The MV has different embryological origins than the PV and AV, which may explain the difference in gene expression levels. However, based on the lack of differences in α-SMA protein between valves, possible genetic differences due to embryological origins do not affect protein synthesis outcomes.

Genetic regulation of α-SMA differs among cell types, and has not been determined in VICs, however there are some consistencies.[106] The promoter region on the

gene is regulated by force-responsive elements, and signalling pathways that have been implicated in transcriptional control include some pathways that have also been implicated in integrin-mediated signalling, such as via MAPKs. Because genetic regulation is different among cell types, the different origins of the AV and PV compared to the MV may explain the difference in gene expression levels.

VIC deoxygenation in the MV is another possibility because it is thicker than the AV and PV. The experimental model used in the present study relied upon diffusion, which may not have been sufficient if the tissue was too thick. However, it is unlikely that the VICs in the MV were in a significantly different metabolic state compared to the other valve tissues. The genes for Cx43 and β-actin were expressed across all of the valves, and, furthermore, β-actin was expressed to a similar degree across all valves which showed that the basal metabolic rates were also similar.

Environmental conditioning of the MV is another possibility because it is in the most mechanically demanding position. It may require larger changes than those that were experimentally induced to increase gene expression levels. However, it is unlikely that mechanical conditions could explain the present results because the AV and MV have a more similar mechanical environment than the AV and PV, so if this were true, the AV would have also shown decreased expression levels, and the PV would have had the highest levels.

As interesting as this genetic difference is, there was no observable difference in the present study between valves with translation to protein. The differences seem to lay in the gene expression levels, and not the extent to which protein is produced. It is then possible that embryological origins define the genetic levels, and additional steps that regulate protein translation, especially for structural proteins like α-SMA, are based on remodelling for adaptation to the mechanical environment, regardless of how the signalling cascade was initiated. This may affect how some valve diseases are approached. Research has suggested that valve disease is influenced by embryological origins, and that disregulation of the remodelling pathways may lead to disease, either congenital or degenerative.[15, 20]

The genetic difference between valves may also have implications for TEHVs because of the long-term duration that would be expected from the implants.

Determination of differences in transcription behaviour in VICs between valves provides further evidence that cell sources need to be chosen carefully. The genetic differences may not have significant effects in normal physiologic environments, but may have long-term effects, especially in modified environments. After the initial remodelling response, aVICs in PV autografts (Ross procedure) become quiescent, but do not return to basal levels.[69] In the case of TEHVs, this may lead to unintended consequences. Other groups have already suggested that each valve has its own remodelling strategy and the observed genetic difference adds further support.[87] The suitability of different cell sources are still being evaluated, and criteria for cell source selection may need to be further narrowed to include more location-specific cell substitutes in order to more accurately replicate the native environment.[107, 108]

'End-point' protein expression has had more study than transcription processes because of the structure-function implications in clinical and TEHV applications. The most common assessment methods are histology and immunohistochemistry.[109] The structure-function relationships are especially important for TEHV research in pursuit of the ideal implant. The essential design criteria include the ability to grow, repair, and remodel itself in order to be durable, as well as no adverse effects, such as obstruction or thrombogenicity.[83] A common design method involves seeding cells onto a scaffold material which is then placed in a bioreactor in order to develop mechanical strength and cellular function.[83, 108] Prototype TEHVs have been developed in this way and successfully implanted in vivo in lambs.[110] Their anatomy resembled native valve structures, including trilaminar architecture and similar VIC and ECM distributions. Evaluation of the mechanical properties of the constructs in comparison to native leaflets and long-term functionality remains challenging because of the destructive nature of most testing methods and inadequate imaging techniques.[109] A better understanding of valve remodelling mechanisms is required in order to be able to better characterize whether a TEHV is 'normal.' This is especially important when considering the long-term applications of these implants.

6.1.3 Evaluation of RT-PCR Process

There are many steps involved in the RT-PCR process, and therefore many steps in which to introduce variability. It arises from multiple points in each step, including RNA stabilization and isolation, RT and PCR, and the detection method. Even with the same user, variability is substantial between samples from the same material and between runs.[111]

The amount of RNA in tissues is inherently variable, and the stability, concentration, and quality can be impacted by how the tissue is handled and prepared. Cells within the tissues used in the current study were unlikely to be negatively impacted during the harvesting and transportation process. There was little chance of degradation because the tissues were obtained immediately after butchering, placed in cold storage during transportation, and were preserved as quickly as possible with RNAlater®, a solution that is well documented to stabilize and protect RNA.[112] The tissues subjected to experimental conditions were also unlikely to have their cells and structure negatively impacted because they were maintained for the duration in biologically supportive conditions at 37°C in supplemented media, and at the conclusion, were also preserved in RNAlater®. Additionally, it has been shown that while proliferation and apoptosis increase with increasing mechanical loads, cell viability and structural integrity are maintained in valve tissue that has undergone cyclic stretch.[74-76] Cell viability was also visually confirmed in experimentally manipulated tissues in the current study using a commercial viability/ cytotoxicity kit during protocol validation (data not shown).

RNA should have remained stable during the tissue and cell disruption process to allow for extraction. The heat generated from the tissue dismembrator was not sustained for an extended duration because cell disruption was performed in bursts. RNA isolation was accomplished using the commercial RNeasy® Mini kit. Further degradation was limited by preventing contamination through use of RNase-free supplies and careful handling. After isolation, storage (-80°C) and concentration by lyophilization (-50°C) were performed at temperatures cold enough to prevent RNA degradation. Aliquots of the RNA solutions were made for testing in order to prevent degradation during multiple freeze/ thaw cycles. Concentration and quality of the extracted RNA were assessed using

a spectrophotometer, and the quality of the samples was found to be within the accepted range.[94]

RT is known to introduce considerable variation into the RT-PCR process. Some sources include differences in RNA concentrations, RNA quality and stability, RNase contamination, and salt or solvent contamination from the RNA isolation process.[111, 113, 114] Differences in RNA concentration affect RT efficiency because the conversion of RNA to cDNA is concentration dependent, however, for the current study, a consistent amount (2 μg) was used across all samples.[113] RNA quality and stability have a strong effect on the primers that generate the cDNA. Oligo-dT was the primer used in this study. It attaches to the 3'-polyadenylate (polyA) tail of the RNA, so this sequence must be present for the reverse transcriptase to begin cDNA synthesis. Additionally, RNA degradation can have an impact on investigations into sequences coded at the distant 5' end because cDNA cannot be synthesized from a sequence that is not present. Oligo-dT may also fall off the RNA molecule before it reaches the end, especially if it is a long sequence. In the present study, the primers for PCR were nearer the 5'-end than the 3'-end, however the RNA sequences were relatively short, so while it is likely that there were some shorter sequences, it is unlikely to have had a significant effect. DNA is a common contaminant, even with RNA isolation kits.[115] There would have been little to no amplification of genetic DNA contaminants in the current study because of the specificity of the oligo-dT primer to the polyA tail of RNA.

PCR is the process where DNA or cDNA is amplified to detectable levels. Efficiency and variability in the reactions are affected by many components and factors. These are important to acknowledge because the exponential nature of signal amplification and the multiple cycles required mean that effects of inconsistencies are also magnified. Some of the contributing factors include the concentrations of the template cDNA, DNA polymerase, and other reaction components, as well as the presence of contaminants, such as DNA, traces from the isolation process, and DNases.[96, 114] Variability in the reaction components is largely due to repetitive pipetting errors, and premixed solutions of the components that can be mixed ahead of time help to reduce this.[96] In the present study, premixed solutions were used where possible (e.g. MasterMix, which contained DNA polymerase, reaction buffer, and nucleotides).

Additionally, the impact of DNA contamination was reduced by using primers that span the intron/exon boundaries of RNA. This allows for selective amplification of only cDNA and not genomic DNA because the primers are unable to bind to the interrupting intron sequence (**Figure 27**). No-template controls were included with every batch to ensure there was no amplification of genomic DNA or other unintended products.

A Primer spans an intron/ exon boundary.
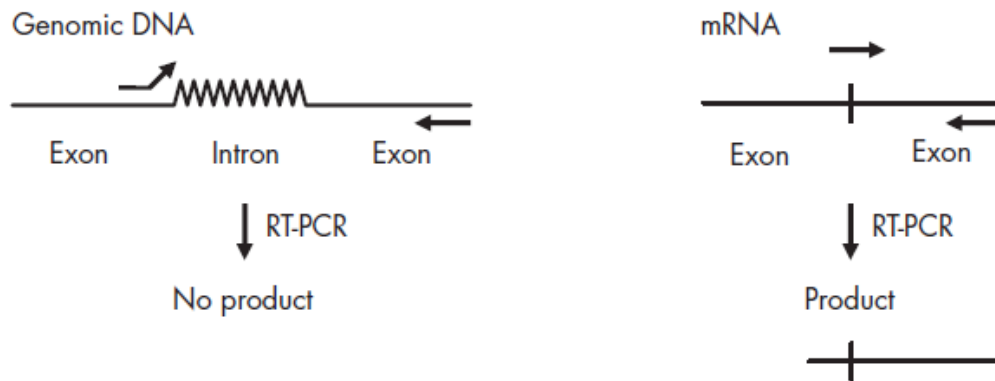
B Primers flank an intron.
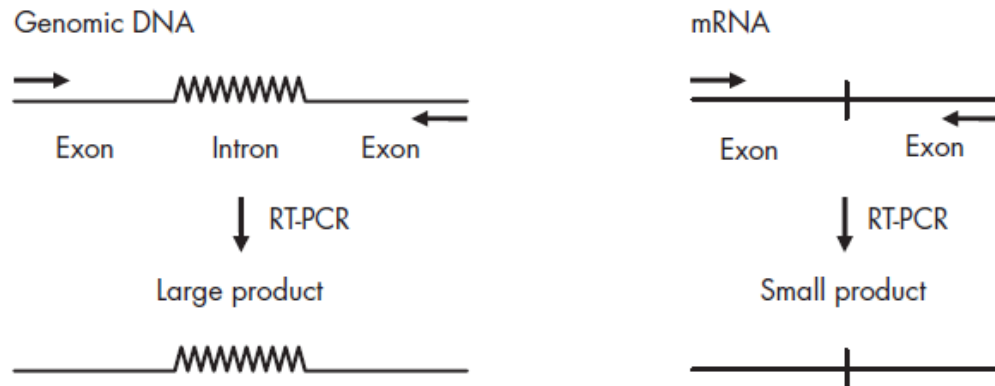
Figure 27 – Effect of primer annealing locations at introns and exons. **(A)** When the primers span an intron/ exon boundary, only RNA is amplified because the primers cannot anneal to the interrupting intron sequence. (B) When primers are located in the exons flanking the intron sequence, both DNA and RNA are amplified. (Figure from Qiagen®[116])

PCR products can be detected and measured in multiple ways. Conventional end-point PCR, which was used in the current study, uses gel electrophoresis to separate the products which are then labelled with ethidium bromide in order to identify them. Assuming the procedure was optimal, there should be one sharp band for each product.[96] The gels are photographed under UV light, and the band intensities are measured from the images using densitometry. These additional steps continue to add variability to the process.

Data normalization is considered an essential component of PCR, whether quantitative or semi-quantitative methods are used.[114] The most common method is to use a reference gene, such as β-actin. Normalization is the ratio of the gene of interest to the reference gene. Reference genes are required to be stably expressed across experimental conditions. They act as internal controls because they have been prepared under the same experimental conditions as the genes of interest. By reporting the ratios between these genes, variability can be reduced that arises from the integrity and concentration of the initial RNA, which is especially relevant for multiple tissue sources, and RT and PCR efficiency.[111, 113, 114] Relative expression is the ratio of one or more conditions compared to a control condition (e.g. unloaded, low-load, and high-load tissues compared to fresh tissues). It reduces variability arising from different tissue sources because it is the ratio of change and not the absolute levels that are compared.

In semi-quantitative RT-PCR, intra-sample variability is estimated to be approximately 40%, and inter-sample variability is approximately 70%.[111] If standard deviations in this study were considered as percentages instead of ratio ranges, most of the data in the present study varied by ~70%, although it ranged as high as 120% in a small number of cases. This could have been reduced with replicated data, which was not completed due to time constraints, as current practices in qualitative real-time RT-PCR suggest each measurement should be conducted in duplicate or triplicate.[111, 114] Many of the differences in this study were less than the 1.2-fold difference required for significant semi-quantitative RT-PCR results.[117] The study results with large enough differences also had larger SEs that masked any potential statistical significance at the current power level.

6.1.4 Evaluation of IHC Process

IHC is a valuable research and clinical tool, but it is an inherently variable process. There are many steps involved, and therefore many steps in which to introduce variability, similar to RT-PCR. The main sources arise from tissue fixation, antigen retrieval, improper antibody optimization and detection, and interpretation.[104, 118] The quality, sensitivity, and specificity of the reagents and process have been improved dramatically, to the point that the largest issue contributing to IHC inconsistency is the lack of procedural standardization.[104]

In the pre-analytical steps, variability mostly arises from tissue handling and fixation aspects, similar to RT-PCR. Biological tissue is inherently variable, and tissues must be preserved as quickly as possible before the onset of degradation. The same steps taken during tissue harvesting, transportation, and experimentation that preserve RNA quality also preserve tissue and cell morphology. At each collection point in the current study, tissues were quickly immersed in 10% phosphate-buffered formalin. Formalin is the most widely used fixative for preserving tissue morphology, and it works by cross-linking amino acids (mainly those containing amino side-chains). The uses of other fixatives have been acknowledged, but formalin remains the gold standard because it is relatively inexpensive and very reliable. Formalin-fixed tissues compose the majority of tissues studied in the literature, which allows for comparisons between different tissues and across studies since they have been conserved in the same manner.[104, 118-120] The tissues used in this study were fixed for approximately 72 hours, and while 24-48 hours is often considered acceptable, there are no standard times. Increased fixation times and overfixation (> 2 weeks) are known to cause increased masking of epitopes (marker regions on the protein(s) of interest) due to the abundance of cross-links, however antigen retrieval (AR) largely overcomes this issue.[104, 120] After fixation, tissues used in the present study were washed and stored in 70% ethanol in order to preserve cross-links and prevent more from forming.[118] Tissues must also be processed and embedded. Any changes in processing can alter the tissues, so this step relies on quality alcohols and xylenes for tissue dehydration, and is usually automated, as was the case in this study when performed at Dalhousie's Histology Research Services Laboratory.[104, 119] Paraffin

wax is the most common embedding agent. It provides a rigid support for the tissues which allows for excellent maintenance of morphology, and sections as thin as 3 μm can be cut, although the section thickness used in the current study, 5 μm, is the most common.[119, 121]

AR is the process of exposing antibody binding sites that have been masked by cross-links or paraffin. This step is greatly affected by the degree of fixation, as well as by the buffers used, the temperatures used, duration of application, and even the cooling period.[104, 118, 121] The most common AR method is HIER. Slides are incubated in buffered solutions at a given pH (range 3-9). The most commonly used buffers are pH 6 citrate and pH 9 Tris-EDTA, both of which were used in the current study.[104, 121] There are multiple methods of applying heat, such as microwaves, steamers, and pressure cookers (used in the present study), but the particular method is not as important as the energy applied.[104, 121]

The antibody itself and its application also can introduce variability. The antibody solution is applied to tissue in order to bind to an epitope. The concentration and pH of the antibody solution, and the temperature and duration of application have some influence on the degree of staining, but it is low compared to other steps.[104, 118] The method of antibody detection and signal amplification confers the majority of sensitivity.[118, 120] The indirect staining method has increased sensitivity compared to the direct method because of signal amplification. Labelled secondary antibodies and amplifiers are applied step-wise to the tissue to bind to unlabelled primary antibodies, and they allow for detection through the visualization of chromogens (coloured compounds). The signal is strong because there are a large number of dye molecules present for each antibody binding site, compared to the direct binding method which has one dye molecule associated to one antibody. The method used in this study was based on the avidin-biotin method, which is known for its bonding strength. The primary antibody, which bound to the epitope, was labelled with a biotinylated linker molecule. Streptavidin was then applied which binds with high affinity to biotin. Streptavidin was linked with multiple peroxidase molecules which form an insoluble brown precipitate in the presence of oxidizing solutions. The amount of time allowed for the chromogens to develop confers additional variability.[104, 121]

Background staining can occur from multiple sources and is usually a combination of factors.[120] Some sources can be eliminated or reduced, while others must simply be considered as potential variables. Hydrophobic interactions are increased with formalin fixation, however their impact is minimized by using solutions that contain detergent, such as Tween® 20, and the addition of a blocking step, such as a casein solution, which were both used in the current study.[118] Endogenous alkaline phosphatase, peroxidase, and biotin may also contribute to background staining, however their effects can be greatly reduced.[118, 120] Alkaline phosphatase is destroyed by both formalin fixation and heat (e.g. HIER). Endogenous peroxidase is blocked with dilute hydrogen peroxide, which was also incorporated into the protocol used in this study. Endogenous biotin is mostly eliminated with formalin fixation. The contribution of these sources to overall staining can be determined based on negative control slides that omitted the primary antibody.

The final contributor to IHC variation occurs with imaging and analysis. Image analysis begins with obtaining high quality digital images of tissues with optimum contrast and resolution. The brightfield images obtained for this study were taken using Kohler illumination, a widely used method of setting the microscope components so that there is bright and even illumination, and a similar intensity is maintained across images.[103, 120] Magnification is the user's choice depending on the features of interest. Three magnifications were evaluated: 200x, 400x, and 630x. The 200x images allowed for inspection of general morphology and distribution of tissue components, however it did not provide sufficient resolution for determining the extent of staining. The images taken with 400x and 630x magnification showed excellent detail, but the 400x images were chosen for evaluation of samples in this study because of the balance between resolution and the number of photographs required based on the objects of interest in the image field.

The images were then processed in Photoshop® before evaluation in order to more easily differentiate between the blue-stained nuclei, the brown positive stain, and the matrix background. The same series of optimization steps were conducted for each photo, and any changes to intensity were adjusted to the same level for all images so that the signal itself was not manipulated. For this study, accurate cell enumeration was

required, and stereology is one of the most widely accepted practices.[103-105] The accuracy of this technique is based on statistics and sampling, and the main determinant of precision is inherent biological variability.[103, 105] This method reduces the amount of work, provides reproducibility, little training is required, and it reduces subjectivity.[103] A minimum of 100 nuclei were counted for each specimen which is the minimum required for a stable estimate.[105] A minimum of three photos were analyzed for each tissue sample. User-induced bias from over- and/or under-sampling 'interesting' (stained) objects could have been reduced by analyzing more images (6-10).[105] Sampling could have also been further randomized by ensuring images were taken of tissues from multiple non-neighbouring sections (by staining non-serial slides). This would have provided a more complete representation of the tissue, and the amount of work would remain the same if the size of the point grid was increased so that at least 100 nuclei were still counted.

SEs were generally ≤5%, and ranged from as low as 3.4% to as high as 6.1% in this study. When expressed as standard deviation for each condition (n = 6), this gave a range of 7-31%, and pooled valves (n = 18) had a range of 14-26%. These values are similar to those found in other studies that contained substantial IHC components (standard deviation range (n = 1-15): 1-44%).[15, 17]

6.2   Significance

This thesis showed that α-SMA gene expression levels are lower in the MV compared to the AV and PV. This is the first study that has demonstrated a genetic difference for α-SMA between valves. Additional knowledge of the transcription processes among different heart valves will provide a more complete understanding of VIC function, as well as add to the body of knowledge on valvular remodelling processes.

Conventional semi-quantitative RT-PCR is limited in that it does not allow for comparison between samples run under different conditions, which was required for valves in this study. Furthermore, its dynamic range is smaller than the difference that was found between loading conditions. While an accurate comparison was unable to be completed for α-SMA expression of the MV to the AV and PV, the MV α-SMA gene expression levels were approximately 50-500 times lower compared to the AV and PV, based on the higher number of cycles required to provide detectable signals. This may indicate genetic differences in valve remodelling pathways although functional outcomes are similar, based on the lack of difference of protein expression levels between valves.

This study found no differences in GJ or α-SMA content in VICs due to loading conditions or valve type. If these relationships hold true, this would suggest that neither native loading conditions nor embryological origins are the primary determinants of VIC responses. This suggests that further research into isolated stretch is required, especially since the current literature has contradictory results with respect to its significance.[75, 77] More complex conditions than simply isolated stretch may be required to elicit measureable changes, such as the presence of biochemical signals. This would further support a potentiating effect, which has been demonstrated ex vivo, and is a possible explanation for in vivo results.[32, 77]

6.3   Summary

In summary, the results from this study show that α-SMA gene expression levels are lower in the MV compared to the AV and PV. This was demonstrated by the higher number of cycles compared to the AV and PV required to produce a measurable signal. This is the first time this genetic difference has been demonstrated.

The overall hypothesis stated that in vitro mechanical loading conditions would affect VIC responses by altering phenotype and communication, and that embryological origins would have a negligible impact on VIC responses. Specifically, increasing mechanical loads would change the VIC phenotype from quiescent to activated, and the level of Cx43, but not Cx26, would increase. The responses would be greater in valve tissues from native high loading conditions. This was not confirmed because there were no significant differences in protein expression due to in vitro mechanical loading conditions for α-SMA (phenotype) or GJs (communication). However, the expected lack of difference due to mechanical loading for Cx26 was confirmed. Neither loading conditions nor embryological origins can be used as the primary classification factor for VIC responses because the results were inconclusive. Measureable responses may require more complex conditions, such as the presence of biochemical mediators. Neither loading conditions nor valve type affected communication or phenotype, however the gene expression levels for phenotype were much lower in the MV compared to the AV and PV. This suggests genetic differences in valve remodelling pathways although functional outcomes are similar.

The main reasons for the lack of significant differences, especially those expected for α-SMA with respect to loading conditions, were likely due to the differences in loading conditions not being large enough, and possibly the lack of statistical power based on the sample size. The components of this pilot study, from stimulation to measurement, were evaluated and suggestions are made below for future work (see Section 6.4).

6.4   Limitations and Suggestion for Future Work

When considering conditioning and origins, a number of environmental and anatomical differences between the valves should be acknowledged. One consideration when comparing high pressure valves on the left side of the heart to low pressure valves on the right is the oxygen content of the blood. This is likely not a major effector for VICs or ECM. The oxygen supply is at 95% saturation in the left side compared to 75% saturation in the right, but these levels are both within range for physiological function.[63]

In vitro oxygenation and VIC viability are another consideration. Valve tissues are quite thin (~ 0.5 mm), but are also non-uniform, and can vary in thickness. Considering that oxygen diffusion in tissues can only travel ~ 0.1 mm, this may cause the VICs to enter a morbid state. This would be a limitation in many other tissue models as well. While the VICs are no longer in their native environment where they have blood circulation at the base of the leaflet and pressure gradients across the leaflets for perfusion, VICs remained viable. This was confirmed during preliminary validation by using a live/dead kit, in which live cells would uptake a green fluorescent dye which indicated ongoing esterase activity, and dead cells displayed a red fluorescent dye to indicate the loss of the cell membrane. Furthermore, other researchers have shown that VICs are still viable at 14 days, although both proliferation and apoptosis increase at pathological strains.[74-77]

VECs were likely partially denuded from the valve tissues, which may have impacted the results because they have been shown to affect VIC mechanical and synthetic behaviour.[14, 45] VECs were visible on IHC sections, but partial denudation cannot be ruled out. Disinfection processes and storage conditions both impact cellular integrity that may have lead to the loss of some VECs, and this may have impacted VIC responses because of their modulatory effect.[45, 122] However, cold antibiotic disinfection causes minimal damage, and tissue handling and experimental stimulation processes in the comparative studies were similar, therefore the extent to which this may have influenced results across studies would have been small.[122]

The mechanical stimulation apparatus applied uniaxial stretch. Biaxial stimulation with appropriate circumferential and radial tensions would have provided a closer

approximation to the physiologic environment and maintained cross-coupling between directions, but circumferential cyclic stretch was a reasonable approximation for this project. Most collagen is aligned circumferentially, and it is the major determinant for valve mechanical properties in this direction. Since VICs are closely associated with collagen, and are known to deform with its realignment, the experimental mechanical environment was a reasonable facsimile for testing VIC responses. Biaxial mechanical testing would have been required if mechanical properties were being tested, but biomechanical responses were not sought in the present model.

There were also limitations of the experimental model regarding tissue strips. First, by cutting a circumferentially-oriented tissue strip from the leaflet, mechanical cross-coupling is eliminated. The majority of the elastin fibres would be cut and some collagen fibres as well. This would eliminate the majority of prestress in the tissue, and the ability of collagen fibres to recoil.[11] This would likely cause increased tissue extensibility. Second, the tissue strips were flat, which would alter the natural stress and strain fields since the natural curvature was absent. The present model used places both sides of the tissue in tension (no compression on the concave aspect), however while the valve is closed membrane tension is experienced throughout the tissue. This does ignore the layer-specific contributions, and the non-uniformity of the tissue. Since the biomechanics were altered from native conditions, this may also have affected VIC responses. Lastly, the ideal sample dimensions in uniaxial testing are long and skinny in order to have a strain distribution independent of the attachment method used. The grip-tissue sample interface and the immediate vicinity would have a complex strain field (Saint-Venant effect) that ideally would be eliminated by tissue excision. This effect could have been further reduced by using longer tissue strips, narrower tissue strips, or a combination. If the dimensions were altered, consideration would also have to be given to the maximum tissue length because the smaller semilunar valve leaflets would be the limiting factor assuming the gauge lengths were to remain equal, and to the minimum tissue width because of earlier failure with the further reduction of mechanical cross-coupling. Strain measurements become more reliable near the center of the tissue strip, although load-control, not strain-control, was used in the present study.

Tissue geometry and loading conditions also contributed to the difference in uniaxial strains found during preliminary work for the present project compared to those used in other strain-controlled studies.[74, 75, 77] The estimated strains for the present project were higher than those in other studies (low: 20-46 % vs. 10-15 %, respectively; high: 45-69 % vs. 15-20 %, respectively) (see Appendix C). The strain measurements were made by placing two markers on circumferential tissue strips in the center third, parallel to the direction of force application, and taking the difference between them from images in their unloaded and loaded states. These estimates are higher for a number of reasons. The tissues strips were relatively short and wide, and this would affect the strain measurement, since they are often higher in non-ideal samples.[123] The impact of this factor was reduced by using the markers near the center of the tissue instead of the grip-to-grip distance, however the tissue dimensions were still non-ideal. Mechanical cross-coupling between layers was also removed, and with the elastin fibres cut, which provides prestress and recoil, the tissues would also be more extensible. These estimates were made for reference only because load-control, not strain-control, was used in the current study. However, the differences in strain conditions found between the present study and the previous studies suggest the possibility that the loading state (both the strain and stress) of the samples may not be comparable. It also suggests that the changes in the loading states may not have been large enough to elicit responses for Cx43 and α-SMA, and that higher loads comparable to sever hypertension may be required.

A major limitation for the RT-PCR component of this study was its lack of dynamic range. Differences between the AV and PV compared to the MV for α-SMA transcription could not be investigated because the MV required different experimental conditions, therefore comparisons could not be made. The MV required 36-39 cycles for visual detection compared to 30 cycles for the AV and PV. Real-time RT-PCR is currently the most widely used method for investigating transcription because it is quantitative, has greater sensitivity, reproducibility, a large range of measurement, and eliminates a number of post-PCR processing steps.[111] Real-time RT-PCR has a dynamic range of $>10^7$ instead of ~10 for semi-quantitative RT-PCR, which would allow for comparison between valves.[111] This method can also detect much smaller significant changes compared to the ≥1.2-fold difference required in semi-quantitative RT-PCR.[117]

Similar to conventional semi-quantitative methods, procedural validation is time-consuming, but once the protocol is established, measurements could be completed much more quickly. Real-time RT-PCR machines generally have high through-put capacities because they have the ability to process plates containing multiple wells for samples. A common plate size, 96 wells, would allow for efficient sample measurements in duplicate or triplicate, which would greatly decrease experimental variability.

Antibody concentrations for IHC staining should be evaluated on fresh tissues based on the amount of positive stain expected, not solely the quality of the staining. Quality of staining was acceptable for this study because the relationships between the valves and loading conditions were of interest, and this could still be determined with a different baseline level of staining. By ensuring that the antibody titre had reasonable staining at the expected 'baseline' for tissues, comparisons between different studies would be easier.

Cell enumeration using stereology should be done using more images from multiple non-serial sections for each tissue in order to reduce user-introduced error from over- or under-sampling stained objects. The amount of work would be the same if the size of the point grid was increased.

Finally, a higher sample number should be used for the next study in order to increase statistical power. Some of the relationships that were just above significance may be significant at a higher power. Any tissues that were lost due to processing would also have a smaller effect on the power. Based on the results from this study and power-sample size calculations, a sample size of ≥ 8 would be appropriate.

References

1. Tirziu D, Giordano F, Simons M. Cell communications in the heart. Circulation. 2010; 122:928.

2. Sacks M, Yoganathan A. Heart valve function: A biomechanical perspective. Phil Trans R Soc B. 2007; 362:1369.

3. National Heart, Lung, and Blood Institute. Healthy heart cross-section <http://www.nhlbi.nih.gov/health//dci/Diseases/hvd/hvd_whatis.html>. Accessed January, 2013. National Institutes of Health, Bethesda, MD, 2011.

4. Berry GJ, Billingham ME. Normal Heart. In: Mills SE (ed). Histology for Pathologists. 3rd ed. Philadelphia: Lippincott Williams & Wilkins, 2007:527.

5. Martini FH, Timmons MJ. The Heart (Fig. 21.7). In: Martini FH, Timmons MJ, Tallitsch RB (eds). Human Anatomy. 4th ed. Benjamin Cummings, 2003:553.

6. Moeller AD. Remodelling of heart valves resulting from the physiological effects of pregnancy [dissertation]. Halifax, NS: Dalhousie University, Canada, 2007.

7. Combs M, Yutzey K. Heart valve development regulatory networks in development and disease. Circ Res. 2009; 105:408.

8. Schoen F. Cardiac valves and valvular pathology - update on function, disease, repair, and replacement. Cardiovasc Pathol. 2005; 14:189.

9. Liu AC, Joag VR, Gotlieb AI. The emerging role of valve interstitial cell phenotypes in regulating heart valve pathobiology. Am J Pathol. 2007; 171:1407.

10. Donnelly K. Cardiac valvular pathology: Comparative pathology and animal models of acquired cardiac valvular diseases. Toxicol Pathol. 2008; 36:204.

11. Vesely I. The role of elastin in aortic valve mechanics. J Biomech. 1998; 31:115.

12. McCarthy K, Ring L, Rana B. Anatomy of the mitral valve: Understanding the mitral valve complex in mitral regurgitation. Eur J Echocardiogr. 2010; 11:i3.

13. Schoen F. Evolving concepts of cardiac valve dynamics the continuum of development, functional structure, pathobiology, and tissue engineering. Circulation. 2008; 118:1864.

14. Simmons C. Aortic valve mechanics: An emerging role for the endothelium. J Am Coll Cardiol. 2009; 53:1456.

15.   Rabkin-Aikawa E, Farber M, Aikawa M, Schoen FJ. Dynamic and reversible changes of interstitial cell phenotype during remodeling of cardiac valves. J Heart Valve Dis. 2004; 13:841.

16.   Akat K, Borggrefe M, Kaden J. Aortic valve calcification: Basic science to clinical practice. Br Heart J. 2008; 95:616.

17.   Aikawa E, Whittaker P, Farber M, et al. Human semilunar cardiac valve remodeling by activated cells from fetus to adult: Implications for postnatal adaptation, pathology, and tissue engineering. Circulation. 2006; 113:1344.

18.   Armstrong EJ, Bischoff J. Heart valve development: Endothelial cell signaling and differentiation. Circ Res. 2004; 95:459.

19.   Gittenberger-de Groot A, Bartelings M, Deruiter M, Poelmann R. Basics of cardiac development for the understanding of congenital heart malformations. Pediatr Res. 2005; 57:169.

20.   Hinton RB, Jr., Lincoln J, Deutsch GH, et al. Extracellular matrix remodeling and organization in developing and diseased aortic valves. Circ Res. 2006; 98:1431.

21.   Latif N, Sarathchandra P, Taylor P, Antoniw J, Brand N, Yacoub M. Characterization of molecules mediating cell-cell communication in human cardiac valve interstitial cells. Cell Biochem Biophys. 2006; 45:255.

22.   Latif N, Sarathchandra R, Taylor R, Antoniw J, Yacoub M. Molecules mediating cell-ECM and cell-cell communication in human heart valves. Cell Biochem Biophys. 2005; 43:275.

23.   Alexander DB, Goldberg GS. Transfer of biologically important molecules between cells through gap junction channels. Curr Med Chem. 2003; 10:2045.

24.   Laird DW. Life cycle of connexins in health and disease. Biochem J. 2006; 394:527.

25.   Dbouk H, Mroue R, El-Sabban M, Talhouk R. Connexins: A myriad of functions extending beyond assembly of gap junction channels. Cell Commun Signal. 2009; 7:4.

26.   Laird DW. Connexin phosphorylation as a regulatory event linked to gap junction internalization and degradation. BBA-Biomembranes. 2005; 1711:172.

27.   Figueroa X, Duling B. Gap junctions in the control of vascular function. Antioxid Redox Sign. 2009; 11:251.

28.   Sohl G, Willecke K. Gap junctions and the connexin protein family. Cardiovasc Res. 2004; 62:228.

29.   Risek B, Guthrie S, Kumar N, Gilula N. Modulation of gap junction transcript and protein expression during pregnancy in the rat. J Cell Biol. 1990; 110:269.

30.   Cowan D, Lye S, Langille B. Regulation of vascular connexin43 gene expression by mechanical loads. Circ Res. 1998; 82:786.

31.   Scott C, Tattersall D, O'Toole E, Kelsell D. Connexins in epidermal homeostasis and skin disease. BBA-Biomembranes. 2012; 1818:1952.

32.   Wang Y, Choe M, Choi S, Jin U, Kim C, Seo E. Increased expression of Connexin43 on the aortic valve in the hypercholesterolemic rabbit model. J Invest Surg. 2009; 22:98.

33.   Shanker A, Green K, Yamada K, Saffitz J. Matrix protein-specific regulation of Cx43 expression in cardiac myocytes subjected to mechanical load. Circ Res. 2005; 96:558.

34.   Salameh A, Wustmann A, Karl S, Blanke K, Apel D, Rojas Gomez D. Cyclic mechanical stretch induces cardiomyocyte orientation and polarization of the gap junction protein connexin43. Circ Res. 2010; 106:1592.

35.   Peters N, Green C, Poole-Wilson P, Severs N. Reduced content of connexin43 gap junctions in ventricular myocardium from hypertrophied and ischemic hearts. Circulation. 1993; 88:864.

36.   Vetter C, Zweifel M, Zuppinger C, et al. Connexin 43 expression in human hypertrophied heart due to pressure and volume overload. Physiol Res. 2010; 59:35.

37.   Brisset A, Isakson B, Kwak B. Connexins in vascular physiology and pathology. Antioxid Redox Sign. 2009; 11:267.

38.   Ou C, Orsino A, Lye S. Expression of connexin-43 and connexin-26 in the rat myometrium during pregnancy and labor is differentially regulated by mechanical and hormonal signals. Endocrinology. 1997; 138:5398.

39.   McNeilly C, Banes A, Benjamin M, Ralphs J. Tendon cells in vivo form a three dimensional network of cell processes linked by gap junctions. J Anat. 1996; 189:593.

40.   Lo I, Chi S, Ivie T, Frank C, Rattner J. The cellular matrix: A feature of tensile bearing dense soft connective tissues. Histol Histopathol. 2002; 17:523.

41.   Wall M, Otey C, Qi J, Banes A. Connexin 43 is localized with actin in tenocytes. Cell Motil Cytoskel. 2007; 64:121.

42.   Wall ME, Banes AJ. Early responses to mechanical load in tendon: Role for calcium signaling, gap junctions and intercellular communication. J Musculoskelet Neuronal Interact. 2005; 5:70.

43.   Waggett A, Benjamin M, Ralphs J. Connexin 32 and 43 gap junctions differentially modulate tenocyte response to cyclic mechanical load. Eur J Cell Biol. 2006; 85:1145.

44.   Ehrlich H, Diez T. Role for gap junctional intercellular communications in wound repair. Wound Rep Reg. 2003; 11:481.

45.   Butcher J, Nerem R. Valvular endothelial cells regulate the phenotype of interstitial cells in co-culture: Effects of steady shear stress. Tissue Eng. 2006; 12:905.

46.   Balachandran K, Sucosky P, Yoganathan A. Hemodynamics and mechanobiology of aortic valve inflammation and calcification. Int J Inflamm. 2011; 2011:263870.

47.   Sacks M. On the biomechanics of heart valve function. J Biomech. 2009; 42:1804.

48.   Tibayan F, Rodriguez F, Langer F, et al. Increases in mitral leaflet radii of curvature with chronic ischemic mitral regurgitation. J Heart Valve Dis. 2004; 13:772.

49.   Balachandran K. Aortic valve mechanobiology - the effect of cyclic stretch [dissertation]. Atlanta, Ga.: Georgia Institute of Technology, 2010.

50.   Grashow J, Sacks M, Liao J, Yoganathan A. Planar biaxial creep and stress relaxation of the mitral valve anterior leaflet. Ann Biomed Eng. 2006; 34:1509.

51.   Billiar K, Sacks M. Biaxial mechanical properties of the natural and glutaraldehyde treated aortic valve cusp - part I: Experimental results. J Biomech Eng. 2000; 122:23.

52.   Ethier RC, Simmons CA. Introductory Biomechanics: From Cells to Organisms. New York: Cambridge University Press, 2007.

53.   Pierlot C, Wells S, Lee JM. Pregnancy-Induced Remodeling of Heart Valves. Atlanta, Georgia: Biomedical Engineering Society Annual Meeting, 2012.

54.   Ingber DE. Cellular mechanotransduction: Putting all the pieces together again. FASEB J. 2006; 20:811.

55.   Huang H, Liao J, Sacks M. In-situ deformation of the aortic valve interstitial cell nucleus under diastolic loading. J Biomech Eng. 2007; 129:880.

56.   Kershaw J, Misfeld M, Sievers H, Yacoub M, Chester A. Specific regional and directional contractile responses of aortic cusp tissue. J Heart Valve Dis. 2004; 13:798.

57.   Bershadsky A, Balaban N, Geiger B. Adhesion-dependent cell mechanosensitivity. Annu Rev Cell Dev Biol. 2003; 19:677.

58.   Rao S, Winter J. Adhesion molecule-modified biomaterials for neural tissue engineering. Front Neuroeng. 2009; 2:6.

59.   Saffitz J, Kleber A. Effects of mechanical forces and mediators of hypertrophy on remodeling of gap junctions in the heart. Circ Res. 2004; 94:585.

60.   Yamada K, Green K, Samarel A, Saffitz J. Distinct pathways regulate expression of cardiac electrical and mechanical junction proteins in response to stretch. Circ Res. 2005; 97:346.

61.   Giepmans B. Gap junctions and connexin-interacting proteins. Cardiovasc Res. 2004; 62:233.

62.   Watson P. Mechanical activation of signaling pathways in the cardiovascular system. Trends Cardiovasc Med. 1996; 6:73.

63.   Aldous I, Lee JM, Wells S. Differential changes in the molecular stability of collagen from the pulmonary and aortic valves during the fetal-to-neonatal transition. Ann Biomed Eng. 2010; 38:3000.

64.   Stephens EH, Grande-Allen KJ. Age-related changes in collagen synthesis and turnover in porcine heart valves. J Heart Valve Dis. 2007; 16:672.

65.   Wells S, Pierlot C, Moeller A. Physiological remodeling of the mitral valve during pregnancy. Am J Physiol Heart Circ Physiol. 2012; 303:H878.

66.   National Heart, Lung, and Blood Institute. What is High Blood Pressure? <http://www.nhlbi.nih.gov/health/health-topics/topics/hbp/>. Accessed July 2013. National Institutes of Health, Bethesda, MD, 2012.

67.   Gorczynski A, Trenkner M, Anisimowicz L, et al. Biomechanics of the pulmonary autograft valve in the aortic position. Thorax. 1982; 37:535.

68.   Joyce E, Liao J, Schoen F, Mayer J, Sacks M. Functional collagen fiber architecture of the pulmonary heart valve cusp. Ann Thorac Surg. 2009; 87:1240.

69.   Schoof P, Takkenberg J, van Suylen R, Zondervan P, Hazekamp M, Dion R. Degeneration of the pulmonary autograft: An explant study. J Thorac Cardiovasc Surg. 2006; 132:1426.

70.   Mookhoek A, de Heer E, Bogers A, Takkenberg J, Schoof P. Pulmonary autograft valve explants show typical degeneration. J Thorac Cardiovasc Surg. 2010; 139:1416.

71.   Weston M, Yoganathan A. Biosynthetic activity in heart valve leaflets in response to in vitro flow environments. Ann Biomed Eng. 2001; 29:752.

72.   Xing Y, Warnock J, He Z, Hilbert S, Yoganathan A. Cyclic pressure affects the biological properties of porcine aortic valve leaflets in a magnitude and frequency dependent manner. Ann Biomed Eng. 2004; 32:1461.

73.   Xing Y, He Z, Warnock J, Hilbert S, Yoganathan A. Effects of constant static pressure on the biological properties of porcine aortic valve leaflets. Ann Biomed Eng. 2004; 32:555.

74.   Balachandran K, Sucosky P, Jo H, Yoganathan A. Elevated cyclic stretch alters matrix remodeling in aortic valve cusps: Implications for degenerative aortic valve disease. Am J Physiol Heart Circ Physiol. 2009; 296:H756.

75.   Balachandran K, Konduri S, Sucosky P, Jo H, Yoganathan A. An ex vivo study of the biological properties of porcine aortic valves in response to circumferential cyclic stretch. Ann Biomed Eng. 2006; 34:1655.

76.   Lacerda CMR, Kisiday J, Johnson B, Orton EC. Local serotonin mediates cyclic strain-induced phenotype transformation, matrix degradation, and glycosaminoglycan synthesis in cultured sheep mitral valves. Am J Physiol Heart Circ Physiol. 2012; 302:H1983.

77.   Merryman W, Lukoff H, Long R, Engelmayr G, Hopkins R, Sacks M. Synergistic effects of cyclic tension and transforming growth factor-beta 1 on the aortic valve myofibroblast. Cardiovasc Pathol. 2007; 16:268.

78.   Konduri S, Xing Y, Warnock J, He Z, Yoganathan A. Normal physiological conditions maintain the biological characteristics of porcine aortic heart valves: An ex vivo organ culture study. Ann Biomed Eng. 2005; 33:1158.

79.   Rodriguez K, Masters K. Regulation of valvular interstitial cell calcification by components of the extracellular matrix. J Biomed Mater Res A. 2009; 90a:1043.

80.   Barber J, Kasper F, Ratliff N, Cosgrove D, Griffin B, Vesely I. Mechanical properties of myxomatous mitral valves. J Thorac Cardiovasc Surg. 2001; 122:955.

81.   Rabkin E, Aikawa M, Stone J, Fukumoto Y, Libby P, Schoen F. Activated interstitial myofibroblasts express catabolic enzymes and mediate matrix remodeling in myxomatous heart valves. Circulation. 2001; 104:2525.

82.   Disatian S, Ehrhart E, Zimmerman S, Orton E. Interstitial cells from dogs with naturally occurring myxomatous mitral valve disease undergo phenotype transformation. J Heart Valve Dis. 2008; 17:402.

83.   Sacks M, Schoen F, Mayer J. Bioengineering challenges for heart valve tissue engineering. Annu Rev Biomed Eng. 2009; 11:289.

84.   Concha M, Aranda PJ, Casares J, et al. The ross procedure. J Card Surg. 2004; 19:401.

85.   Stradins P, Lacis R, Ozolanta I, et al. Comparison of biomechanical and structural properties between human aortic and pulmonary valve. Eur J Cardio-Thorac. 2004; 26:634.

86.   Rabkin-Aikawa E, Aikawa M, Farber M, Kratz J, Garcia Cardena G. Clinical pulmonary autograft valves: Pathologic evidence of adaptive remodeling in the aortic site. J Thorac Cardiovasc Surg. 2004; 128:552.

87.   Aldous I, Veres S, Jahangir A, Lee JM. Differences in collagen cross-linking between the four valves of the bovine heart: A possible role in adaptation to mechanical fatigue. Am J Physiol Heart Circ Physiol. 2009; 296:H1898.

88.   Merryman WD, Liao J, Parekh A, Candiello JE, Lin H, Sacks MS. Differences in tissue-remodeling potential of aortic and pulmonary heart valve interstitial cells. Tissue Eng. 2007; 13:2281.

89.   Merryman WD, Youn I, Lukoff HD, et al. Correlation between heart valve interstitial cell stiffness and transvalvular pressure: Implications for collagen biosynthesis. Am J Physiol Heart Circ Physiol. 2006; 59:224.

90.   Bouchard-Martel J, Roussel E, Drolet M, Arsenault M, Couet J. Interstitial cells from left-sided heart valves display more calcification potential than from right-sided valves: An in-vitro study of porcine valves. J Heart Valve Dis. 2009; 18:421.

91.   Nkomo V, Gardin J, Skelton T, Gottdiener J, Scott C. Burden of valvular heart diseases: A population-based study. Lancet. 2006; 368:1005.

92.   Goldbarg SH. Insights into degenerative aortic valve disease. J Am Coll Cardiol. 2007; 50:1205.

93. Thayer P, Balachandran K, Rathan S, et al. The effects of combined cyclic stretch and pressure on the aortic valve interstitial cell phenotype. Ann Biomed Eng. 2011; 39:1654.

94. Invitrogen® - Life Technologies®. RNA Quantitation is an Important and Necessary Step Prior to most RNA Analysis Methods RNA Technical Resources from Ambion®. 2012; RNA Isolation - TechNotes.

95. Cromey D. Avoiding twisted pixels: Ethical guidelines for the appropriate use and manipulation of scientific digital images. Sci Eng Ethics. 2010; 16:639.

96. McPherson MJ, Moller SG. PCR. 2nd ed. New York, NY: Taylor & Francis Group, 2006.

97. Durbin AD, Gotlieb AI. Advances towards understanding heart valve response to injury. Cardiovasc Pathol. 2002; 11:69.

98. Laird D, Puranam K, Revel J. Turnover and phosphorylation dynamics of Connexin43 gap junction protein in cultured cardiac myocytes. Biochem J. 1991; 273:67.

99. Lampe P, Lau A. The effects of connexin phosphorylation on gap junctional communication. Int J Biochem. 2004; 36:1171.

100. Kadle R, Zhang J, Nicholson B. Tissue-specific distribution of differentially phosphorylated forms of Cx43. Mol Cell Biol. 1991; 11:363.

101. Jahn E, Classenlinke I, Kusche M, Beier H, Traub O. Expression of gap junction connexins in the human endometrium throughout the menstrual-cycle. Hum Reprod. 1995; 10:2666.

102. Dal-Bianco J, Aikawa E, Bischoff J, Guerrero J, Handschumacher M, Sullivan S. Active adaptation of the tethered mitral valve insights into a compensatory mechanism for functional mitral regurgitation. Circulation. 2009; 120:334.

103. Mandarim-de-Lacerda CA, Fernandes Santos C, Aguila M. Image analysis and quantitative morphology. In: Hewitson T, Darby I (eds). Histology Protocols (Methods in Molecular Biology). Clifton, N.J.: Humana Press, 2010:211.

104. Goldstein N, Hewitt S, Taylor C, Yaziji H, Hicks D. Recommendations for improved standardization of immunohistochemistry. Appl Immunohistochem Mol Morphol. 2007; 15:124.

105. Mouton PR. Principles and Practices of Unbiased Stereology: An Introduction for Bioscientists. Baltimore: Johns Hopkins University Press, 2002.

106. Wang J, Zohar R, McCulloch C. Multiple roles of alpha-smooth muscle actin in mechanotransduction. Exp Cell Res. 2006; 312:205.

107. Schmidt D, Hoerstrup S. Tissue engineered heart valves based on human cells. Swiss Med Wkly. 2006; 136:618.

108. Rabkin E, Schoen FJ. Cardiovascular tissue engineering. Cardiovasc Pathol. 2002; 11:305.

109. Hjortnaes J, Bouten C, Van Herwerden L, Grundeman P, Kluin J. Translating autologous heart valve tissue engineering from bench to bed. Tissue Eng Pt B-Rev. 2009; 15:307.

110. Rabkin E, Hoerstrup S, Aikawa M, Mayer J, Schoen F. Evolution of cell phenotype and extracellular matrix in tissue-engineered heart valves during in-vitro maturation and in-vivo remodeling. J Heart Valve Dis. 2002; 11:308.

111. Pfaffl MW. Quantification strategies in real-time PCR. In: Bustin SA (ed). A-Z of Quantitative PCR. La Jolla, CA, USA: International University Line, 2004:87.

112. Invitrogen® - Ambion® RNA (Protocol). RNAlater® Tissue Collection: RNA Stabilization Solution. Life Technologies Corporation. 2011.

113. Bustin S, Benes V, Nolan T, Pfaffl M. Quantitative real-time RT-PCR - a perspective. J Mol Endocrinol. 2005; 34:597.

114. Bustin SA, Benes V, Garson JA, et al. The MIQE guidelines: Minimum information for publication of quantitative real-time PCR experiments. Clin Chem. 2009; 55:611.

115. Bustin S. Quantification of mRNA using real-time reverse transcription PCR (RT-PCR): Trends and problems. J Mol Endocrinol. 2002; 29:23.

116. Qiagen (General Protocol). RNA: Guidelines for RT-PCR. 67.

117. Marone M, Mozzetti S, De Ritis D, Pierelli L, Scambia G. Semiquantitative RT-PCR analysis to assess the expression levels of multiple transcripts from the same sample. Biol Proc Online. 2001; 3:19.

118. Ramos-Vara J. Technical aspects of immunohistochemistry. Vet Pathol. 2005; 42:405.

119. Werner M, Chott A, Fabiano A, Battifora H. Effect of formalin tissue fixation and processing on immunohistochemistry. Am J Surg Pathol. 2000; 24:1016.

120.   Buchwalow IB, Böcker W. Immunohistochemistry Basics and Methods. Berlin; London: Springer, 2010.

121.   Hewitson T, Wigg B, Becker G. Tissue preparation for histochemistry: fixation, embedding, and antigen retrieval for light microscopy. In: Hewitson T, Darby I (eds). Histology Protocols (Methods in Molecular Biology). Clifton, N.J.: Humana Press, 2010:3.

122.   Crescenzo D, Hilbert S, Messier R, Domkowski P, Barrick M. Human cryopreserved homografts - electron-microscopic analysis of cellular injury. Ann Thorac Surg. 1993; 55:25.

123.   Waldman S, Lee JM. Effect of sample geometry on the apparent biaxial mechanical behaviour of planar connective tissues. Biomaterials. 2005; 26:7504.

Appendix A – Supply List

Stimulation

Company and Products	Catalog Number
Oulton's Meats (Windsor, NS)	
Porcine heart valves	---
BD Falcon	
6-Well sterile tissue culture plate	353046
Custom	
Grips, plates, slide guide, weights	---
Fisher Scientific	
10% neutral buffered formalin	23-245-684
Invitrogen	
Dulbecco's Modified Eagle's medium	11995-073
Fetal bovine serum	A2617DJ
Fungizone	15290-018
RNAlater®	AM7024
Live/ dead viability/ cytotoxicity kit	L3224
Kimberly-Clark	
Kimguard KC100 sterilization wrap, 50 cm x 50 cm	10720
Qosina	
Stimulation containers – bottom (90 mL, 48 mm opening)	99983
Stimulation containers – top (90 mL, 53 mm opening)	99982

RNA Extraction and RT-PCR

Company and Products	Catalog Number
B. Braun Biotech (Sartorius)	
Glass beads (1 mm diameter)	BBI-8541809
BioShop	
Agarose (biotechnology grade)	AGA001.500
TBE buffer, 10x ez-pak (bioultrapure grade)	TBE101.105
Fermentas (now part of Thermo Fisher Scientific)	
Top Vision® LE GQ Agarose	R0491
Taq DNA polymerase	EP0402
GeneRuler® 100 bp plus DNA ladder	SM0323
6x DNA loading dye	R0611
2x RNA loading dye	R0641
RiboRuler® high range RNA ladder	SM1823
IDT Technology	
Primers	Custom
Invitrogen	
Ambion® RNAlater	AM7024
SuperScript® III First Strand Synthesis System for RT-PCR	18080-051
Ethidium bromide	15585-011
Qiagen	
RNeasy® Mini Kit	74106
Roche	
FastStart PCR MasterMix	04710436001
Sigma Aldrich Canada	
β-Mercaptoethanol	M-6250-250ML
Sorenson BioScience	
10 μL Barrier tip pipettes, sterile	380000
100 μL Barrier tip pipettes, sterile, low binding	36060T
1000 μL Barrier tip pipettes, sterile, low binding	14200T
Thermo Fisher Scientific	
Nalgene® cryogenic vial (sterile), PP, 1.2 mL	5000-0012
Glass beads solid (3 mm diameter)	11-312A

Immunohistochemistry

Company and Products	Catalog Number
Abcam	
Rabbit polyclonal to GJB2 (Cx26)	ab38584
Rabbit polyclonal IgG	ab27478
Dako	
Protein block	X0909
Biotinylated universal link (kit)	K0690
Streptavidin horseradish peroxidase (kit)	K0690
Diaminobenzidine horseradish peroxidase	K3468
Monoclonal mouse anti-human smooth muscle actin	M0851
Mouse IgG2a	X 0943
Invitrogen	
Hydrogen peroxide	216763-100mL
Santa Cruz	
Connexin 43 (C-20) (Rabbit polyclonal)	sc-6560-R
Rabbit polyclonal IgG	sc2027
Sigma Aldrich	
Mayer's hematoxylin solution	MHS32-1L
Thermo Fisher Scientific	
Fisherbrand® Superfrost® Plus microscope slides	12-550-15
Fisherbrand® microscope cover glasses	12-545-M
Richard-Allan Scientific® Cytoseal® 60 mounting medium	8310-16

Instruments

Company and Products	Catalog Number
Stimulation	
Custom	
Cycling apparatus	---
RNA Extraction and RT-PCR	
B. Braun Biotech	
Mikro-Dismembrator U	BBI-8531730
Biometra	
T*personal* Combi PCR machine	050-552
BioRad	
PowerPac basic power supply	164-5050
Mini sub cell GT	166-4270
Labconco	
FreeZone 4.5 Liter freeze dry system	7740040
Thermo Fisher Scientific	
GeneQuant® Pro spectrophotometer	10035024
Immunohistochemistry	
Leica	
Microtome	RM2255
Tissue processor	ASP300
Zeiss	
Axioplan 2 microscope	*
Axiocam HRc digital camera	*

* Accessed at the Cellular Microscopy Digital Imaging (CMDI) facility at Dalhousie University

Appendix B – Solutions

The PBS and buffer solutions used for stimulation and histology were formulated as 20x stock solutions (100x for antibiotics). They were diluted to 1x solutions and pH balanced if required before use.

Company and Products	Quantity	Catalog Number
PBS (1x)		
Sigma Aldrich		
Potassium phosphate monobasic	0.2 g/L	229806-25G
Sodium chloride	8.0 g/L	S1679-1KG
Sodium phosphate dibasic	1.15 g/L	S9763-500G
Citrate buffer, pH 6 (1x)		
Sigma Aldrich		
Citric acid monohydrate	0.265 g/L	C7129-500G
Hydrochloric acid, 1.0 N	As req'd	H9892-100ML
Invitrogen		
50% Tween® 20 solution	0.5 mL/L	AM7024
Tris-EDTA buffer, pH 9 (1x)		
Sigma Aldrich		
Trizma hydrochloride	1.58 g/L	T3253-250G
Ethylenediaminetetraacetic acid	0.29 g/L	E9884-100G
Sodium hydroxide, 0.1N	As req'd	2105-50ML
Invitrogen		
50% Tween® 20 solution	0.5 mL/L	AM7024
Ampicillin-streptomycin (1x)		
Sigma Aldrich		
Ampicillin	0.10 g/L	A1593-25G
Streptomycin	0.10 g/L	S9137-25G

Appendix C – Raw data

This section contains the raw data collected for this study.

Heart ID	Valve	Fresh	No	Low	High
1	AV	1.00	0.76	0.12	4.99
2	AV	1.00	0.38	0.04	0.25
3	AV	1.00	0.41	0.91	0.03
4	AV	1.00	1.32	0.28	1.47
5	AV	1.00	0.18	0.00	0.00
6	AV	1.00	0.61	0.06	1.70
1	PV	1.00	0.28	0.95	3.29
2	PV	ND	1.00	0.43	1.20
3	PV	1.00	0.83	2.44	5.48
4	PV	1.00	0.38	0.10	1.50
5	PV	1.00	3.16	1.38	1.98
6	PV	1.00	0.23	0.07	0.13
1	MV	ND	ND	ND	ND
2	MV	ND	ND	ND	ND
3	MV	ND	ND	ND	ND
4	MV	1.00	0.03	0.34	0.37
5	MV	1.00	0.23	ND	ND
6	MV	ND	ND	ND	ND

Table 11 – Raw RT-PCR data for α-SMA. Data is expressed relative to fresh tissues. ND represents non-detectable signals at the measured level. (Section 5.1.1)

Heart ID	Valve	Fresh	No	Low	High
1	AV	79.05	79.40	63.75	53.92
2	AV	44.45	31.40	52.24	28.80
3	AV	62.96	64.75	30.96	18.26
4	AV	62.86	22.41	58.98	45.39
5	AV	37.71	24.69	48.61	70.58
6	AV	36.68	37.29	15.40	19.69
1	PV	64.98	60.32	38.45	77.87
2	PV	59.87	37.83	14.87	53.45
3	PV	29.54	43.46	2.29	29.92
4	PV	41.76	29.35	72.45	68.44
5	PV	44.99	31.41	64.73	40.72
6	PV	64.48	17.36	68.21	65.23
1	MV	48.16	59.47	74.91	52.79
2	MV	49.91	25.74	46.67	23.85
3	MV	72.88	17.94	47.77	70.94
4	MV	46.84	67.78	24.21	18.35
5	MV	67.92	9.53	52.45	21.21
6	MV	45.08	19.05	47.53	34.95

Table 12 – Raw % positively stained cells for α-SMA IHC. (Section 5.1.2)

Heart ID	Valve	Fresh	No	Low	High
1	AV	1.00	2.48	4.15	3.87
2	AV	1.00	1.06	3.48	2.61
3	AV	ND	1.00	0.95	0.55
4	AV	1.00	1.93	3.83	4.83
5	AV	1.00	1.14	1.99	0.58
6	AV	1.00	0.90	0.93	1.40
1	PV	1.00	1.11	0.47	1.13
2	PV	1.00	2.10	2.52	1.10
3	PV	1.00	0.20	0.30	0.16
4	PV	1.00	1.30	1.76	1.70
5	PV	1.00	4.31	6.51	5.89
6	PV	1.00	2.12	0.43	0.42
1	MV	1.00	3.34	4.99	4.14
2	MV	1.00	2.34	3.07	0.28
3	MV	1.00	1.50	0.17	0.01
4	MV	1.00	0.20	0.66	1.11
5	MV	1.00	0.75	2.45	2.59
6	MV	1.00	1.00	3.18	0.55

Table 13 – Raw RT-PCR data for Cx43. Data is expressed relative to fresh tissues. ND represents non-detectable signals at the measured level. (Section 5.2.1)

Heart ID	Valve	Fresh	No	Low	High
1	AV	28.76	40.74	51.53	44.95
2	AV	16.62	23.31	33.74	24.69
3	AV	56.31	56.36	48.02	25.47
4	AV	54.04	33.61	53.06	74.03
5	AV	81.77	46.64	51.34	56.75
6	AV	41.49	50.10	48.86	69.04
1	PV	61.62	18.71	83.74	69.78
2	PV	21.61	10.85	50.24	33.61
3	PV	35.09	55.63	28.28	TL
4	PV	69.49	42.29	57.14	TL
5	PV	30.89	32.51	TL	66.81
6	PV	34.78	52.80	45.38	68.25
1	MV	72.37	68.83	97.55	34.57
2	MV	28.01	20.86	62.15	33.63
3	MV	51.77	25.97	TL	86.23
4	MV	60.58	82.15	55.20	66.27
5	MV	48.42	59.37	39.46	77.59
6	MV	24.38	36.76	48.31	34.45

Table 14 – Raw % positively stained cells for Cx43 IHC. TL represents tissues lost during processing. (Section 5.2.2)

Heart ID	Valve	Fresh	No	Low	High
1	AV	81.62	62.96	22.82	61.33
2	AV	64.75	66.21	58.15	31.87
3	AV	49.90	73.26	73.19	36.13
4	AV	59.26	53.58	53.30	51.83
5	AV	43.52	80.03	53.98	57.01
6	AV	41.68	72.77	62.73	72.77
1	PV	68.50	46.88	92.86	93.49
2	PV	62.98	33.91	24.81	71.09
3	PV	42.46	32.87	23.50	33.59
4	PV	51.30	56.67	51.31	34.95
5	PV	54.82	61.56	77.39	51.78
6	PV	63.78	73.29	91.38	70.47
1	MV	35.72	66.61	84.60	50.03
2	MV	75.61	33.53	99.52	70.75
3	MV	27.65	36.36	12.96	18.89
4	MV	73.62	38.24	52.22	60.76
5	MV	52.44	88.61	75.47	45.49
6	MV	58.12	57.45	65.72	59.24

Table 15 – Raw % positively stained cells for Cx26 IHC. (Section 5.3)

Valve	Condition (n=3)	No Weight (mm)	With Weight (mm)	% Stretch (With-No/ No x 100)
AV	Low	2.54	2.94	15.75
		2.65	3.19	20.38
		2.78	3.42	23.02
				Avg = 19.72
	High	1.74	2.43	39.66
		2.20	3.43	55.91
		2.12	2.96	39.62
				Avg = 45.06
MV	Low	2.35	2.59	10.21
		1.90	2.21	16.32
		2.69	3.55	31.97
				Avg = 19.50
	High	1.73	2.27	31.21
		2.03	3.76	85.22
		2.76	5.00	81.16
				Avg = 65.86
PV	Low	2.66	3.69	38.72
		2.45	3.90	59.18
		2.33	3.29	41.20
				Avg = 46.37
	High	2.75	4.18	52.00
		1.81	3.56	96.69
		1.83	2.89	57.92
				Avg = 68.87

Table 16 – Preliminary strain data for each valve and loading condition. Strains were determined by measuring the distance between two small markers attached to the leaflet surface in the unloaded and the loaded state. (Section 4)

Slide	Count 1 (%)	Count 2 (%)	Difference (%)
1	67.3	65.8	1.5
2	68.8	74.8	6.0
3	97.5	98.8	1.2
4	34.6	33.2	1.4
5	35.1	43.3	8.2
6	40.7	35.1	5.6
7	51.5	46.9	4.7
8	45.0	43.9	1.1
9	61.6	54.4	7.2
10	18.7	19.7	0.9
11	83.7	86.4	2.6
12	69.8	78.8	9.0
			Avg = 4.1

Table 17 – Point count repeatability. Twelve slides that had been stained at the same time were counted twice using the point count method. The grid overlay was placed randomly for each image and each count. (Section 4)

Appendix D – Enlarged IHC Image

This enlarged image is the fresh PV tissue from **Error! Reference source not found.** (Section 5.1.2). It shows in greater detail the tissue and features of interest for α-SMA staining specifically, and IHC staining in general. The brown stained cells are positive for the antibody. The blue unstained cells are stained with hematoxylin. The light blue in the background is the ECM.
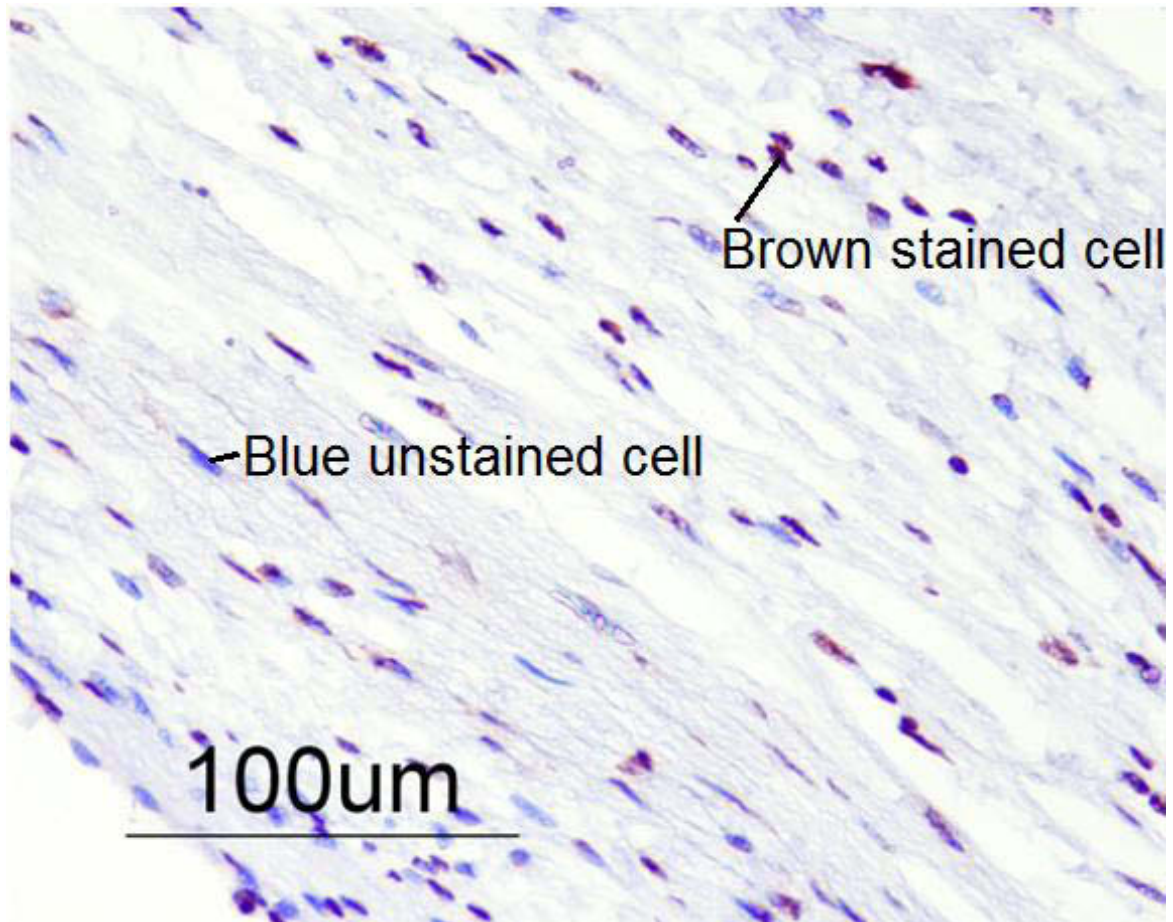
Appendix E – Power Analysis

Post hoc calculations were done using G*Power © (version 3.1.5) for MANOVA. The sample size for future work was calulated using data from the present study. (Section 6)

F tests - MANOVA: Repeated measures, within-between

Analysis: Compute required sample size

Input: α err prob   =   0.05

             Power (1-β err prob)   =   0.8

             Number of groups   =   3

             Number of measurements   =   4

Output: Total sample size   =   22

In order to have equal sample numbers in each group, n = 8 for each group would be required.

Appendix F – Copyright Permissions

PEARSON

Legal/Permissions
One Lake Street
Upper Saddle River, NJ 07458
Fax: 201-236-3290
Phone: 201-236-3564
Cheryl.Freeman@Pearson.com

Mar 25, 2013

PE Ref # 176686

KAREN L. O'MALLEY
Dalhousie University
Halifax, NS
CANADA B3H 4R2

Dear Ms. O'Malley:

You have our permission to include content from our text, *HUMAN ANATOMY, 4th Ed.*
by MARTINI, FREDERIC H.; TIMMONS, MICHAEL J.; TALLITSCH, ROBERT B.,
in your Master of Applied Science studies at DALHOUSIE UNIVERSITY.

Content to have 5 printed copies, plus online distribution through Library and Archives of Canada
(published in PDF format):

- Figure 21.7 Gap junction formation in heart valves in response to mechanical loading

Please credit our material as follows:
Figs. 21.3 p. 553 from HUMAN ANATOMY, 4th ed. by Frederic H. Martini, Michael J. Timmons
and Robert B. Tallitsch. Copyright © 2003 by Frederic H. Martini, Inc. Michael J. Timmons

Sincerely,

Cheryl Freeman, Permissions Administrator

March 14, 2013

Andrew Moeller

I am preparing my Master of Applied Science thesis for submission to the Faculty of Graduate Studies at Dalhousie University, Halifax, Nova Scotia, Canada. I am seeking your permission to include an image with some modification from the following document in the thesis:

Moeller AD. Remodelling of heart valves resulting from the physiological effects of pregnancy [dissertation]. Halifax, NS: Dalhousie University, Canada, 2007.
    Image: Figure 1.1.2, p. 4

Canadian graduate theses are reproduced by the Library and Archives of Canada (Formerly National Library of Canada) through a non-exclusive, world-wide license to reproduce, load, distribute, or sell theses. I am also seeking your permission for the material above to be reproduced and distributed by the LAC (NLC). Further details about the LAC (NLC) thesis program are available on the LAC (NLC) website (www.nlc-bcn.ca).

Full publication details and a copy of this permission letter will be included in the thesis.

Yours sincerely,

Karen O'Malley

_____

Permission is granted for:

a)   the inclusion of the material described above in your thesis.

b)   for the material described above to be included in the copy of your thesis that is sent to the Library and Archives of Canada (formerly National Library of Canada) for reproduction and distribution.

Name: Andrew Moeller   Title: Internal Medicine Resident

Signature: Date: 2013/03/14

January 17, 2013

Katherine E. Yutzey
Division of Molecular Cardiovascular Biology
Cincinnati Children's Hospital Medical Center ML7020
240 Albert Sabin Way
Cincinnati, OH   45229

I am preparing my Master of Applied Science thesis for submission to the Faculty of Graduate Studies at Dalhousie University, Halifax, Nova Scotia, Canada. I am seeking your permission to include an image with some modification from the following document in the thesis:

Combs M, Yutzey K. Heart valve development regulatory networks in development and disease. Circ Res. 2009; 105(5):408.
        Image: Figure 1, p. 409

Canadian graduate theses are reproduced by the Library and Archives of Canada (Formerly National Library of Canada) through a non-exclusive, world-wide license to reproduce, load, distribute, or sell theses. I am also seeking your permission for the material above to be reproduced and distributed by the LAC (NLC). Further details about the LAC (NLC) thesis program are available on the LAC (NLC) website (www.nlc-bcn.ca).

Full publication details and a copy of this permission letter will be included in the thesis.

Yours sincerely,

Karen O'Malley
_____

Permission is granted for:

a)   the inclusion of the material described above in your thesis.

b)   for the material described above to be included in the copy of your thesis that is sent to the Library and Archives of Canada (formerly National Library of Canada) for reproduction and distribution.

A License Agreement between Karen L O'Malley and Wolters Kluwer Health was obtained. License number: 3107761426299.

January 17, 2013

Klaus Willecke
Institut für Genetik
Abteilung Molekulargenetik
Universität Bonn
53117 Bonn, Germany

I am preparing my Master of Applied Science thesis for submission to the Faculty of Graduate Studies at Dalhousie University, Halifax, Nova Scotia, Canada. I am seeking your permission to include an image with some modification from the following document in the thesis:

Söhl G, Willecke K. Gap junctions and the connexin protein family. Cardiovasc Res. 2004; 62(2):228.
        Image: Figure 1, p. 229

Canadian graduate theses are reproduced by the Library and Archives of Canada (Formerly National Library of Canada) through a non-exclusive, world-wide license to reproduce, load, distribute, or sell theses. I am also seeking your permission for the material above to be reproduced and distributed by the LAC (NLC). Further details about the LAC (NLC) thesis program are available on the LAC (NLC) website (www.nlc-bcn.ca).

Full publication details and a copy of this permission letter will be included in the thesis.

Yours sincerely,

Karen O'Malley
_____

Permission is granted for:

a)   the inclusion of the material described above in your thesis.

b)   for the material described above to be included in the copy of your thesis that is sent to the Library and Archives of Canada (formerly National Library of Canada) for reproduction and distribution.

A License Agreement between Karen L O'Malley and Oxford University Press was obtained. License number: 3073850885362.

January 17, 2013

ASME
22 Law Drive
PO Box 2900
Fairfield, NJ   07007-2900

I am preparing my Master of Applied Science thesis for submission to the Faculty of Graduate Studies at Dalhousie University, Halifax, Nova Scotia, Canada. I am seeking your permission to include an image with some modification from the following document in the thesis:

Huang H, Liao J, Sacks M. In-situ deformation of the aortic valve interstitial cell nucleus under diastolic loading. J Biomech Eng. 2007; 129(6):880.
      Image: Figure 9, p. 887

Canadian graduate theses are reproduced by the Library and Archives of Canada (Formerly National Library of Canada) through a non-exclusive, world-wide license to reproduce, load, distribute, or sell theses. I am also seeking your permission for the material above to be reproduced and distributed by the LAC (NLC). Further details about the LAC (NLC) thesis program are available on the LAC (NLC) website (www.nlc-bcn.ca).

Full publication details and a copy of this permission letter will be included in the thesis.

Yours sincerely,

Karen O'Malley
_____

Permission is granted for:

a)   the inclusion of the material described above in your thesis.

b)   for the material described above to be included in the copy of your thesis that is sent to the Library and Archives of Canada (formerly National Library of Canada) for reproduction and distribution.

A License Agreement between Karen L O'Malley and ASME was obtained. Invoice number: 2002417167.

January 17, 2013

Dr. Jessica O. Winter
William G. Lowrie Department of Chemical and Biomolecular Engineering
Department of Biomedical Engineering
The Ohio State University
335 Koffolt Laboratories
140 W 19th Avenue
Columbus, OH   43210

I am preparing my Master of Applied Science thesis for submission to the Faculty of Graduate Studies at Dalhousie University, Halifax, Nova Scotia, Canada. I am seeking your permission to include an image with some modification from the following document in the thesis:

Rao S, Winter J. Adhesion molecule-modified biomaterials for neural tissue engineering. Front Neuroeng. 2009; 2:6.
        Image: Figure 1, p. 2

Canadian graduate theses are reproduced by the Library and Archives of Canada (Formerly National Library of Canada) through a non-exclusive, world-wide license to reproduce, load, distribute, or sell theses. I am also seeking your permission for the material above to be reproduced and distributed by the LAC (NLC). Further details about the LAC (NLC) thesis program are available on the LAC (NLC) website (www.nlc-bcn.ca).

Full publication details and a copy of this permission letter will be included in the thesis.

Yours sincerely,

Karen O'Malley
_____

Permission is granted for:

a)   the inclusion of the material described above in your thesis.

b)   for the material described above to be included in the copy of your thesis that is sent to the Library and Archives of Canada (formerly National Library of Canada) for reproduction and distribution.

Written permission was provided by the author, and can be found on the following page.

Sure.

-J

--
Dr. Jessica Winter
Associate Professor
William G. Lowrie Department of Chemical and Biomolecular Engineering
Department of Biomedical Engineering
140 W 19th Ave
Columbus, OH 43210
(614) 247-7668
http://chbmeng.ohio-state.edu/~winter